LBL-38595
UC-404

Lawrence Berkeley Laboratory
UNIVERSITY OF CALIFORNIA

Materials Sciences Division

Ultrafast Dynamics of Coulomb Correlated Excitons in GaAs Quantum Wells

M.-A. Mycek
(Ph.D. Thesis)

December 1995

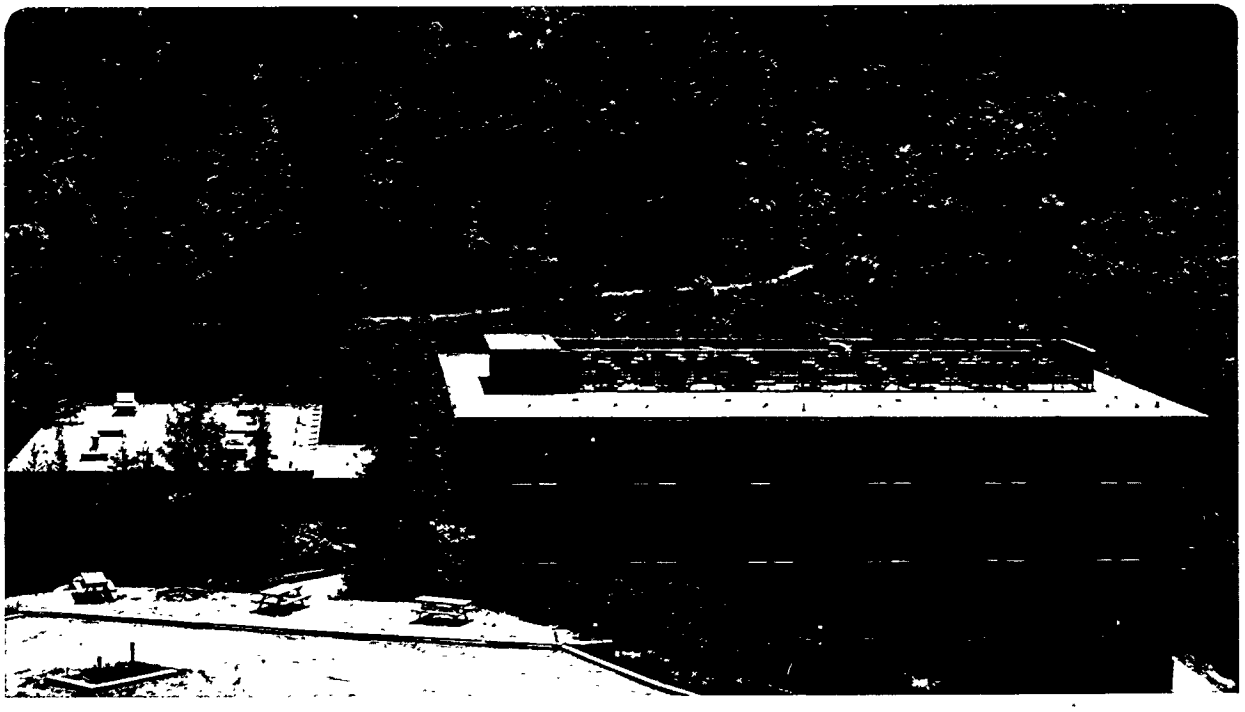

Prepared for the U.S. Department of Energy under Contract Number DE-AC03-76SF00098

DISCLAIMER

LBL 38595
UC-404

ULTRAFAST DYNAMICS OF COULOMB CORRELATED EXCITONS IN GaAs QUANTUM WELLS

Mary-Ann Mycek
Ph.D. Thesis

DEPARTMENT OF PHYSICS
University of California, Berkeley

and

MATERIALS SCIENCES DIVISION
Lawrence Berkeley National Laboratory
University of California
Berkeley, CA 94720

DECEMBER 1995

This work was supported by the Director, Office of Energy Research, Offie of Basic Energy Sciences, Materials Sciences Division, of the U.S. Department of Energy under Contract No. DE-AC03-76SF00098.

Ultrafast Dynamics of Coulomb Correlated Excitons in GaAs Quantum Wells

by

Mary-Ann Mycek

B.S. (Rochester Institute of Technology) 1989
M.A. (University of California, Berkeley) 1991

A dissertation submitted in partial satisfaction of the

requirements for the degree of

Doctor of Philosophy

in

Physics

in the

GRADUATE DIVISION

of the

UNIVERSITY of CALIFORNIA, BERKELEY

Committee in charge:

Professor Daniel S. Chemla, Chair
Professor Paul L. McEuen
Professor A. Paul Alivisatos

1995

Ultrafast Dynamics of Coulomb Correlated Excitons in GaAs Quantum Wells

by

Mary-Ann Mycek

Abstract

Ultrafast Dynamics of Coulomb Correlated Excitons in GaAs Quantum Wells

by

Mary-Ann Mycek

Doctor of Philosophy in Physics

University of California, Berkeley

Professor Daniel S. Chemla, Chair

We measure the transient nonlinear optical response of room temperature excitons in gallium arsenide quantum wells via multi-wave mixing experiments. The dynamics of the resonantly excited excitons is directly reflected by the ultrafast decay of the induced nonlinear polarization, which radiates the detected multi-wave mixing signal. We characterize this ultrafast coherent emission in both amplitude and phase, using time- and frequency-domain measurement techniques, to better understand the role of Coulomb correlation in these systems.

To interpret the experimental results, the nonlinear optical response of a dense medium is calculated using a model including Coulomb interaction. We contribute three new elements to previous theoretical and experimental studies of these systems. First, surpassing traditional time-integrated measurements, we temporally resolve the amplitude of the ultrafast coherent emission. Second, in addition to measuring the third-order four-wave mixing signal, we also investigate the fifth-order six-wave mixing response. Third, we characterize the ultrafast phase dynamics of the nonlinear emission using

interferometric techniques with an unprecedented resolution of approximately 140 attoseconds.

We find that effects arising from Coulomb correlation dominate the nonlinear optical response when the density of excitons falls below $3x10^{11}cm^{-2}$, the saturation density. Under these conditions, Coulomb interactions are unscreened and there exist two contributions to the multi-wave mixing emission. A prompt response from field scattering occurs via the phase-space filling effects of the Pauli exclusion principle, while a delayed response from polarization wave scattering occurs via the Coulomb interactions between excitons. In four-wave mixing, polarization wave scattering produces a non-exponential decay to the time-resolved signal and a corresponding non-linear phase evolution in the emitted pulse. In six-wave mixing, polarization wave scattering manifests itself as an asymmetry in the time-integrated lineshape.

These signatures of Coulomb correlation are investigated for increasing excitation density to gradually screen the interactions and test the validity of the model for dense media. Our results are found to be qualitatively consistent with both the predictions of the model and with numerical solutions to the semiconductor Bloch equations. Importantly, our results also indicate current experimental and theoretical limitations, which should be addressed in future research.

This dissertation is dedicated
to the memory of my mother,
Sophie M. Mycek,
who taught me to ask questions
and to my father,
Edwin E. Mycek,
who taught me to persist.

TABLE OF CONTENTS

ACKNOWLEDGMENTS

Once upon a time, a long, long time ago, I checked a box on a standardized questionnaire. The form asked about the highest educational degree you imagine yourself attaining. I was very young, liked school a lot, and reasoned I would continue my education as long as possible. Having absolutely no idea what the three letters meant, I marked "Ph.D," simply because it was the last in a long progression of boxes. I can hardly believe that now, many, many years later, I have indeed become a Doctor of Philosophy. My journey has been an unforgettable and infinitely rewarding experience.

If there is one person who is most responsible for guiding me along the way, it is my dissertation advisor, Prof. Daniel S. Chemla. More than anyone else, he has shown me by example the dedication and hard work it takes to be a research scientist. Over the years, he has been consistently generous with his time and good-humor. It has been both a pleasure and a privilege to work with him. I thank him for allowing me to share his enthusiasm and wonder for a fascinating field of research.

There have been several faculty members at U.C. Berkeley who showed me great kindness and encouragement during my time here. In particular, I thank Profs. Marvin Cohen, Paul McEuen, and Paul Alivisatos, who served on my committee during my last year, and Profs. J.D. Jackson and Marjorie Olmstead.

During the course of my graduate research, I had the opportunity to collaborate with a number of visiting scientists. Theorists, including Profs. Wilfried Schafer, the late Stefan Schmitt-Rink, and Ilias E. Perakis, have contributed greatly to my interpretation of experimental results, while experimentalists, including Prof. Rainer Ulbrich and Dr. Jean-

Yves Bigot, have shared with me their secrets for success in the laboratory. I consider myself very fortunate, indeed, to have worked with such outstanding scientists: More than anyone else, though, Jean-Yves has taught me the methods of good scientific research. He is a valued friend and colleague, and much of this dissertation is the result of our joint efforts in the lab.

Financial support has been crucial to my progress in graduate school and I am deeply indebted to the National Physical Science Consortium (NPSC) for providing fellowship funds during six years. I especially want to thank L. Nan Snow, the director of the NPSC, for being a friend, advisor, and role-model to me, and many other fellows, during this time. Through the NPSC I met two very special persons: my mentor, Dr. Tom Klitsner of Sandia National Laboratories, who has given me unfailing support and guidance throughout my graduate career, and Oscar Dubon, my cohort in Materials Science. Oscar and I began graduate school together, worked in the same building at Lawrence Berkeley Lab during five years, and made a pact to graduate together. I am happy to say we have met our goal.

I will never forget the many people who made being at Berkeley a distinctly pleasurable experience, from start to finish. I want to thank them for their years of friendship, humor, and support. Whether puzzling over problem sets 'til dawn with Aephraim Steinberg and Jim Vickers during the first two years of classes or puzzling over lab equipment with David Botkin, Sarah Bolton, Beth Parks, Chandu Karadi, and Sandeep Jauhar during later years, these people surely made the daily experience of graduate school much more fun than it would have been without them. I extend many thanks, too, to

those students who went before me and never failed to provide sound and valued advice. Foremost among them is Vin Crespi, who is both a good friend and an excellent teacher of condensed matter theory. Special appreciation is sent to long-time and long-distance friends from undergraduate days, Jayanne English and Denise Chen. From different corners of the globe, we shared the trials and triumphs of graduate school as we each made our way through, year after year. Finally, my dissertation partner Bruce McWilliams deserves special mention. We are good friends and former housemates who banded together to work on the writing portion of our dissertations. I owe to Bruce this manuscript, completed in a timely fashion, and all my knowledge of Agricultural Economics. When we file our dissertations together tomorrow, it will be a wonderful day for us both.

The acknowledgments for this dissertation would not be complete without thanking my family for the support and love they have given me during these many years away from them. They started me on this journey of wondering why, and why not, many years ago and have taught me the meaning of courage, honor, and tenacity along the way. I have never regretted this path.

Finally, my husband John M. Card has made these last years in Berkeley the best years of my life. He brings to me a special joy which turns the tallest mountains into hills. I look forward to climbing many more mountains with him.

M.-A. Mycek

Berkeley, December 14, 1995

Chapter 1

Introduction

1.1 Motivation

Understanding the properties of electronic excitations in semiconductors is of interest to scientists and engineers alike. To modify the electronic response of the material for device applications, for example, an understanding of the fundamental physical processes contributing to the response is of paramount importance. Thus it is crucial to recognize that the properties of electronic excitations in semiconductors are strongly influenced by both Coulomb interaction, because the particles are charged, and state filling effects arising from the Pauli exclusion principle, because the particles are fermions. Although there are several methods available to study these semiconductor excitations (for example, transport techniques), we will use optical probes, which are ideal for investigating the response of excitations in direct band-gap GaAs.

Coulomb correlation and Pauli exclusion influence both the *linear* and the *nonlinear* optical properties of semiconductors. [1.1] When a photon with energy greater than the band-gap is incident on the material, an electron-hole pair is created. Because the two particles are oppositely charged, they form an interacting system rather like a hydrogen atom, where the particle masses are the conduction and valence band effective masses ($m_e^* \approx 0.066m_e$, $m_{hh}^* \approx 0.5m_e$ (heavy-hole) in GaAs) and where the Coulomb

potential is screened by the dielectric constant of the material ($\varepsilon \approx 13$ in GaAs). The bound states of the interacting electron and hole are the exciton states. (Compared to the hydrogen atom, the excitonic Bohr radius is large ($a_0^* \approx 140$ Å in GaAs), while the binding energy, the excitonic Rydberg, is small ($Ry^* \approx 4.2$ meV in GaAs). An excellent description of excitons can be found in the reference [1.2].) The bound exciton appears in the linear absorption spectrum of the material as a resonance slightly below the semiconductor band-gap. Naturally, the Coulomb interaction is inherent to the formation of excitons. Because the exciton is composed of two fermions, state filling effects due to Pauli exclusion also play a role in the creation of excitons. When there are a sufficient number of free carriers present to screen the Coulomb potential and block phase space, the exciton dissociates, as observed in nonlinear optical experiments. [1.1] [1.3] Thus, physical processes resulting from the interplay between Pauli exclusion and Coulomb correlation influence the optical response of the semiconductor. These are the fundamental phenomena which we are interested in understanding via optical studies of GaAs. To do this, we performed transient multi-wave mixing experiments on excitons in GaAs quantum wells, which we describe below.

1.2 Semiconductor heterostructures

Experimental studies of semiconductor optical response have been greatly aided by advances in semiconductor growth technology, such as molecular beam epitaxy (MBE).

In addition to producing crystals of very high quality, which is essential for homogeneously broadened resonances, MBE is used to create semiconductor heterostructures by growing thin (typically about 100 Å thick) layers of alternating band-gap semiconductors. Electronic wavefunctions are confined along the growth direction within the lower-gap material, thus forming quasi-2D "quantum wells" (QWs). [1.4] For GaAs QWs, it is important to note that the quantum confinement lifts the degeneracy of the heavy- and light-hole (hh, lh) excitons because of their differing masses. As described in elementary text books on quantum mechanics, these structures have a series of quantum well states denoted n = 1, 2, 3, etc., labeling the confined hh and lh excitons. Currently, via a variety of growth techniques, further confinement in semiconductors to quasi-1D quantum wires and quasi-0D quantum dots is also available. [1.5] As one might expect, quantum confinement influences both the linear and the nonlinear optical properties of the material. For excitons in quasi-2D GaAs QWs, there is a greater overlap of the electron and hole wavefunctions, compared to the bulk semiconductor, which leads to an enhanced absorption at the hh- and lh-exciton resonances. [1.1] The exciton resonances in *bulk* GaAs are visible only at low temperatures, since the increasing phonon population at higher temperatures broadens the bulk exciton resonances until they disappear. Importantly, because of the quantum confinement effect, the GaAs hh- and lh-exciton QW resonances remain pronounced, even at room temperature. In this way, we have employed MBE grown QW samples to study the optical response of quasi-2D excitons in GaAs at room temperature.

1.3 Dynamics

The quasi-2D confinement described above influences not only steady-state optical properties of the semiconductor, but also *dynamical processes* in the material, for example the screening of the Coulomb correlation [1.6], which in turn affect the transient optical response of the system. Because the dynamics of the electronic excitations in semiconductors are very fast (on the order of ps or fs) it is necessary to use ultrashort laser pulses to resolve them. Under optical excitation, a coherent and oscillating polarization is induced in the semiconductor, which undergoes Rabi flopping. [1.7] Once the pulsed field is gone, the induced polarization loses coherence via scattering (incoherent) processes and dephases (typically in fs or ps). This induced polarization radiates a field, which we measure and attempt to characterize as fully as possible to obtain information on the dynamic incoherent processes. After the induced polarization has dephased, a quasi-equilibrium excitation distribution is formed which ultimately (in ns) recombines with the valence band. (This evolution is well summarized in reference [1.5].) Using sufficiently short pulses to excite and subsequently probe the semiconductor, it is possible to resolve these dynamic processes. For instance, the dephasing dynamics of e-h pairs in non-equlibrium Fermi seas has been studied via transient pump-probe and multi-wave mixing experiments. [1.8] Furthermore, photon echo experiments using 8 fs pulses to excite carriers in GaAs QWs have shown how quantum confinement alters the screening of the Coulomb potential. [1.6] Here, we investigate the dephasing dynamics of a simpler system: the single bound state of the n = 1 hh-exciton in GaAs QWs at room

temperature, where we study the interplay of Coulomb correlation and Pauli exclusion on the transient multi-wave mixing signal.

Effects of Coulomb correlation and Pauli exclusion on the transient nonlinear optical response of excitons in QWs have been studied previously via four-wave mixing (FWM) experiments on InGaAs. [1.9] Here, we extend those experiments to room temperature excitons in GaAs QWs and additionally measure three new quantities. First, we characterize the multi-wave mixing emission via *time-resolved* (TR) measurements, which provide information beyond the traditional time-integrated (TI) measurements employed in [1.9]. Second, we study the effects of Coulomb correlation on the induced nonlinear polarization to fifth-order by measuring *six-wave mixing* (SWM) signals. Third, we go beyond the traditional amplitude characterization of the coherent emission by also measuring the *ultrafast phase dynamics* of the multi-wave mixing signal. This allows us to extract from the multi-wave mixing emission the most information possible on the dynamics of the induced nonlinear polarization. From our measurements we observe directly in the time domain the competition between processes arising from Pauli exclusion and Coulomb correlation.

1.4 Outline of dissertation

We begin the discussion by presenting in Ch.2 the theoretical model we use to calculate the induced nonlinear polarization in the semiconductor. We obtain from the model a series of "signatures" for Coulomb correlation which appear in multi-wave mixing

experiments. We will test the validity of these predictions in this dissertation by fully characterizing the coherent multi-wave mixing emission.

The experimental apparatus we constructed to perform the multi-wave mixing measurements and characterization is fully detailed in Ch.3. After describing the GaAs multiple quantum well samples and the fs-modelocked Ti:Sapphire laser, we discuss the multi-wave mixing optical set-up. The various time and frequency domain measurements we perform to characterize both the excitation laser pulse and the coherent emission from the sample are then presented in detail.

Our experimental results are presented in Chapters 4-6. The results of TR FWM measurements, including numerical fits to the TR data, appear in Ch.4. From the fits, we observe directly the interplay between Pauli exclusion and Coulomb correlation in the FWM coherent emission. The results of TI and TR SWM measurements are presented in Ch.5. Again, we detect signatures for Coulomb correlation, which appear in the TI SWM lineshape at low excitation density. Finally, the phase characterization of the FWM signal is presented in Ch.6. Here we show experimental results for both selective excitation of the hh-exciton resonance and the simultaneous excitation of hh- and lh-excitons. In the former case we observe the nonlinear phase dynamics at low excitation density which is the signature of Coulomb correlation predicted from the theoretical model. In the latter case, we observe the nonlinear phase dynamics coupled with a quantum beat.

We summarize and conclude the dissertation in Ch.7, where we also discuss important theoretical and experimental limitations discovered by the research presented here. In light of our results, we discuss the directions of future research in this field.

References

[1.1] S. Schmitt-Rink, D.S. Chemla, D.A.B. Miller: *Linear and nonlinear optical properties of semiconductor quantum wells*, Advances in Physics, Vol.38, No.2, pp.89-188 (1989).

[1.2] R.S. Knox: *Theory of Excitons*, Academic Press, (1963).

[1.3] see, S. Schmitt-Rink, D.S. Chemla, D.A.B. Miller: *Theory of transient excitonic optical nonlinearities in semiconductor quantum-well structures*, Physical Review B, Vol.32, No.10, pp.6601-6609 (1985), and references therein.

[1.4] G. Bastard: *Wave Mechanics Applied to Semiconductor Heterostructures*, Halsted Press, (1988).

[1.5] see, for example, N. Peyghambarian, S.W. Koch, A. Mysyrowicz: *Introduction to Semiconductor Optics*, Prentice-Hall, (1993).

[1.6] J.-Y. Bigot, M.T. Portella, R.W. Schoenlein, J.E. Cunningham, C.V. Shank: *Two-dimensional carrier-carrier screening in a quantum well*, Physical Review Letters, Vol.67, No.5, pp.636-639 (1991).

[1.7] S.T. Cundiff, A. Knorr, J. Feldmann, S.W. Koch, E.O. Gobel, H. Nickel: *Rabi flopping in semiconductors*, Physical Review Letters, Vol.73, No.8, pp.1178-1181 (1994).

[1.8] M.-A. Mycek, J.-Y. Bigot, I.E. Perakis, D.S. Chemla: *Measuring the ultrafast dynamics of Coulomb correlation effects: Dephasing in non-equilibrium Fermi seas*, Journal of the Optical Society of America B, to appear in March 1996.

[1.9] M. Wegener, D.S. Chemla, S. Schmitt-Rink, W. Schafer: *Line shape of time-resolved four-wave mixing*, Physical Review A, Vol.42, No.9, pp.5675-5683 (1990).

Chapter 2

Theoretical Model: Signatures of Coulomb Correlation in Ultrafast Wave Mixing Experiments

2.1 Introduction

It is well known that light incident on a material induces a polarization in the medium, which, in turn, radiates a field. The former process is governed by the microscopic constitutive relations appropriate for the medium, while the latter process is determined by the Maxwell equations. For the optically thin samples investigated in this dissertation (see Ch.3.), the wave equation indicates that the temporal dependence of the emitted field and the induced polarization are the same. Thus, we are left to model the microscopic description of the light-matter interaction in the experiments presented in Chapters 4-6. We have performed multi-wave mixing experiments on GaAs multiple quantum well structures using intense beams of light from an ultrashort pulsed laser to induce several orders of transient nonlinear polarization. We then measured the coherent radiation emitted from the semiconductor using a variety of techniques to fully characterize the

signal and thus gain information on the physical processes contributing to the optical response.

For a simple atomic system, the nonlinear optical response is well described by the optical Bloch equations (OBE) [2.1] for a two-level system. Collections of two-level systems, such as dilute gases, require the density matrix formalism where the temporal evolution of the system is determined from the Liouville equation and relaxation processes (polarization dephasing and population lifetime) are accounted for phenomenologically. This approach has been fully developed in many excellent references [2.2] [2.3] [2.4] and successfully applied to multi-wave mixing experiments in a variety of systems, such as atomic vapors and dye molecules in solution [2.4]. However, the above formalism has limited success in dense media, such as semiconductors, where effects resulting from Coulomb correlation can dominate both the linear and nonlinear optical response. [2.5] The most complete description of the nonlinear optical response of semiconductors to date is given by numerical solutions to the semiconductor Bloch equations (SBE) in k-space [2.6] [2.7] [2.8], where effects from band dispersion, multiple bands, and valence-band mixing are included in the formalism. In addition, the *static* screening of the Coulomb interaction for excited electron hole pairs is treated exactly. Although the SBE approach has been highly successful at matching experimental results [2.9] [2.10] [2.11], one drawback to the lengthy numerical calculations is that much of the physical insight is lost in the process.

In this chapter, we present a model for the optical response of dense media based on *interacting* two-level systems. This highly simplified version of the two-band SBE is

valid for selective, weak excitation of the lowest bound state (1s) exciton and is equivalent to a local-field model, as described in reference [2.7]. This approach has the advantage of capturing the important physics, including effects due to Coulomb correlation, which are critical to interpreting the semiconductor response, while keeping the physical insight gained from an analytical solution to the Liouville equation. This type of model has been used before [2.12] [2.13] to successfully interpret anomalies in the four-wave mixing response from semiconductors, which were attributed to Coulomb correlation. Here, we add three new points to the discussion. First, we carry out the calculation to *fifth*-order to interpret not only four-wave mixing (FWM) signals, but also *six*-wave mixing (SWM) signals. Second, we determine from the analytical results for impulsive excitation both the time-integrated (TI) and the time-*resolved* (TR) response for both FWM and SWM measurements. Third, we investigate the effects of Coulomb correlation on not only the amplitude of the coherent emission but also on the *phase*. These results provide us with clear signatures of Coulomb correlation which we will later use to interpret the data presented in Chs.4, 5, and 6.

We begin the discussion by presenting the phenomenological model we use to describe the interacting two-level systems in section 2.2. Next, in section 2.3, we discuss the TI and TR measurements performed to characterize the multi-wave mixing signals and outline the approach used for a general solution to the problem. We then present the temporal dependence of the nonlinear polarization calculated for δ-function pulsed excitation in section 2.4. These results provide us with signatures for Coulomb correlation

in TI and TR multi-wave mixing which we explicitly state in section 2.5. Finally, in section 2.6 we summarize our findings and conclude.

2.2 Theoretical model

To better understand the physical processes contributing to the nonlinear optical response of our samples, we must first develop a model for the light-matter interaction which is appropriate for a semiconductor. As explained in the introduction, two extreme cases for material optical response are the isolated two-level system, described by the OBE [2.1], and the semiconductor, whose most complete description to date is given by numerical solutions to the SBE [2.7]. We begin this section by outlining the well known density matrix formalism appropriate for dilute media, where interactions within the collection of two-level systems are neglected. For semiconductors, neglecting Coulomb interactions is unjustified and this approach has been found to be inadequate. [2.12] Thus, for dense media, we present a model based on *interacting* two-level systems, which we fully develop in the remainder of the chapter. As we will show, this model allows analytical solutions under impulsive excitation, while capturing the essential physics of Coulomb correlation in the semiconductor.

2.2.1 Dilute media

The transient nonlinear optical response of dilute media, such as atomic vapors and gases, is obtained by solving the Liouville equation for the density matrix describing the ensemble of two-level systems. For the case of *independent* two-level systems, the procedure [2.2] and results for four-wave mixing experiments [2.4] have been written explicitly many times. We will not duplicate this process here, since the solutions presented in following sections for *interacting* two-level systems naturally reduce to these results when the interaction terms are neglected. Instead, we sketch here an outline of the solution for dilute media as an aid to following the more complicated case for dense media, presented in detail below.

Let $|a\rangle$ and $|b\rangle$ label the lower and upper levels of the two-level system. The density matrix ρ for the ensemble is

$$\rho=\begin{bmatrix} n_{aa} & \psi^{*}_{ba} \\ \psi_{ba} & n_{bb} \end{bmatrix}$$

where the diagonal elements n_{jj} represent the population in level $|j\rangle$ and the off-diagonal elements ψ_{ij} represent the transition amplitude between levels. The evolution of ρ is determined by the Liouville equation, $\frac{\partial\rho}{\partial t}=\frac{2\pi}{ih}[H,\rho]+\left(\frac{\partial\rho}{\partial t}\right)_{relax}$. Here, the Hamiltonian H is given by $H = H_0 + H_{int}$, with H_0 being the Hamiltonian of the unperturbed system and H_{int} being the Hamiltonian describing the light-matter interaction, while $(\partial\rho/\partial t)_{relax}$

accounts for the interaction of the two-level systems with their surrounding environment as the perturbed ρ relaxes back to thermal equilibrium. Thus we have

$$\frac{\partial \rho}{\partial t}=\frac{2\pi}{ih}\left[\left\{\begin{bmatrix} E_a & 0 \\ 0 & E_b \end{bmatrix}+\begin{bmatrix} 0 & -\mu^* E^*(t) \\ -\mu E(t) & 0 \end{bmatrix}\right\},\rho\right]+\left(\frac{\partial \rho}{\partial t}\right)_{relax}$$

where E_j are the unperturbed energy levels, $\mu E(t)=\langle a|er\cdot E|b\rangle$ gives H_{int} in the dipole approximation, and the relaxation terms are treated phenomenologically

$$\frac{\partial}{\partial t}\left(n_{ij}-n_{ij}^{(0)}\right)_{relax}=\frac{-1}{(T_1)_j}\left(n_{ij}-n_{ij}^{(0)}\right) \qquad \text{and} \qquad \left(\frac{\partial \psi_{ij}}{\partial t}\right)_{relax}=\frac{-1}{(T_2)_{ij}}\psi_{ij}$$

by introducing the longitudinal and transverse relaxation rates, known as the population lifetime, T_1, and the polarization dephasing time, T_2, respectively.

Once the evolution of the density matrix ρ(t) is known, the ensemble average of a physical observable M is found from: $\langle M\rangle=Tr(\rho\overline{M})$. For example, assuming a homogeneously broadened system, the macroscopic polarization P(t) is given by $\langle P(t)\rangle=Tr(\rho\overline{P})=Tr(\rho N\overline{\mu})=N\mu^*\psi(t)$, where N is the number density of two-level systems and $\overline{\mu}$ is the dipole matrix operator. To find the *nonlinear* polarization, a perturbation approximation is employed for the density matrix $\rho = \rho^{(0)} + \rho^{(1)} + \rho^{(2)} + \rho^{(3)} + ...$ and for the macroscopic polarization $\langle P\rangle = \langle P^{(1)}\rangle + \langle P^{(2)}\rangle + \langle P^{(3)}\rangle + ...$, where the relation

$\langle P^{(n)}(t)\rangle = Tr(\rho^{(n)}\overline{P}) = N\mu^{*}\psi^{(n)}(t)$ holds for each expansion order (n). Introducing the expansion for ρ into the Liouville equation, collecting terms of equal order in the field, and assuming that initially the system is in thermal equilibrium, with the population in the ground state, gives a hierarchy of coupled equations for $\psi^{(1)}$, $n^{(2)}$, $\psi^{(3)}$, $n^{(4)}$, $\psi^{(5)}$, etc. For a given excitation condition, e.g. a sequence of time-delayed optical pulses with given wavevector directions for a specific wave-mixing geometry, the system of equations are solved iteratively for the nonlinear polarization in a particular wavevector direction, e.g. the four- or six-wave mixing direction. As we will show, the same general procedure outlined here is also used to calculate the nonlinear polarization for the collection of interacting two-level systems, where the model is different and the solutions are far more complex.

When propagation effects can be neglected (see Ch.3), the wave equation tells us that the induced nonlinear polarization $P^{(n)}(t)$ and the corresponding emitted radiation $E_{signal}(t)$ have the same time dependence. Thus, by measuring and characterizing the coherent emission $E_{signal}(t)$ we indirectly measure the induced transient nonlinear polarization, which sheds light on the dynamical physical processes responsible for the nonlinear optical response of the material. For example, in dilute media transient FWM experiments measure the polarization dephasing time T_2. [2.4] A problem arises, however, when the results obtained for dilute media are applied to dense materials, such as semiconductors [2.12], where Coulomb correlation effects cannot be neglected. As we show below, the model presented above may be modified to account for such interactions.

2.2.2 Dense media

A dense medium may be modeled as a collection of N *interacting* two-level systems, as described in the Appendix. In this case, and using the notation developed in the Appendix, the optical response of the system is governed by the time-dependent transition amplitude $\psi(t)$, giving the induced polarization P(t), and by the excited state population n(t), which are determined by the solutions to the coupled equations

$$\left[\frac{\partial}{\partial t}+\Gamma+i\Omega\right]\psi(t)=i[1-2n(t)]\mu E(t)-2iVn(t)\psi(t) \qquad \text{Eqn.2-1}$$

$$\left[\frac{\partial}{\partial t}+\gamma\right]n(t)=-2\mathrm{Im}\left[\mu E(t)\psi^{*}(t)\right] \qquad \text{Eqn.2-2}$$

where $h/2\pi \equiv 1$, E(t) is the externally applied field, Ω is the transition frequency, μE is the Rabi frequency, and V represents the effective interaction energy due to the presence of Coulomb correlation. The transverse and longitudinal relaxation rates are introduced phenomenologically and denoted by $\Gamma = (T_2)^{-1}$ and $\gamma = (T_1)^{-1}$, respectively. For a homogeneously broadened system and in the dipole approximation, appropriate for our experiment (see Chs.3 and 4), the induced polarization is given by $P(t) = N\mu^*\psi(t)$. Because the transition amplitude determines the induced polarization, $\psi(t)$ is often referred to simply as the induced polarization wave in the material.

Although highly simplified compared to the complete k-space description of the SBE formalism, the above equations contain a wealth of physical insight into the optical

response of interacting systems. The population n(t) is seen to depend nonlinearly upon the energy absorbed, being limited by relaxation via the lifetime T_1, as for a two-level system. In fact, by neglecting interactions (setting V = 0) the two equations reduce to the OBE for a saturable two-level system. Thus, as for independent two-level systems, the above equations are coupled, meaning that the development and evolution of the induced polarization depends upon the population, and vice versa. We will demonstrate this explicitly below when calculating the successive orders of nonlinear polarization.

The transition amplitude $\psi(t)$ is also limited by relaxation, via the polarization dephasing rate $\Gamma = (T_2)^{-1}$, and is further affected by the two nonlinear terms on the right side of the equation. In the first term, phase space filling (PSF) plays a role as Pauli exclusion reduces the strength of the coupling of the applied field to the system by reducing the Rabi frequency μE via saturation. As we show below for multi-wave mixing experiments, the term $\propto [n(t)\mu E(t)]$ can be viewed qualitatively as the scattering of the applied field E(t) in the presence of the population n(t). We denote this effect as the PSF contribution to the emission and will discuss its significance at great length below. In the second term, the Coulomb potential V mediates the interaction of the induced polarization wave $\psi(t)$ with the population n(t). Again, this term, $\propto [Vn(t)\psi(t)]$, can be viewed qualitatively as the scattering of the induced polarization wave $\psi(t)$ in the presence of the population n(t). We denote this effect as the polarization wave scattering (PWS) contribution to the emission and emphasize that it is does not exist for a collection of independent two-level systems. We notice from the form of the above equations that, in the presence of the same population n(t), if the applied field and the induced polarization

wave have distinct time dependencies, the two nonlinear contributions PSF and PWS will have different temporal evolutions. This is indeed the case, as we demonstrate below, and, in fact, PWS can have a profound influence on the nonlinear optical response of the system. Therefore the PWS contribution can be viewed as a *signature* for Coulomb correlation. Importantly, the model described above provides the same qualitative information as the complete numerical solution of the SBE for the nonlinear optical response of semiconductors in multi-wave mixing experiments, without losing physical insight in the process.

2.3 Multi-wave mixing signals

Before proceeding with the solution to the model for dense media (Eqns.2-1, 2-2) presented above, we first introduce the experimental techniques we have employed to induce the nonlinear polarization which generates the multi-wave mixing signals we measure. For the four-wave mixing (FWM) and six-wave mixing (SWM) experiments presented in this dissertation, we have employed the two-pulse wave-mixing geometry sketched in Fig.2.1. (The optical set-up and all measurement techniques are described in detail in Ch.3.) Two beams of time-delayed excitation pulses in wavevector directions k_1 and k_2 are incident on the sample. When the two pulses overlap, they interfere and create a grating. Photons scatter off this grating into the background free and momentum conserving directions $m(k_2-k_1)+k_2$, where m labels the diffraction order. For example, the first-order diffracted signal, m = 1, is the FWM signal emitted in direction $(k_2-k_1)+k_2$ =

$2k_2$-k_1. The second-order diffracted signal, m = 2, is the SWM signal emitted in direction $2(k_2-k_1)+k_2 = 3k_2-2k_1$. It is this coherent emission, called $E_{signal}(t)$, that we measure as the multi-wave mixing signal for a specific direction. This emission is depicted for FWM in Fig.2.1.

As we know from the wave equation, where propagation effects are neglected for optically thin samples (see Ch.3), the time dependence of these diffracted signals is the same as the time dependence of the induced nonlinear polarization. To determine this time dependence, we introduce a perturbation expansion for $\psi(t)$ and n(t), described in the procedure outlined for dilute media above, into the Eqns.2-1, 2-2 and collect terms of equal order in the field. For each expansion order ($n = 2m+1$), the nonlinear polarization is given by

$$P^{(n)}(t)=N\mu^{*}\psi^{(n)}(t) \qquad \text{Eqn.2-3}$$

thus $E_{signal}(\, m(k_2-k_1)+k_2, t) \propto P^{(n)}(t) \propto \psi^{(n)}(t)$. So, for the first-order diffracted signal , m = 1, $n = 3$, and we are interested in calculating $\psi^{(3)}(t)$ for the FWM direction $2k_2$-k_1. Similarly, for the second-order diffracted signal , m = 2, $n = 5$, and we must calculate $\psi^{(5)}(t)$ for the SWM direction $3k_2$-$2k_1$.

It is important to emphasize that the excitation pulses k_1 and k_2 need not overlap temporally for this coherent emission to occur. This is true because the first pulse, say k_1, incident on the sample induces a polarization which decays with the polarization dephasing time T_2. Thus, when the second pulse k_2 arrives at a later time Δt, it will interfere with the

remaining coherent polarization from pulse k_1. Thus a grating is still formed, photons from pulse k_2 are still scattered, and the coherent emission $E_{signal}(t)$ is still generated. Naturally, the efficiency of this process depends upon the timing of pulse k_2 (i.e. Δt) relative to the decay rate of the coherent polarization (i.e. T_2). The sooner pulse k_2 arrives after pulse k_1, the more induced polarization from k_1 remains coherent, the larger the scattered signal.

Ideally, we would like to fully characterize the scattered field $E_{signal}(t)$ in both amplitude and phase, to obtain as much information as possible on the corresponding nonlinear polarization $P^{(n)}(t)$. Because dephasing processes in semiconductors are very fast (on the order of picoseconds or even femtoseconds), historically it was not possible to directly resolve $E_{signal}(t, \Delta t)$ on a femtosecond time scale due to the limitations of electronic detection. For this reason, the time-integrated (TI) measurement technique was developed, which uses a slow-detector to integrate the total energy emitted as a function of the time-delay Δt between excitation pulses, as sketched in Fig.2.1(a). The TI trace, $S_{TI}(\Delta t)$, is thus given by

$$S_{TI}(\Delta t) = \int_{-\infty}^{+\infty} \left| P^{(n)}(t, \Delta t) \right|^2 dt \qquad \text{Eqn.2-4}$$

As we will see below, for dilute media $S_{TI}(\Delta t)$ decays exponentially with the polarization dephasing time T_2, thus giving the same information as $P^{(n)}(t, \Delta t)$. In this way the TI measurement *indirectly* provides information on the nonlinear polarization $P^{(n)}(t, \Delta t)$.

For dense media, however, the $S_{TI}(\Delta t)$ measurement is *not* sufficient for characterizing the nonlinear polarization $P^{(n)}(t, \Delta t)$. As we will show, there is a clear need to *directly* obtain the profile of $P^{(n)}(t, \Delta t)$. This is accomplished via time-resolved (TR) measurements, where we come very close to determining the amplitude of the ultrafast emission. We achieved temporal resolution of the multi-wave mixing signal by optically gating the coherent emission via sum-frequency generation in a nonlinear crystal using a cross-correlation geometry (see Ch.3 for details). As shown in Fig.2.1(b), instead of sending the coherent emission from the sample directly to a slow detector, as in the TI measurement, we optically gate the multi-wave mixing emission using a time-delayed reference pulse "k_3" from the laser. Thus, the TR signal $S_{TR}(T, \Delta t)$ for a fixed time-delay Δt is given by

$$S_{TR}(T,\Delta t)=\int_{-\infty}^{+\infty}\left|P^{(n)}(t,\Delta t)\right|^2\left|E_{laser}(t-T)\right|^2 dt \qquad \text{Eqn.2-5}$$

where it is easy to see that if the reference pulse from the laser $E_{laser}(t-T)$ were a δ-function pulse $\delta(t-T)$, then $S_{TR}(T, \Delta t)$ would *exactly* reproduce $|P^{(n)}(t, \Delta t)|^2$. Thus, for finite reference pulses, $S_{TR}(T, \Delta t)$ gives the temporal profile of the coherent emission convolved with the reference pulse from the laser.

We may now proceed with the general solution to the coupled Eqns.2-1, 2-2, for the nonlinear polarization wave $\psi^{(n)}(t)$. We assume that the applied excitation field $E(t)=\tilde{E}(t)e^{-i\omega t}$, where $\tilde{E}(t)$ is the envelope of the pulse and ω is the carrier frequency.

When the perturbation expansion described above is performed, the first-, third-, and fifth-order nonlinear polarization waves are given by

$$\psi^{(1)}(t)=ie^{-i\omega t}\int_{-\infty}^{t}e^{-i(\Omega-\omega-i\Gamma)(t-t')}\mu\tilde{E}(t')dt' \qquad \text{Eqn.2-6(a)}$$

$$\psi^{(3)}(t)=-2ie^{-i\omega t}\int_{-\infty}^{t}e^{-i(\Omega-\omega-i\Gamma)(t-t')}n^{(2)}(t')[\mu\tilde{E}(t')+V\psi^{(1)}(t')]dt' \qquad \text{Eqn.2-6(b)}$$

$$\psi^{(5)}(t)=-2ie^{-i\omega t}\int_{-\infty}^{t}e^{-i(\Omega-\omega-i\Gamma)(t-t')}\{n^{(4)}(t')[\mu\tilde{E}(t')+V\psi^{(1)}(t')]+n^{(2)}(t')V\psi^{(3)}(t')\}dt'$$

Eqn.2-6(c)

where we emphasize that the terms proportional to V do not exist for the case of independent two-level systems. Clearly these interaction terms will have an impact on the FWM and SWM signals generated by $\psi^{(3)}(t)$ and $\psi^{(5)}(t)$, respectively. From Eqns.2-6, we see that the induced linear polarization wave $\psi^{(1)}(t)$ decays exponentially with the polarization dephasing time $T_2 = \Gamma^{-1}$, and is *not* modified by the Coulomb interaction V. The induced nonlinear polarizations, however, are both affected by V. In $\psi^{(3)}(t)$, for example, not only does the applied field $\tilde{E}(t)$ scatter off the induced population grating $n^{(2)}(t)$, but also the induced polarization wave $\psi^{(1)}(t)$ scatters off the induced population grating $n^{(2)}(t)$, via the potential V. These two terms reflect the phase space filling (PSF) and polarization wave scattering (PWS) processes described in section 2.2 and indicate

that, unlike independent two-level systems, *in dense media both the applied field and the induced polarization wave contribute to the scattered coherent emission.*

To solve for the nonlinear polarization waves $\psi^{(n)}(t)$, we must begin by specifying the characteristics of the applied field. For the multi-wave mixing experiments described in this dissertation, the timing conventions for the two excitation pulses are given by

$$\tilde{E}(t)=E_1(t)\exp(ik_1r)+E_2(t-\Delta t)\exp(ik_2r) \qquad \text{Eqn.2-7}$$

In the general case of pulses of arbitrary shape, analytical solutions to the Eqns.2-6 may be too difficult to find. The equations may then be solved numerically using the exact pulse envelope and duration. (See Ch.4.) One special and important case of interest is impulsive excitation by δ-function pulses, where it is easy to obtain analytical solutions to Eqns.2-6 which capture the essential physics in the problem and provide us with clear signatures for Coulomb correlation. We present the results of such a calculation in the following sections.

2.4 Analytical result for δ-function pulse excitation

When the ultrashort pulses used to excite the semiconductor have a duration which is very much shorter than the polarization dephasing time, T_2, and the population lifetime T_1, it is appropriate to approximate the pulses by δ-function pulses. This allows analytical

solutions to Eqns.2-6 which display the same important features obtained via numerical solutions for finite pulse durations. (See Ch.4.) Using Eqns.2-3, 2-6, and 2-7, with $E_1(t) = E_1\,\delta(t)$ and $E_2(t) = E_2\,\delta(t-\Delta t)$, the first-order polarization is found to be

$$P^{(1)}(t,\Delta t) \propto iN|\mu|^2\left[E_2 e^{ik_2 r} e^{-i(\Omega-i\Gamma)(t-\Delta t)}\Theta(t-\Delta t)+E_1 e^{ik_1 r} e^{-i(\Omega-i\Gamma)t}\Theta(t)\right] \quad \text{Eqn.2-8}$$

where $\Theta(t)$ is the Heaviside step-function. As expected, each pulse induces a first-order polarization which decays exponentially in time with the polarization dephasing time $T_2 = \Gamma^{-1}$. From Eqn.2-8, we determine the second-order population, and subsequently the third-order polarization with wavevector $2k_2\text{-}k_1$ to be

$$P^{(3)}(t,\Delta t) \propto -2iN|\mu|^4\left[E_1^* E_2^2 e^{i(2k_2-k_1)r} e^{-i(\Omega-i\Gamma)t} e^{2i(\Omega-\omega)\Delta t}\right]\times$$

$$\left\{\left[\frac{1}{2}+iV\frac{1-e^{-\gamma(t-\Delta t)}}{\gamma}\right]\Theta(t-\Delta t)\Theta(\Delta t)+\left[iV\frac{1-e^{-\gamma t}}{\gamma}\right]e^{+2\Gamma\Delta t}\Theta(t)\Theta(-\Delta t)\right\}$$

Eqn.2-9

This polarization produces the coherent FWM emission in direction $2k_2\text{-}k_1$. Setting $V = 0$, we have the well-known result for a homogeneously broadened collection of independent two-level systems [2.4]: for $\Delta t > 0$, the third-order polarization decays exponentially in time with the polarization dephasing time $T_2 = \Gamma^{-1}$ and for $\Delta t < 0$, there is no third-order polarization in direction $2k_2\text{-}k_1$. For interacting two-level systems, when $V \neq 0$, there are

several important signatures here for Coulomb correlation. First, there exists a third-order polarization in direction $2k_2$-k_1 for $\Delta t < 0$. Second, for $\Delta t > 0$, there are two distinct contributions to the nonlinear polarization arising from PSF and PWS, as explained above, which have different, and non-exponential in the case of PWS, time dependencies. Third, the PSF and PWS contributions differ by i and are therefore out of phase with one another. Thus, the presence of PWS should affect in the instantaneous frequency dynamics of the coherent FWM emission. We will demonstrate how these signatures manifest themselves in TI and TR FWM experiments in the next section. Using the result in Eqn.2-9, we next obtain the fourth-order population, and finally find the fifth-order polarization with wavevector $3k_2$-$2k_1$ to be

$$P^{(5)}(t,\Delta t) \propto -2iN|\mu|^6 \left[E_1^{*2} E_2^3 e^{i(3k_2-2k_1)r} e^{-i(\Omega-i\Gamma)t} e^{3i(\Omega-\omega)\Delta t}\right] \times$$

$$\left\{ iVe^{-\Gamma\Delta t}\left[\frac{1-e^{-\gamma(t-\Delta t)}}{\gamma}\right]\left[1+iV\frac{1-e^{-\gamma(t-\Delta t)}}{\gamma}\right]\Theta(t-\Delta t)\Theta(\Delta t) \right.$$

$$\left. +iV^2\left[\frac{1-e^{-\gamma t}}{\gamma}\right]^2 e^{+3\Gamma\Delta t}\Theta(t)\Theta(-\Delta t)\right\} \qquad \text{Eqn.2-10}$$

This is a very interesting result, because *neglecting interactions by setting $V = 0$ seems to destroy the entire fifth-order signal.* In fact, for the case of independent two-level systems, there is no fifth-order emission for time-delays other than $\Delta t = 0$, when the two excitation pulses are co-incident on the sample. In this case and for $\Delta t = 0$, only, the fifth-order polarization decays exponentially in time with the polarization dephasing time $T_2 =$

Γ^{-1}. We find from Eqn.2-10, when interactions are included in the model, that there is emission present for time-delays other than $\Delta t = 0$ and that this emission has a non-exponential time-dependence. Thus, this result provides clear signatures for Coulomb correlation in SWM experiments. We discuss how these signatures appear in TI and TR SWM experiments below.

2.5 Signatures of Coulomb correlation

We begin by describing the signatures of Coulomb correlation which are found in transient FWM experiments. From the result for $P^{(3)}(t)$ with wavevector $2k_2$-k_1, Eqn.2-9, we determine the lineshape of the experimentally measured TR and TI FWM signals using the Eqns.2-5 and 2-4, respectively, and assuming δ-function laser pulses. The result for TR FWM in direction $2k_2$-k_1 is

$$S_{TR}(T,\Delta t) \propto \left|P^{(3)}(T,\Delta t)\right|^2$$

$$\propto \left[\frac{1}{4}+V^2\left(\frac{1-e^{-\gamma(T-\Delta t)}}{\gamma}\right)^2\right]e^{-2\Gamma T}\Theta(T-\Delta t)\Theta(\Delta t)$$

$$+V^2\left(\frac{1-e^{-\gamma T}}{\gamma}\right)^2 e^{+4\Gamma\Delta t}e^{-2\Gamma T}\Theta(T)\Theta(-\Delta t) \qquad \text{Eqn.2-11(a)}$$

The TR FWM lineshape given by the above equation is sketched in Fig.2.2. Fig.2.2(a) depicts the exponential decay with time constant $T_2/2$ when $V = 0$, as expected for the case of a homogeneously broadened collection of independent two-level systems. [2.4] Fig.2.2(b) shows the *two* contributions to the signal when interactions are included ($V \neq 0$). One is the *prompt* emission due to scattering of the electric field via PSF, as for independent two-level systems, and the other is the *delayed* emission resulting from scattering of the induced polarization wave via PWS, which is unique to interacting systems. Thus, one signature for Coulomb correlation in FWM experiments is the *non-exponential decay* of the TR FWM lineshape.

The corresponding result for TI FWM in direction $2k_2$-k_1 is

$$S_{TI}(\Delta t) \propto \left[\frac{1}{4\Gamma} + \frac{V^2}{\Gamma(\gamma+2\Gamma)(\gamma+\Gamma)}\right] e^{-2\Gamma\Delta t}\Theta(\Delta t) + \left[\frac{V^2}{\Gamma(\gamma+2\Gamma)(\gamma+\Gamma)}\right] e^{+4\Gamma\Delta t}\Theta(-\Delta t) \qquad \text{Eqn.2-11(b)}$$

The TI FWM lineshape given by the above equation is also sketched in Fig.2.2. Fig.2.2(c) depicts the exponential decay with time constant $T_2/2$ for positive time-delays ($\Delta t > 0$) when $V = 0$, as expected for the case of a homogeneously broadened collection of independent two-level systems. [2.4] Fig.2.2(d) shows the signal at negative time-delay ($\Delta t < 0$) which appears when interactions are included ($V \neq 0$). This signal is another manifestation of PWS, which is unique to interacting systems. The TI FWM lineshape, in

this case, is found to decay exponentially for negative time-delays with time constant $T_2/4$, at twice the rate of the positive time-delay signal. Thus, another signature for Coulomb correlation in FWM experiments is the *signal at negative time-delay* which appears in the TI FWM lineshape. This signature and the distinctive time-dependence have been observed in TI FWM measurements on both GaAs and InGaAs multiple quantum well structures. [2.14] (We note that in optically thick samples (10μm thick, for GaAs) propagation effects lead to a FWM signal for negative time delays, even for the model of independent two-level systems. [2.15] [2.16] This is not the case for the optically thin samples used in our experiments, as explained in Ch.3.)

From the result for $P^{(5)}(t)$ with wavevector $3k_2$-$2k_1$, Eqn.2-10, we determine the lineshape of the experimentally measured TR and TI SWM signals using the Eqns.2-5 and 2-4, respectively, and assuming δ-function laser pulses. The result for TR SWM in direction $3k_2$-$2k_1$ is

$$S_{TR}(T,\Delta t)\propto\left|p^{(5)}(T,\Delta t)\right|^2$$

$$\propto V^2\left[\left(1+V^2\left(\frac{1-e^{-\gamma(T-\Delta t)}}{\gamma}\right)^2\right)\left(\frac{1-e^{-\gamma(T-\Delta t)}}{\gamma}\right)^2\right]e^{-2\Gamma(T-\Delta t)}e^{-4\Gamma\Delta t}\Theta(T-\Delta t)\Theta(\Delta t)$$

$$+\left[V^4\left(\frac{1-e^{-\gamma T}}{\gamma}\right)^4 e^{+6\Gamma\Delta t}\right]e^{-2\Gamma T}\Theta(T)\Theta(-\Delta t) \qquad \text{Eqn.2-12(a)}$$

The TR SWM lineshape given by the above equation has a complicated time-dependence, but the general features are sketched in Fig.2.3. Fig.2.3(a) depicts the exponential decay with time constant $T_2/2$ when interactions are neglected and $V = 0$. Fig.2.3(b) shows the two contributions to the signal when interactions are included ($V \neq 0$). Although the particular form is more complicated than the TR FWM results presented above, the qualitative features are the same. One is the *prompt* contribution to the emission resulting from the scattering of the electric field via PSF, as for independent two-level systems, and the other is the *delayed* contribution to the emission due to scattering of the induced polarization wave via PWS, which is unique to interacting systems. Thus, a signature for Coulomb correlation in SWM experiments is the *non-exponential decay* of the TR SWM lineshape. Unfortunately, as we explain in Chs.3 and 5, TR SWM lineshapes are very difficult to measure at the low excitation densities where effects that arise from Coulomb correlation dominate the optical response. (As we explain in later chapters, at high excitation densities the Coulomb correlation is screened by the large number of free electron-hole pairs from exciton ionization. Thus, Coulomb correlation effects are dominant at lower excitation densities.) Therefore, we were not able to verify this signature of Coulomb correlation in TR SWM. We turn, therefore, to the TI SWM measurement, where it was possible to measure the optical response at very low excitation densities.

The result for TI SWM in direction $3k_2$-$2k_1$ is

$$S_{TI}(\Delta t) \propto \left[\frac{V^2}{\Gamma(\gamma+2\Gamma)(\gamma+\Gamma)}\right] \times$$

$$\left\{\left[\frac{1}{2}+\frac{3V^2}{(3\gamma+2\Gamma)(2\gamma+\Gamma)}\right]e^{-4\Gamma\Delta t}\Theta(\Delta t)+\left[\frac{3V^2}{(3\gamma+2\Gamma)(2\gamma+\Gamma)}\right]e^{+6\Gamma\Delta t}\Theta(-\Delta t)\right\}$$

Eqn.2-12(b)

The TI SWM lineshape given by the above equation is also sketched in Fig.2.3. Fig.2.3(c) depicts the coherent spike expected when V = 0, since, in this case, coherent SWM emission is only present when the two excitation pulses are co-incident on the sample. For finite excitation pulse widths, therefore, we expect the TI lineshape to reflect the pulse envelope and be symmetric about $\Delta t = 0$. Fig.2.3(d) depicts the TI lineshape when interactions are included ($V \neq 0$). In this case, SWM emission is present for both positive and negative time-delays. Furthermore, the TI SWM lineshape is found to decay exponentially for negative time-delays with time constant $T_2/6$, which is *faster* than the rate for positive time-delays, $T_2/4$. Thus, a signature for Coulomb correlation in SWM experiments is the *asymmetry of the TI SWM lineshape*. Because TI measurements can be made for very low excitation densities, when Coulomb interaction effects are most pronounced, we were able to verify this signature of Coulomb correlation in the TI SWM measurements presented in Ch.5.

Up to this point in the discussion we have presented signatures of Coulomb correlation which appear in the *amplitude* measurements of TI and TR multi-wave mixing signals. If we recall the discussion surrounding Eqn.2-9, where it was indicated that there

is a relative phase difference between the prompt PSF and the delayed PWS contributions to the coherent FWM emission, one would expect to observe a *dynamic evolution to the phase or instantaneous frequency of the emitted pulse.* Examining Eqn.2-9 for small, positive time-delays Δt indicates that for small times t, i.e. when $\gamma t << 1$,

$$P^{(3)}(t,\Delta t \geq 0) \propto \left[\frac{1}{2} + iV\frac{1-e^{-\gamma t}}{\gamma}\right] \approx \left[\frac{1}{2} + iVt\right]$$

Writing $P^{(3)}(t) \equiv r\, e^{i\varphi(t)}$, we find that $\varphi(t) \approx \arctan[2Vt]$, for small t. Thus, there is indeed a nonlinear phase dynamics associated with the FWM emission when effects arising from Coulomb correlation are included. This fact has been demonstrated via numerical solutions to the semiconductor Bloch equations, where the static Coulomb interaction is treated exactly. [2.17] This signature in phase cannot be measured via the amplitude TI and TR measurements described above. Instead, we performed interferometric correlation measurements of the FWM signal, which are described in detail in the next chapter.

2.6 Summary and conclusions

We have presented a model to describe the nonlinear optical response of dense media, such as semiconductors, which includes the effect of Coulomb correlation on the induced nonlinear polarization. Assuming impulsive excitation and a homogeneously broadened system, we used this model to calculate both TI and TR lineshapes for both FWM and

SWM. In addition to the amplitude response predicted from this model, we also considered the instantaneous frequency dynamics of the FWM emission. We obtained a series of signatures for Coulomb correlation observable in FWM and SWM measurements at low excitation densities, which are unique to interacting systems. After describing the technical details of the experiments in the following chapter, we systematically test the validity of these predictions in Chs.4, 5, and 6.

References

[2.1] see, for example, L. Allen and J.H. Eberly: *Optical resonance and two-level atoms*, Dover Publications (1987).

[2.2] Y.R. Shen: *The Principles of Nonlinear Optics*, John Wiley & Sons, Chapter 2 (1984).

[2.3] P.N. Butcher and D. Cotter: *The Elements of Nonlinear Optics*, Cambridge University Press, Chapter 6 (1990).

[2.4] T. Yajima and Y. Taira: *Spatial optical parametric coupling of picosecond light pulses and transverse relaxation effect in resonant media*, Journal of the Physical Society of Japan, Vol.47, No.5, pp.1620-1626 (1979).

[2.5] S. Schmitt-Rink, D.S. Chemla, and D.A.B. Miller: *Linear and nonlinear optical properties of semiconductor quantum wells*, Advances in Physics, Vol.38, No.2, pp.89-188 (1989).

[2.6] N. Peyghambarian, S.W. Koch, A. Mysyrowicz: *Introduction to Semiconductor Optics*, Prentice-Hall, Ch.3 (1993).

[2.7] W. Schafer: *Manybody-effects in nonlinear optics of semiconductor structures*, in *Optics of Semiconductor Nanostructures*, F. Henneberger, S. Schmitt-Rink, E.O. Gobel, eds., Academie Verlag, pp. 21-50 (1993).

[2.8] R. Binder, S.W. Koch, M. Lindberg, W. Schafer, F. Jahnke: *Transient many-body effects in the semiconductor optical Stark effect: A numerical study*, Physical Review B, Vol.43, No.8, pp.6520-6529 (1991).

[2.9] D.S. Kim, J. Shah, T.C. Damen, W. Schafer, F. Jahnke, S. Schmitt-Rink, K. Kohler: *Unusually slow temporal evolution of femtosecond four-wave-mixing signals in intrinsic GaAs quantum wells: Direct evidence for the dominance of interaction effects*, Physical Review Letters, Vol.69, No.18, pp.2725-2728 (1992).

[2.10] W. Schafer, F. Jahnke, S. Schmitt-Rink: *Many-particle effects on transient four-wave-mixing signals in semiconductors*, Physical Review B, Vol.47, No.3, pp.1217-1220 (1993).

[2.11] H. Wang, K. Ferrio, D.G. Steel, Y.Z. Hu, R. Binder, S.W. Koch: *Transient nonlinear optical response from excitation induced dephasing in GaAs*, Physical Review Letters, Vol.71, No.8, pp.1261-1264 (1993).

[2.12] M. Wegener, D.S. Chemla, S. Schmitt-Rink, and W. Schafer: *Line shape of time-resolved four-wave mixing*, Physical Review A, Vol.42, No.9, pp.5675-5683 (1990).

[2.13] S. Schmitt-Rink, S. Mukamel, K. Leo, J. Shah, D.S. Chemla: *Stochastic theory of time-resolved four-wave mixing in interacting media*, Physical Review A, Vol.44, No.3, pp.2124-2129 (1991).

[2.14] K. Leo, M. Wegener, J. Shah, D.S. Chemla, E.O. Gobel, T.C. Damen, S. Schmitt-Rink, and W. Schafer: *Effects of coherent polarization interactions on time-resolved degenerate four-wave mixing*, Physical Review Letters, Vol.65, No.11, pp.1340-1343 (1990).

[2.15] P. Schillak and I. Balslev: *Theory of propagation effects in time-resolved four-wave mixing*, Physical Review B, Vol.48, No.13, pp.9426-9433 (1993).

[2.16] M.N. Belov, E.A. Manykin, M.A. Selifanov: *Self-consistent theory of time-resolved four-wave mixing*, Optics Communications, Vol.99, pp.101-104 (1993).

[2.17] D.S. Chemla, J.-Y. Bigot, M.-A. Mycek, S. Weiss, W. Schafer: *Ultrafast phase dynamics of coherent emission from excitons in GaAs quantum wells*, Physical Review B, Vol.50, No.12, pp.8439-8453 (1994).

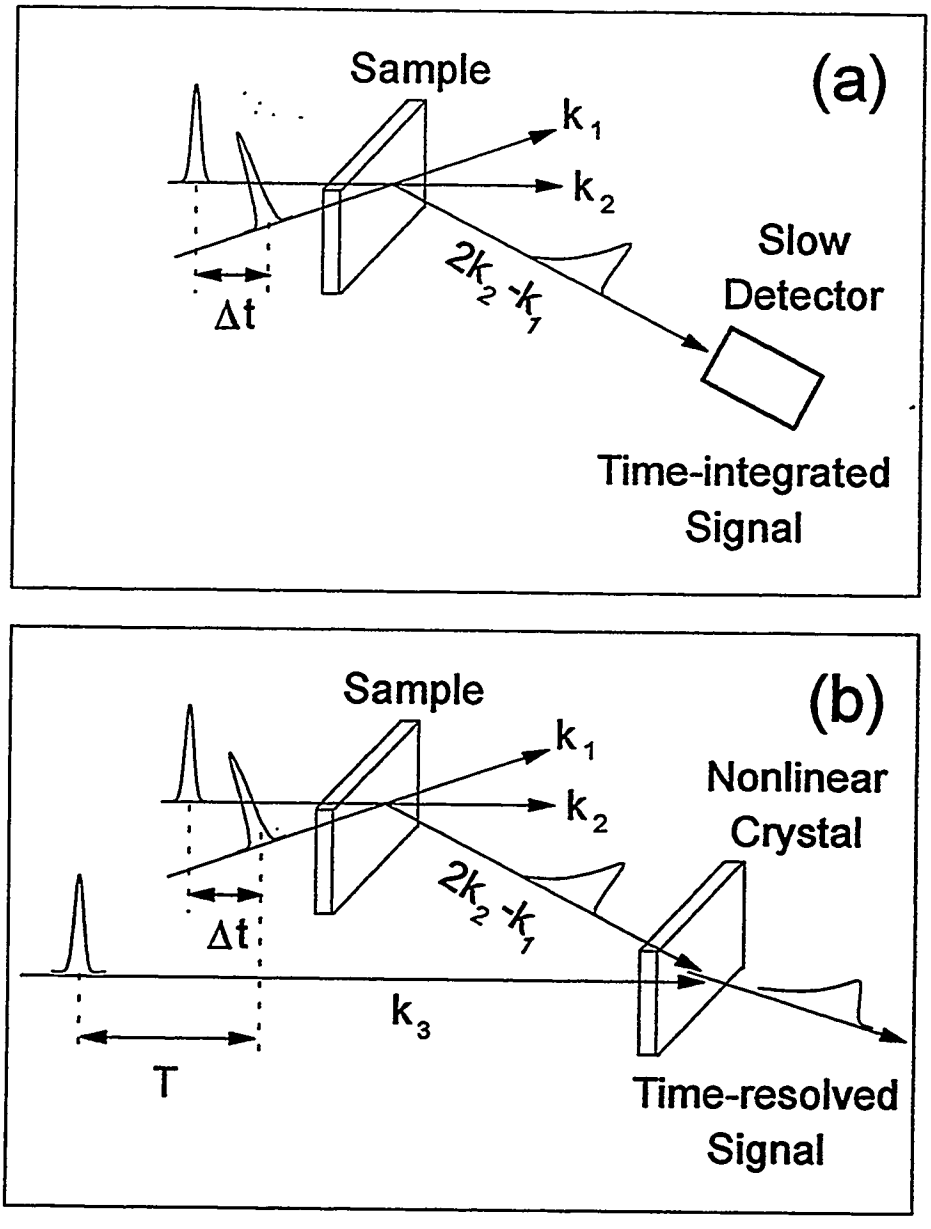

Figure 2.1: Schematic view of (a) time-integrated (TI) and (b) time-resolved (TR) measurements for the four-wave mixing (FWM) signal in direction $2k_2$-k_1. The higher order six-wave mixing (SWM) signal in direction $3k_2$-$2k_1$ is measured in the same way.

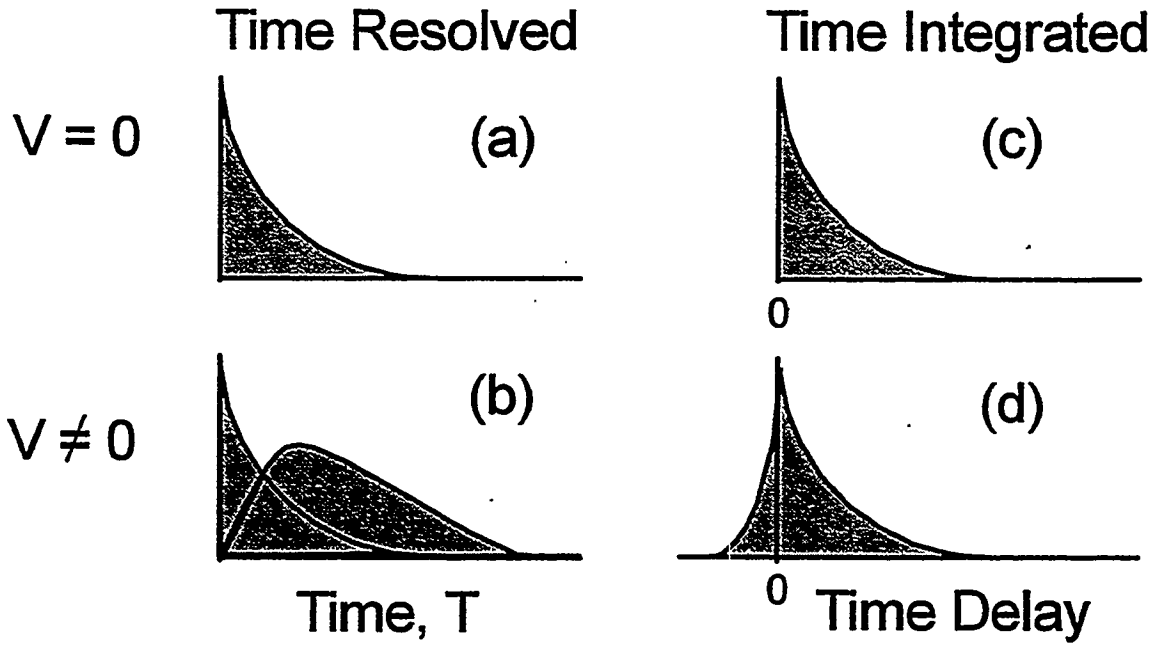

Figure 2.2: Comparison of time resolved and time integrated four-wave mixing signals in the absence (V = 0) and presence (V ≠ 0) of Coulomb interaction.

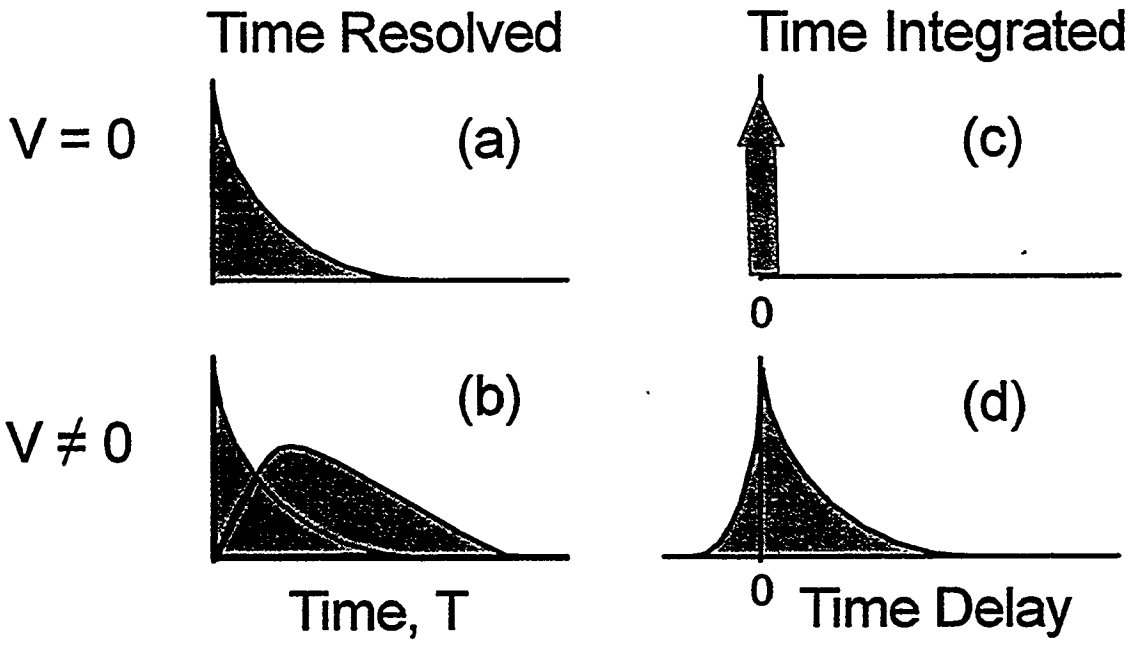

Figure 2.3: Comparison of time resolved and time integrated six-wave mixing signals in the absence ($V = 0$) and presence ($V \neq 0$) of Coulomb interaction.

Chapter 3

Experimental Instrumentation and Techniques

3.1 Introduction

Measuring the transient nonlinear optical response of semiconductors is a difficult task for several reasons. High quality materials, free of defects or impurities, are essential for homogeneously broadened lines, but often difficult to obtain. Even a good quality sample has limitations if experiments on bound state excitons are desired. For bulk GaAs, one must minimize the phonon population, which broadens the exciton resonance until it disappears at high temperatures, by working at low temperatures. Alternatively, to study excitons at room temperature, one must use the quantum confinement effect of quasi two-dimensional (2D) quantum wells (QWs) grown by molecular-beam epitaxy (MBE). [3.1] Because the polarization dephasing times in such systems are on the order of picoseconds, or even femtoseconds, measurements of dynamics require ultrashort pulsed lasers for excitation. These laser systems are quite expensive and often difficult to operate in a reliable manner. In nonlinear experiments on coherent emission from semiconductors, one must also consider signal detection issues. In four-wave mixing (FWM), for example, interesting effects occur at low excitation densities, when the energy per emitted pulse is

very low, on the order of a few femtojoules. Thus, laser sources must be extremely stable and combined with state of the art detection schemes. Historically, these were severe limitations for experimentalists. Nonetheless, as advances were made in ultrashort pulsed lasers and sample fabrication technologies and guided by results from atomic physics, FWM measurements on semiconductors were realised.

In this chapter we describe the apparatus and measurement techniques used in the femtosecond wave mixing experiments presented in this dissertation. We begin by describing, in section 3.2, the preparation of the optically thin GaAs multiple quantum well (MQW) samples we have investigated. Section 3.3 discusses the specifications of the ultrashort pulsed Titanium:sapphire ($Ti:Al_2O_3$) laser used in these studies and gives a brief overview of the history surrounding the development of this particular modelocked laser. We detail the optical set-up constructed for the multi-wave mixing experiments in section 3.4, while section 3.5 discusses the methods and equipment we employed for full characterization of both the excitation laser pulse and the coherent emission from the sample. After describing the data processing procedures, we conclude in section 3.6.

3.2 Multiple quantum well samples

The samples investigated were high quality GaAs MQWs grown on a GaAs substrate by molecular beam epitaxy in the crystal direction [0 0 1]. The structures typically consisted of 50 periods of 100 Å thick GaAs wells with $Al_{0.3}Ga_{0.7}As$ barrier layers. The samples were held at room temperature for all experiments described in this dissertation. Details

of the structures, including their linear absorption spectra, will be shown with the experimental results in subsequent chapters. In order to permit transmission experiments, the GaAs substrate was removed from the sample by selective chemical etching [3.2] and the sample itself was antireflection coated on both sides in order to minimise Fabry-Perot effects. Finally, the coated sample was mounted with glue on a sapphire disk to allow for heat dissipation under laser irradiation. Experiments were performed in transmission with the optical axis of the excitation beam along the growth direction, i.e. perpendicular to the plane of the wells.

We estimate the absorption coefficient, α, by measuring the transmission, through the MQW sample, of a laser beam of measured incident intensity I_0. For a typical sample with 50 periods of $\ell = 100$ Å wells, i.e. total absorbing length $L = 0.5$ μm, the transmitted intensity I_t was measured to be typically around $0.7I_0$. Following the Beer-Lambert law [3.3] [3.4] $I_t = I_0 e^{-\alpha L}$ and neglecting losses due to reflection, we have $\alpha L \approx 0.3 < 1$ as the *maximum* value for the entire MQW structure. Thus, $\alpha \approx 6 \times 10^3 cm^{-1}$, which is the order of magnitude of values published in the literature and determined from much more precise measurements [3.5]. For a single quantum well of thickness $\ell = 100$ Å, we find $\alpha \ell = \alpha L / 50 \approx 10^{-2} \ll 1$. Clearly, for the structures studied in these experiments, the quantum wells are optically thin and propagation effects are negligible, which is consistent with the theoretical models presented in Ch.2.

3.3 Ti:Sapphire oscillator

To perform transient, coherent, nonlinear optical experiments in semiconductors, the excitation source must satisfy several important requirements. First, because the carrier dynamics in these materials are very fast, on the order of picoseconds or even less, femtosecond pulses are necessary to provide adequate temporal resolution. Second, the laser wavelength must be tunable (and in the near-IR, for GaAs) to allow for state-selective excitation over a variety of sample temperatures and quantum well-widths. Third, in order to probe the nonlinear optical response, there must be sufficient energy per pulse to generate and subsequently measure higher order signals. Finally, high repetition rates and extreme, long-term stability are both important considerations for optimum signal-to-noise ratios. As we show below, the passively modelocked Ti:Sapphire oscillator used in these experiments has all of the above characteristics and more. Before listing the specifications of our system, though, we first describe some of the interesting history surrounding this increasingly important laser.

The first demonstration of sub-100-femtosecond pulses directly generated from a Ti:Sapphire laser was reported in early 1991. [3.6] The laser relied upon self-modelocking and intracavity dispersion compensation to achieve unprecedented pulse durations for that medium. The announcement of what was soon dubbed "magic modelocking" by the community spurred intense research into both the theory [3.7] and applications of Ti:Sapphire laser technology. [3.8] [3.9] The basic design of the laser (which was pumped by a CW Argon-ion laser) was quite simple: a linear cavity with two end mirrors, two curved mirrors for focusing into the Ti:Sapphire rod, and two prisms for

dispersion compensation. By carefully controlling the third order dispersion within the laser cavity, pulses as short as 17 fs were reported less than two years after the seminal paper [3.10] and, within a few months, that record was again broken with the announcement of 11 fs Ti:Sapphire pulses. [3.11] In addition to producing extremely short pulses, extremely high powers were also quickly achieved when Ti:Sapphire regenerative amplifiers were coupled with the Ti:Sapphire oscillators: millijoules per pulse were produced at 20 Hz repetition rates [3.12] and microjoules per pulse at 250 kHz. [3.13] Since those early days of Ti:Sapphire research, major advances continue to occur, making the earlier systems seem primitive by comparison. A few of the developments toward more compact, higher repetition rate, femtosecond sources include an all solid-state passively modelocked Ti:Sapphire oscillator using a MQW as a saturable absorber [3.14] and the introduction of specially designed dielectric mirrors for prism-less dispersion compensation. [3.15] [3.16]

The laser used for the experiments presented in this dissertation was the first commercial femtosecond Ti:Sapphire system sold. It was the NJA-1 purchased from Clark Instruments and operational in our laboratory by the summer of 1991. Although we may not present the details of the cavity design for proprietary reasons, we may say that the laser cavity is similar to the "standard" and original design described above, using prisms for dispersion compensation and a slit for tuning. In addition to the main cavity, a sub-cavity with a dye-jet acting as a saturable absorber was added to passively modelock the system. Although it is difficult to prove, we do believe that the saturably absorbing dye-jet contributed greatly to the overall stability and reliability of this laser. As we will

show in subsequent chapters, this exceptional performance allowed us to make interferometric measurements of ultrafast dynamics with attosecond resolution. The only disadvantages of working with the dye-jet are the consistent maintenance required for the dye concentrations and difficulties with moisture retention during humid weather. The oscillator itself was pumped with typically 5W of all-lines radiation from a CW Argon-ion laser and both the long- and short-term beam pointing stability of the pump laser were found to be crucial for optimum performance. The Coherent Innova 300 and 400 Argon-ion lasers were both employed and found to be satisfactory, after the mechanical stability of the 400 was improved by the manufacturer. The Ti:Sapphire rod was cooled using house-LCW (low conductivity water), though after these experiments were completed a water chiller (Neslab RTE-series) was used for cooling and found to further improve stability. The laser and all optical set-ups were constructed on breadboards (Newport; Thorlabs) atop a "floating" isolation table (TMC) to minimize the transfer of mechanical vibrations to the optical components.

Typical specifications for the laser as used for the experiments are as follows. The system operated at approximately 85 MHz repetition rate (≈12 ns between pulses), as measured by detecting leakage from the rear cavity mirror with a fast photodiode connected to a 400 MHz oscilloscope (Tektronix, 2465B). The pulse train was constantly monitored on the oscilloscope for stability, which was found to be excellent (≈0.1%). Typical powers after the output coupler were in the range 150-300mW (1.8-3.5 nJ/pulse), as measured with a digital power meter (Newport 815-series). Pulses from the oscillator were measured to be nearly transform-limited Gaussian pulses with a typical spectral

bandwidth of 10-12 nm and with temporal durations between 80-120 fs. (We discuss laser pulse characterization in greater detail in section 3.5.) The mode quality was assessed visually by reflecting and expanding the beam with a curved mirror onto a screen and found to be TEM_{00}. The tuning range of the laser is dependent upon both the coatings on the cavity optics and the particular dye used in the saturable absorber. With the original set of optics, the tuning range extended from approximately 780 to 830nm using HITC-Iodide, to about 860nm by additionally using IR-140 dye, and to 900nm by additionally using IR-143. (All dyes were purchased from Exciton, Inc.)

It should be noted that it is possible to obtain higher output powers, coupled with longer (*picosecond*) pulses, from the Ti:Sapphire oscillator by simply using higher pump powers. High power, *femtosecond* pulses were produced by using a "bow-tie" style dye (LDS-821, Exciton) amplifier (BTA-1, Clark Instruments), pumped by a copper-vapor laser (Oxford Laser) and constructed for the purpose of white-light continuum generation for pump-probe experiments. [3.17] [3.18] As explained in the next section, it was not necessary to use such intense pulses for the transient wave mixing experiments presented in this dissertation.

3.4 Multi-wave mixing

In this section we describe the experimental apparatus constructed to *generate* ultrafast coherent emission from GaAs quantum wells. (The various methods used to *detect* the nonlinear signals are detailed in section 3.5.) Beginning with a basic overview of the

optical set-up, we then define the timing conventions used throughout this dissertation. Next, the excitation density, an important parameter varied in the experiments, is estimated for a typical incident intensity. Finally, we discuss the procedure developed to obtain the spatial and temporal overlap of pulses necessary to produce the multi-wave mixing signals.

3.4.1 Optical set-up and timing conventions

The optical set-up used in the multi-wave mixing experiments is shown schematically in Fig.3.1. As we performed the series of measurements reported in the following chapters, data was acquired and confirmed, equipment was modified and replaced, and several versions of this set-up were constructed. Although the cosmetic details may vary, the basic principals and important components are common to all versions, as summarized here.

We performed transient two-pulse four- and six-wave mixing experiments in the self-diffraction geometry, as shown in the figure. The linearly polarized infrared (IR) laser beam from the Ti:Sapphire oscillator was split into two beams using a 1 mm thick beam splitter (CVI) held in an extremely stable mount (Klinger, Micro-controle) and coated to reflect 60% of the beam at wavelength 800 nm, transmitting the rest. This created two paths, or pulses, for the self-diffraction wave-mixing geometry, where the transmitted beam, known as the *probe* pulse, k_1, was half as intense as the reflected beam, known as the *pump* pulse k_2. After the beam splitter, both the probe and the pump beams were retro-reflected to allow for time-delays of pulses and directed toward the sample. The

two beams were made parallel over a distance of several meters and separated by a distance of approximately 0.5 cm. The beams were aligned symmetrically about the optical axis of a 1-inch diameter bi-convex focusing lens anti-reflection coated for the IR (Newport, AR.16) with focal length of typically 5.0 cm or 6.29 cm, labeled as "Lens 1" in the figure. This lens focused the parallel beams onto the sample, which was mounted on a 3-D ("XYZ") translation stage in order to quickly locate the optimum focus of the lens and to vary the spot on the sample. The transmitted beams (pump, probe, and the emitted four- and six-wave mixing signals in directions $2k_2$-k_1 (FWM) and $3k_2$-$2k_1$ (SWM)) were then either blocked (k_2 and usually k_1) or re-collimated (FWM, SWM, and k_1, occasionally used as a reference laser pulse) with another lens labeled "Lens 2" in the figure. The typical focal length of Lens 2 was 3.8 cm or 10.0 cm. The re-collimated beams were spatially filtered using irises (Thorlabs, Inc.) to eliminate stray light and then aligned into detectors, spectrometers, or Michelson interferometers, to be described later.

To perform transient multi-wave mixing measurements, the two excitation pulses k_1 and k_2 must be time delayed with respect to one another. In our experiments, time $t = 0$ is *defined* as when the probe pulse k_1 is incident on the sample. The timing of the probe pulse is never altered and therefore it is the reference for all other pulses used for experiments (k_2) and detection (a third pulse, split off from the laser beam before the pump and probe, to be known as pulse k_3). In the experiments, we measure coherent FWM radiation emitted in direction $2k_2$-k_1. For independent two-level systems emitting in this direction, positive time-delay $\Delta t > 0$ is defined when pulse k_2 *follows* pulse k_1. [3.19] Thus, for $\Delta t > 0$: k_1 arrives first, at $t = 0$, and k_2 arrives later, at time $t = \Delta t$. On the other

hand, for $\Delta t < 0$: k_2 arrives first, at $t = \Delta t = -|\Delta t|$, and k_1 arrives later, at $t = 0$. These are the timing conventions which are used throughout this dissertation: for both the analytical derivations of Ch.2. and the experimental set-up and data of this and the following chapters.

In order to create the time-delay, the pump pulse k_2 is directed into an optical path delay line which controls its timing with respect to pulse k_1. As shown in Fig.3.1, a delay line consists of a retro-reflector (in our case, a homemade version consisting of a pair of mirrors oriented at 90° to one another) mounted on a programmable stepper motor (Klinger MC4, MD4). In our experiments the motors had step sizes of $D = 0.1$ μm and ranges of a few cm. Because of the retro-reflection, each single step creates an optical path length twice as long as the step size itself. Thus the smallest time delay that can be created between pulses is $\Delta t_{min} = 2D / c \approx 0.66$ fs, which is sufficiently small for precision timing of the 100 fs pulses used to excite the sample in the wave mixing experiments. As we will discuss below, this minimum time delay of 0.66 fs is also sufficiently small for accurate temporal resolution in the time-resolved (TR) amplitude measurements (where pulse profiles are a few hundred fs long), but it is *not* sufficiently small for the accuracy required in interferometric measurements, where the resolution must be much smaller than the *optical cycle* itself, which is 2.8 fs at wavelength $\lambda \approx 850$nm. We will explain in the section on detection how we overcome this limitation, using these same stepper motors.

3.4.2 Estimating excitation density

It is interesting and important to note the power of the pump and probe beams for a typical experiment. The mirrors used to direct the IR beams were 1 inch diameter protected silver mirrors (Newport ER.2) which were found to be ≈98% reflective at 45° angle of incidence and around wavelength $\lambda \approx 850$ nm. Considering the large number of mirrors used to direct the beam from the oscillator and through the wave mixing optical set-up, there are considerable power losses by the time the beams reach the sample. In a typical experiment with 200 mW at the output coupler of the laser, there is approximately 140 mW available before the beamsplitter in Fig.3.1. Approximately two-thirds of this is syphoned-off for use in a third beam (k_3, to be used for detection via up-conversion, and explained fully below), leaving total power $P \approx 47$ mW to be split amongst the pump and probe beams. Thus beginning with 200 mW at the oscillator, we are typically left with only 31 mW for the pump beam and 16 mW for the probe. At a repetition rate $R \approx 85 \times 10^6\ s^{-1}$, this corresponds to an energy per pulse $= P / R \approx 0.5$ nJ at the sample. Fortunately, as will be demonstrated when we discuss estimating the induced exciton density at the sample, this is still ample power to saturate the sample. Thus we have available to us a wide variation in excitation density, even after using most of the available power from the oscillator for detection via upconversion techniques.

In order to estimate the excitation density produced in the sample by the pump and probe beams, it is also necessary to measure the spot size, ω_0, produced by the focusing lens (Lens 1 in Fig.3.1). The spot size was measured by the standard "knife-edge"

technique [3.20] [3.21], which measures the power as the beam is partially blocked or cut by a single edge. Assuming a Gaussian beam-profile, a typical spot size was determined to be in the range $\omega_0 \approx$ 12-30 μm, depending upon the exact focusing lens used. For the purposes of estimating the excitation density, this spot size is equivalent to a spot of area $S = \pi\omega_0^2 / 2$. Thus the typical incident energy per cm^2 at the sample U_0 = (energy per pulse) / $S \approx$ (0.5 nJ) / (8×10^{-6} cm^2) $\approx 6\times10^{-5}$ J/cm^2. We may now calculate the excitation density, N_x, which is the number of excitons per square cm induced in the sample by the excitation pulses: $N_x = QU_A / h\nu$, where Q is the quantum efficiency, introduced to account for losses ($Q \approx 0.8$), U_A is the total energy absorbed per square cm, and hν is the energy per photon. The photon energy for excitation around wavelength 850 nm is $h\nu \approx 2.3\times10^{-19}$ J. Neglecting losses due to reflection, the Beer-Lambert law introduced in section 3.1 gives $U_A \approx (\alpha \ell)U_0 \approx 10^{-2}U_0 \approx 6\times10^{-7}$ J/cm^2, for $\alpha \ell \ll 1$. Thus, we have the typical excitation density $N_x \approx 2\times10^{12}$ cm^{-2} produced at the sample by the pump and probe pulses, beginning with an output power from the oscillator of only 200 mW. This excitation density is well above the saturation density for the sample $N_{sat} \approx 3\times10^{11}$ cm^{-2} [3.1] [3.5] and so we have available to us a wide range of excitation densities to study. The density of excitons was lowered by attenuating the intensity of the pump and probe beams in front of the sample, using neutral density filters (Melles Griot), until reaching the detection limit.

3.4.3 Spatial and temporal overlap

It goes without saying that to produce the multi-wave mixing signal, the pump and probe pulses must coincide both spatially and temporally on the sample. Overlapping two micron-sized pulses of femtosecond duration requires a precise and systematic approach and can be difficult to achieve in practice. Nonetheless, the procedure developed for these experiments is a reliable one which can be used to both align the set-up initially and to bring the signal back after unanticipated optical misalignment. It should be noted that this procedure is used for both multi-wave mixing and sum-frequency generation (SFG), described below and used to characterize the laser pulses and to time-resolve the multi-wave mixing signal.

The temporal overlap of the pulses is adjusted ultimately using the motorized stepper motor. Therefore, upon initial construction and alignment it is not necessary to ensure that the optical paths for the two beams, pump and probe, are identical in length. They must, however, be close enough to ensure that zero delay-time $\Delta t = 0$ is within the range of the stepper motor. Once this is achieved, the spatial overlap is made. This is accomplished by mounting the sample on the XYZ-translation stage, near the focus of Lens 1, and placing a screen behind it. The highest powers available (without damaging the sample) are used and the transmitted pump and probe beams (which are expanded, since the collimating Lens 2 is not yet in place) are viewed on the screen with an IR-viewer (Find-R-Scope, FJW Optical Systems). When one of the beams hits a particle of dust or another type of irregularity on the surface of the sample, it makes an interference or speckle pattern *distinctive* to that feature. The sample is then moved along the optical

axis of the lens until both beams display that same pattern. When this happens, the two beams are focused to the same spot and are therefore spatially overlapped. We note that the addition of a simple imaging system (consisting of a light bulb, lenses for magnification, a Cohu solid state CCD camera, and monitor screen) can greatly aid this process, especially when the sample is not easily accessible, as in a cryostat. Once the spatial overlap is assured, temporal overlap of the pulses is easily accomplished by moving the stepper motor until the desired signal is observed. For SFG, a blue spot visible by eye appears between the pump and probe beams. For multi-wave mixing, the diffracted beams appear on both sides of the pair of pump and probe beams and are observed using the IR-viewer. For fainter signals, lock-in detection is used, as described in the next section.

3.5 Signal detection

This section discusses the methods employed to detect the multi-wave mixing signals generated by the optical set-up illustrated in Fig.3.1 Ideally, we would like to be able to fully characterize the ultrafast coherent emission from the GaAs MQW, both in amplitude and in phase. Before that is possible, however, we must begin with a complete characterization of the optical pulse from the laser used to excite the material. We describe first the two techniques we have used for ultrashort laser pulse characterization. Then, we define the five complimentary experimental techniques we have employed to characterize the multi-wave mixing signals in amplitude and phase and discuss the

accuracy of our measurements. Finally, we discuss data collection and processing, before concluding this chapter.

3.5.1 Laser pulse characterization

Ultrashort laser pulse characterization is an active and important field of research unto itself. Because femtosecond optical pulses are currently beyond the temporal resolution of electronic detectors (even the fastest photodiodes and streak-cameras provide only picosecond resolution, at best) we must rely on other methods, especially nonlinear optical autocorrelation methods which mix femtosecond pulses with time-delayed replicas of themselves. Although perfect characterization of an ultrashort pulse requires infinite orders of optical correlations, in practice correlations are typically measured out to second-order only. This is due to the finite pulse powers available from the laser.

Traditionally, the simplest and most common way to characterize ultrashort laser pulses was to measure the time-bandwidth product (TBP) $\Delta\nu_p\Delta\tau_p$, where $\Delta\nu_p$ is the full-width at half-maximum (FWHM) of the spectral width of the pulse and $\Delta\tau_p$ is the FWHM of the temporal duration of the laser pulse intensity. [3.22] For a laser pulse with optical field $E_{laser}(t) = A_{laser}(t)\, e^{i\varphi(t)}$ given by amplitude $A_{laser}(t)$ and phase $\varphi(t)$, the TBP $\Delta\nu_p\Delta\tau_p$ will have a specific theoretical value for transform-limited pulses. [3.23] [3.24] This value depends upon the shape of the amplitude envelope (e.g. Gaussian 0.44, hyperbolic secant 0.31) and assumes the pulse is "chirp-free," i.e. $\varphi(t)$ has no nonlinear terms and therefore simply represents the carrier frequency ω_{laser} of the laser pulse: $\varphi(t) = \omega_{laser}t$. In

this way, a measured TBP which is close to some theoretical value is an indication that the pulse is relatively chirp-free and gives an idea of the actual shape of the envelope.

We have measured the TBP for the excitation pulses used in our experiments by spectrally and temporally resolving the laser pulse. The FWHM of the power spectrum, $\Delta\nu_p$, was measured by aligning the laser beam into a 25 cm spectrometer (SPEX) with an optical multichannel analyser (OMA) (EG&G Electronics; 1024 photodiodes) mounted at the output port. The position of the grating (600 grooves/mm; blazed for 750 nm) was controlled manually using a CD2A Compudrive (SPEX). The system was calibrated by using lines from an Argon lamp (Oriel) and had an overall resolution of approximately 0.25 meV.

The laser pulse duration, $\Delta\tau_p$, was measured by the standard method of non-collinear intensity autocorrelation. [3.25] In this measurement, two time-delayed replicas of the infrared laser pulse are mixed via second harmonic generation (SHG) [3.26] in a thin, highly transparent nonlinear crystal like potassium dihydrogen phosphate (KDP). If the laser pulses are separated in time by time-delay Δt, then the non-collinear intensity autocorrelation trace $S_{NC\text{-}IAC}$ is given by

$$S_{NC-IAC}(\Delta t)=\int_{-\infty}^{+\infty} I_{laser}(t)\cdot I_{laser}(t-\Delta t)dt \qquad \text{Eqn.3-1}$$

where $I_{laser} = |E_{laser}|^2$. For Gaussian pulses, it is easily demonstrated that the actual duration of the laser pulse intensity $\Delta\tau_p$ is the FWHM of $S_{NC\text{-}IAC}(\Delta t)$ divided by 1.414.

[3.23] [3.24] In order to measure $S_{NC\text{-}IAC}(\Delta t)$, the optical set-up of Fig.3.1 was employed, with the sample replaced by a 300μm thick KDP crystal (Cleveland Crystals, cut for 800nm). In this geometry, the SHG pulse at the visible blue frequency $2\omega_{laser}$ is emitted in the momentum conserving direction ($k_1 + k_2$), along the optical axis of the lens, and is spectrally filtered with a blue bandpass filter (BG40 color glass, Newport) to reject any stray IR light scattered from the laser pulses. The SHG signal is spatially filtered with irises, then directed to a photomultiplier tube (PMT) optimal for detection of blue light (Hamamatsu 931A, mounted in a Products for Research housing and typically powered at around 400 Volts). The signal measured at the PMT was sent to a lock-in amplifier from Stanford Research Systems (SR510). To provide a reference for the lock-in amplifier, both beams k_1 and k_2 were chopped (typically at a few hundred Hz) before Lens 1 by a mechanical light beam chopper from Ithaco (HMS Series 221). The double chopping technique was employed so that the signal isolated by the lock-in *must* necessarily arise from both beams. This is consistent with the SHG measurement and this same technique was also used in the multi-wave mixing detection described below. In this way, we are assured that the signal measured by the lock-in amplifier is the correct one and not a stray or background signal. Typical values for the TBP that we measured are in the range $\Delta\nu_p\Delta\tau_p \approx 0.45 - 0.50$. Thus the pulses from the oscillator are nearly transform limited Gaussian pulses.

We should note two important points. First, our apparatus is designed so that the laser pulse characterization is performed *at the position of the sample*. Thus, the pulses we measure are identical to the pulses used to excite the MQW structure. This will prove

to be very important to our analysis of the data in the following chapters. Second, the maximum of the intensity autocorrelation $S_{NC\text{-}IAC}(\Delta t)$ locates for us the zero time-delay $\Delta t = 0$ of the experiment. Once this is known, all data taken using the same optical set-up, after the sample is exchanged for the KDP crystal, will have the same zero-delay $\Delta t = 0$. Knowing when the pulses are coincident to within a few fs will also prove to be crucial to the interpretation of the data.

Although the traditional TBP approach provides a simple way to detect chirp in the laser pulse, it is not an extremely sensitive measurement, because the intensity autocorrelation $S_{NC\text{-}IAC}(\Delta t)$ varies only as the square of the electric field. A further limitation is that it does not uniquely determine the pulse. Importantly, there is a way to improve upon the sensitivity of the second-order autocorrelation. Instead of using the non-collinear geometry described above, the beams are mixed co-linearly, such that there is an interference of the electric fields of the two pulses before the doubling takes place. This produces an *interferometric* autocorrelation which depends upon the fourth power of the field. For this reason, this measurement is known as a second-order interferometric autocorrelation $S_{2\text{-}IAC}$ and is given by

$$S_{2-IAC}(\tau)=\int_{-\infty}^{+\infty}\left|E_{laser}(t)+E_{laser}(t-\tau)\right|^2\Big|^2 dt \qquad \text{Eqn.3-2}$$

where τ is the time delay between pulses. It has been shown that using the high sensitivity interferometric $S_{2\text{-}IAC}(\tau)$ measurement, coupled with simultaneous measurements of the

power spectrum and the intensity autocorrelation $S_{NC\text{-}IAC}(\Delta t)$, it is possible to accurately extract amplitude and *phase* characteristics from fs laser pulses. [3.23] [3.24]

The optical set-up for the $S_{2\text{-}IAC}(\tau)$ measurement is the Michelson interferometer shown in Figure 3.2. Using a beamsplitter (Oriel) coated to transmit 40% of the IR beam, the input beam from the laser is split into two beams which travel down the arms of the interferometer and are reflected at 0° angle of incidence from 1 inch diameter mirrors. One of the pulses is time-delayed with respect to the other by mounting the mirror atop a stepper motor identical to the one used in the multi-wave mixing set-up. (We will discuss how to achieve sub-femtosecond resolution below.) A compensator (identical to the beamsplitter, but uncoated, from Oriel) is placed in one of the arms to ensure that each pulse experiences the same dispersion. The beams are then recombined and sent *co-linearly* along the optical axis of a bi-convex lens (focal length ≈ 6.3cm), which focuses the beams onto a 300μm thick KDP crystal. Blue light is emitted via SHG when the two pulses are coincident, as explained above. The detection of the blue light is identical to the intensity autocorrelation, although in this set-up the beam is mechanically chopped before the beam splitter.

An example of a second-order interferometric autocorrelation $S_{2\text{-}IAC}(\tau)$ measured for pulses from the Ti:Sapphire oscillator is shown as the thin solid line in Fig.3.3. The fringe pattern contained within upper and lower envelopes is the characteristic form for $S_{2\text{-}IAC}(\tau)$. In such a measurement, the presence of chirp is immediately apparent by distinctive features in the wings of the trace. [3.24] We checked this experimentally by placing a 10 cm long glass rod (BK7) in the path of the beam before the Michelson interferometer and

measuring the broadening with $S_{2\text{-IAC}}(\tau)$. In this case, we saw a pronounced thickening and modulation of the wings of the trace, due to the chirp induced on the pulse. The fact that the pulse in Fig.3.3 does not demonstrate such features also indicates that the chirp produced by the optical elements themselves was negligible. To verify that this pulse is chirp-free, we have fit the data to the $S_{2\text{-IAC}}(\tau)$ predicted theoretically for a *chirp-free* Gaussian pulse of approximately 80 fs pulse duration (thick solid line). Clearly, the fit is excellent within the resolution of the experiment. Thus we can say with confidence that the pulses from the Ti:Sapphire oscillator are nearly transform-limited Gaussian pulses with durations typically between 80-120 fs.

A discussion of ultrashort laser pulse characterization would not be complete without mentioning some of the more recent advances in the field. It is important to note that the techniques we have just described have severe limitations in that either they do not adequately and uniquely determine the pulse characteristics (TBP) or they are difficult to implement since the optical apparatus can be quite tedious to align (interferometric autocorrelations). Recently developed techniques combine *complete* characterization of ultrashort laser pulses with relative ease of use. They rely upon *simultaneous* time- and frequency-domain measurements of the ultrashort optical pulse. An example is the chronocyclic representation [3.27] and its application to phase measurements for fs pulses. [3.28] However, the single most important recent advance in the field of ultrashort laser pulse characterization has been the development of frequency-resolved optical gating (FROG) techniques. [3.29] [3.30] The FROG measurement consists of two parts: experiment and algorithm. The experimental apparatus mixes two time-delayed replicas of

the laser pulse in a nonlinear optical medium and spectrally resolves the mixed signal as a function of time-delay. This produces a simultaneous time- and frequency-domain representation of the pulse which is known as the FROG trace. The phase retrieval algorithm fits the FROG trace and in doing so generates the *complete* intensity I(t) and phase $\varphi(t)$ of the incident pulse. [3.31] [3.32] [3.33] The FROG technique, now commercially available, is well regarded for its high sensitivity to chirp, its general applicability (any optical nonlinearity may be used), its ease of construction, and its robust algorithm. In fact, FROG was recently used to completely specify in amplitude and phase 13-fs pulses from a self-mode-locked Ti:Sapphire laser, which represents the shortest characterization performed to date. [3.34]

Although in principle these various methods of optical waveform characterization are applicable to *any* ultrashort optical pulse, including the coherent wave mixing emission in our experiments, in practice this is not the case. The above techniques have been developed for *laser* pulse characterization, and thus require pulses with nJ or at the very least μJ of energy per pulse. The measured coherent emission from the MQW samples used in our experiments is a few *fJ* of energy per pulse, at the lowest excitation densities we could detect. Thus, to date there is no single technique available for ultrafast pulse characterization of very small signals, which we can apply to the experiments in MQWs.

3.5.2 Full characterization of the coherent emission

To completely characterize the ultrafast coherent multi-wave mixing emission from quasi-2D excitons in the GaAs MQW structures investigated in our studies, we must determine

both the amplitude and the phase of the emitted pulse. As we have seen, because of the low energy per pulse of the multi-wave mixing emission, the techniques commonly used for ultrashort laser pulse characterization are not applicable. For this reason, we developed a different approach using five distinct intensity and interferometric techniques in the time- and frequency-domains simultaneously. Although we do not extract the *exact* envelope A(t) and phase $\varphi(t)$, we do obtain information on the temporal profile of the amplitude and the instantaneous frequency dynamics of the ultrafast emission. [3.35]

As we demonstrated in Ch.2, in multi-wave mixing the pump and probe pulses induce several orders of nonlinear polarization in the material, which radiate coherently in the different momentum conserving directions. Recall that for a given direction and time-delay between pump and probe pulses Δt, the nonlinear polarization, $P(t, \Delta t)$, and the multi-wave mixing coherent emission, $E_{signal}(t, \Delta t)$, have the same time dependence. We are interested in characterizing $E_{signal}(t, \Delta t)$ as fully as possible precisely because its time dependence in amplitude and phase is a direct reflection of the evolution of the macroscopic nonlinear polarization $P(t, \Delta t)$. This polarization is, of course, influenced by dephasing processes due to collisions and by many-body effects due to Coulomb interactions. Ultimately, it is these physical processes which we would like to understand better for the semiconductor systems under study.

Neglecting interactions (e.g. setting $V = 0$ in the model for dense media presented in Ch.2 [3.19]), for a homogeneously broadened collection of independent two-level systems, the polarization $P(t, \Delta t) \sim e^{-\Gamma t}$ decays exponentially in time with dephasing time $T_2 \equiv \Gamma^{-1}$, for a fixed time-delay Δt. Historically, it was not possible to directly resolve P(t,

Δt) on a femtosecond time scale, because of the limitations of electronic detection. For this reason, the time-integrated (TI) measurement technique was developed, which uses a slow-detector to integrate the total energy emitted as a function of the time-delay Δt between excitation pulses. The TI trace, $S_{TI}(\Delta t)$, is given by

$$S_{TI}(\Delta t)=\int_{-\infty}^{+\infty}|P(t,\Delta t)|^2\,dt \qquad \text{Eqn.3-3}$$

Importantly, for independent two-level systems $S_{TI}(\Delta t)$ decays exponentially with the polarization dephasing time T_2, thus giving the same information as P(t, Δt). The TI technique for characterizing the amplitude of the coherent emission is presented in Fig.3.4, which shows the multi-wave mixing set-up of Fig.3.1 plus the amplitude detection schemes. The pump and probe beams are mechanically chopped for lock-in detection and the multi-wave mixing signal is collimated, spatially filtered, and aligned into a GaAs slow detector (RCA31034A PMT, mounted in a water cooled Products For Research housing), which measures the integrated intensity of the beam versus time-delay Δt. In this way the TI measurement *indirectly* provides information on the nonlinear polarization P(t, Δt).

The discussion thus far has neglected Coulomb interaction effects, which, as we showed in Ch.2, can lead to deviations from the exponential decay of P(t, Δt). These signatures of Coulomb correlation can be detected by analysing the lineshape of the coherent emission. There is clearly a need to *directly* obtain the profile of P(t, Δt), and by time-resolved (TR) measurements we come as close as we can to determining the

amplitude of the ultrafast emission. We achieved temporal resolution of the multi-wave mixing signal by using sum-frequency generation (SFG) [3.36] [3.37] in a cross-correlation geometry, similar to the SHG measurements discussed for laser pulse characterization via second-order intensity autocorrelation. As shown in Fig.3.4, instead of sending the coherent emission from the sample directly to a slow detector, as in the TI measurement, we optically gate the multi-wave mixing emission via SFG in a 300μm thick nonlinear KDP crystal, using a time-delayed reference pulse "k_3" from the laser. The optics (beam splitter and retro-reflector) and stepper motor producing the time delay T for pulse k_3 are as described in section 3.4 (see Fig.3.1) and the detection of the blue sum-frequency light is identical to the intensity autocorrelation measurement detailed above (Eqn.3-1). Thus, the TR signal $S_{TR}(T, \Delta t)$ for a fixed time-delay Δt is given by

$$S_{TR}(T,\Delta t)=\int_{-\infty}^{+\infty}|P(t,\Delta t)|^2\left|E_{laser}(t-T)\right|^2 dt \qquad \text{Eqn.3-4}$$

where it is easy to see that if the reference pulse from the laser $E_{laser}(t-T)$ were a δ-function pulse $\delta(t-T)$, then $S_{TR}(T, \Delta t)$ would *exactly* reproduce $|P(t, \Delta t)|^2$. Thus, for finite reference pulses, $S_{TR}(T, \Delta t)$ gives the temporal profile of the coherent emission convolved with the reference pulse from the laser, which we know from the previous section to be nearly transform-limited and Gaussian in lineshape.

It is important to mention three points about the TR method. First, the measurement is made for fixed time-delay Δt between the pump and probe pulses, and so

the sample is under a fixed excitation condition. This is very different from the TI technique, which in fact measures a variation with changing time-delay. Second, by definition the TI measurement integrates over the real-time response of the nonlinear polarization, thus losing information preserved in the TR signal. Third, although the time delay T represents the real-time evolution of the coherent emission, there is no way for us to determine the zero of absolute time, t = 0, from this measurement. (Recall that time t = 0 is defined as being when probe pulse k_1 is incident upon the sample.) This is true, because both the reference pulse k_3 and the multi-wave mixing signal follow different optical paths than pulse k_1. Thus, from the experiment, we know only the calibration of the T-axis without knowing absolutely where the origin of time t is. As we show in the following chapter, however, it will be possible to determine t = 0 from numerical fits to the TR data.

The above methods characterize the amplitude of the coherent emission in the time domain. In the frequency domain, we measure the power spectrum of the emitted pulse for a fixed time-delay Δt, $S_{PS}(\omega, \Delta t)$, by aligning the multi-wave mixing beam into the spectrometer and OMA system described in the section on laser pulse characterization above. The power spectrum is given by

$$S_{PS}(\omega,\Delta t)=I(\omega,\Delta t)=\left|E_{signal}(\omega,\Delta t)\right|^2=\left|P(\omega,\Delta t)\right|^2 \qquad \text{Eqn.3-5}$$

For independent, homogeneously broadened two-level systems, the power spectrum of the coherent emission is a Lorentzian centered at the resonant exciton frequency and any

asymmetry in the shape is an indication that chirp is present in the emitted pulse. As we saw in Ch.2, chirp is another signature of Coulomb correlation. By using mirrors placed upon kinematic mounts (Thorlabs), we were able to rapidly switch between power spectrum measurements of the multi-wave mixing signal and the laser pulse. In this way we were able to constantly monitor and measure the excitation laser pulse characteristics during the course of the experiments. Importantly, the power spectrum of the laser pulse was measured both *directly* from the laser and *after* propagation through the same optics as the multi-wave mixing signal. This allows us to automatically compensate for the dispersion induced on the pulses by the optical elements in the set-up and to directly compare the two spectra.

This fact, that the multi-wave mixing signal can be directly compared with the laser pulse through the same dispersive optical path, thus accounting for effects like broadening and chirp, is especially important for the phase measurements. These instantaneous frequency measurements were made by directing the coherent emission from the sample into the optical set-up of the Michelson interferometer in Fig.3.2. The first-order interferometric autocorrelation was measured by aligning the co-linear beams directly into the GaAs slow detector used for the TI experiment described above. Recall that the pulse energies of multi-wave mixing signals are too low for second-order autocorrelations, so the lens and nonlinear crystal in the figure are removed for this measurement. The resulting fringe pattern is recorded as the time delay τ is varied. The first-order interferometric autocorrelation $S_{1\text{-}IAC}(\tau, \Delta t)$ of the multi-wave mixing signal is measured for fixed time-delay Δt and is given by

$$S_{1-IAC}(\tau,\Delta t)=\int_{-\infty}^{+\infty}\left|P(t-\tau,\Delta t)+P(t,\Delta t)\right|^2 dt \qquad \text{Eqn.3-6}$$

A typical example of the $S_{1\text{-}IAC}(\tau)$ trace for the laser pulse is shown in Fig.3.5. Because the autocorrelation is symmetric in τ, only half the trace is shown. The fringes appear within upper and lower envelopes characteristic of the first-order interferometric measurement. The noisy feature apparent around $\tau = 95$ fs is likely due to a mis-step of the stepper motor. Sources of error are discussed in greater detail below. At the wavelength $\lambda \approx 850$ nm, the optical cycle is approximately 2.8 fs and so in a typical $S_{1\text{-}IAC}(\tau, \Delta t)$ trace there are on the order of a few hundred fringes. A close-up view of a few of the fringes demonstrates the accuracy of the measurement, as shown in Fig.3.6(a). Each point on the fringe corresponds to a single step of the programmable stepper motor and there are 21 points per fringe, which gives us *sub-femtosecond resolution* of better than 0.14 fs. This is the type of accuracy necessary to detect changes in the instantaneous frequency of the ultrafast coherent emission.

Coupled with the high temporal resolution, we also have superior reproducibility, which we attribute in large part to the stability of the Ti:Sapphire oscillator. This is illustrated in Fig.3.6(b), which presents the differential fringe spacing (DFS) between successive $S_{1\text{-}IAC}(\tau)$ measurements of the laser pulse. As we explain in detail below, the DFS measures the difference between two interferometric measurements by tracking the relative positions of the fringes. In multi-wave mixing experiments, (see Ch.6), the

coherent emission trace is usually measured relative to the trace from the reference laser pulse. Here, for the purpose of demonstrating the reproducibility, Fig.3.6(b) shows the DFS for successive interferometric traces of the laser pulse itself. As we can see from the figure, there is virtually no difference between the two successive measurements to within λ / 10. As described below, this is consistent with the fact that we are limited by the surface roughness of the interferometer mirrors, which are specified to be better than λ / 20.

The DFS is a measure of the instantaneous frequency of the coherent emission from the sample and is determined in two steps. First, interferometric $S_{1\text{-}IAC}(\tau, \Delta t)$ traces are taken for the multi-wave mixing signal and for the reference pulse from the laser. Letting $N(\tau)$ be the number of fringes in a $S_{1\text{-}IAC}(\tau)$ trace from delay $\tau = 0$ to delay τ, $N_{WM}(\tau)$ and $N_{laser}(\tau)$ are determined from their respective traces. (This is equivalent to assigning a number to each successive fringe and recording its position in time.) Next, the differential fringe spacing is computed as the difference between the temporal positions of the corresponding fringes: $DFS(\tau) = N_{laser}(\tau) - N_{WM}(\tau)$, as shown in Fig.3.7. In this way, we measure the evolution of the instantaneous frequency of the multi-wave mixing pulse sent into the Michelson interferometer, relative to the reference pulse. For the case of "linear chirp" sketched in Fig.3.7, where the carrier frequency of the coherent emission (ω_{laser}-a) is shifted from the central frequency of the reference laser pulse (ω_{laser}), it is easy to understand intuitively and to prove mathematically that $DFS(\tau)$ is linear in time, as is $\Delta\varphi(t) = -at$, the phase shift between the two pulses. It is not possible to prove this result for the general case of nonlinear chirp, but we have verified numerically on test pulses that

DFS(τ) does in fact reproduce the phase difference between the reference pulse and the test pulse. This result coupled with the fact that the power spectrum and amplitude measurements are smooth, well-behaved functions without discontinuities gives us confidence that we extract from the DFS(τ) measurement information on the instantaneous frequency dynamics of the coherent emission.

There are several important experimental points to discuss regarding the interferometric measurements. First, the sub-femtosecond resolution (~ 0.14 fs) required for interferometric accuracy was obtained using the same programmable stepper motors as the amplitude measurements. As we discussed in the section on the multi-wave mixing set-up, these stepper motors have 0.1 μm step sizes, implying a minimum time-delay of 0.66fs. To achieve the smaller time delays, the direction of travel of the stepper motor was oriented at an angle to the direction of the incident laser beam. By doing so, we could easily obtain step sizes giving a resolution of about 70 attoseconds (40 steps per fringe). However, such resolution would only slow the data collection process without adding new information, and so we chose to acquire data with lower (140 attosecond) resolution. The disadvantage of running the stepper motor at an angle to the beam path is that as the stepper motor moves, it translates the mirror laterally and the beam travels over the surface of the mirror. Thus one limitation to our experiment is determined by the surface roughness of the mirrors used in the interferometer, as indicated in Fig.3.6.

A second important experimental point involves the calibration of the interferometric set-up. Because the angle of orientation of the stepper motor is difficult to measure precisely on the optical breadboard itself, after construction we did not know *a*

priori the calibration of the step size. To determine the number of steps per femtosecond, we aligned CW beams (from a HeNe laser and also from the Ti:Sapphire oscillator) into the interferometer and measured $S_{1\text{-}IAC}(\tau)$. Simultaneous power spectrum measurements of the CW beams provided the laser wavelength, and once the optical cycle was known, we were able to accurately calibrate the interferometer for future measurements.

Third, it is worth emphasizing that we measure the phase or instantaneous frequency of the multi-wave mixing signal via a *differential* measurement. In determining the function $DFS(\tau)$, we automatically subtract *systematic* sources of error in the experiment, because the reference used is an unchirped pulse from the laser (the probe pulse k_1) passing through the same optical set-up as the multi-wave mixing signal, missing the sample, of course, but including the sapphire substrate. Systematic errors eliminated in this way include chirp induced on the multi-wave mixing signal by propagation through and reflection from optical components, patterns in the travel of the stepper motor, and features on the surface of the interferometer mirror. We cannot, however, subtract away other sources of error in the interferometric measurements, such as effects due to mis-steps of the stepper motor (see Fig.3.5), laser instabilities, and air turbulence. Although the stability of the Ti:Sapphire laser was not a major problem, the air currents in the laboratory were. To isolate the Michelson interferometer from these currents, it was typically covered after alignment by a plastic box with holes allowing beams into and out of the set-up.

Finally, there is an interesting effect due to the finite window in time and frequency within which we perform the experiments. In theory, the first-order interferometric

autocorrelation $S_{1\text{-}IAC}(\tau)$ and the power spectrum $S_{PS}(\omega)$ of a pulse are related by Fourier transform. Thus, in principle, there is no need to build interferometers when one may simply measure the power spectrum of the multi-wave mixing emission and take the Fourier transform. In practice, however, we find that by Fourier transforming one measurement we cannot reproduce the other. This is demonstrated in Fig.3.8, which shows experimentally measured $S_{1\text{-}IAC}(\tau)$ and $S_{PS}(\omega)$ and their fast Fourier transforms (FFT). The $S_{PS}(\omega)$ measurement contains 1024 points in the frequency domain and $S_{1\text{-}IAC}(\tau)$ is measured with 4096 data points. The discrepancy results from the finite experimental window, as opposed to infinite theoretical window, in frequency and time and the finite accuracy of the FFT algorithm. Although the FFT captures some of the important features, such as the beating in time and peaks in frequency, it clearly does not reproduce the direct measurement itself.

Because the first-order interferometric autocorrelation of the multi-wave mixing signal is symmetric in time, we also performed the first-order interferometric *cross*-correlation $S_{1\text{-}ICC}(u, \Delta t)$ measurement to provide the sign of the phase shifts in time. The cross-correlation is performed for fixed time-delay Δt between pulses and is given by

$$S_{1-ICC}(u,\Delta t)=\int_{-\infty}^{+\infty}\left|P(t,\Delta t)+E_{laser}(t-u)\right|^2 dt \qquad \text{Eqn.3-7}$$

where the coherent emission interferes with a reference pulse from the laser delayed by time u. The set-up is the Mach-Zender interferometer shown in Fig.3.9. One arm of the

interferometer contains the multi-wave mixing optical set-up of Fig.3.1, which generates the coherent emission from the sample, while the other arm contains the time delayed reference pulse from the laser. The multi-wave mixing beam and the reference laser beam are made co-linear and aligned into the GaAs slow detector used for the first-order interferometric autocorrelation. The sub-femtosecond time-delay is achieved as described for the interferometric measurement above. Data from such a measurement will be presented in Ch.6, where their interpretation will also be important for establishing the degree of inhomogeneous broadening in the sample.

3.5.3 Data collection and processing

Power spectrum measurements at the OMA were interfaced via GPIB to either a 386 or 486 PC and controlled by software (Princeton Applied Research, Model 1471A Detector Interface). The collected data was translated into ASCII format and then processed in the ASYST programming language. All traces in the time-domain were controlled by a scanning program written in ASYST, which incremented the stepper motors while collecting data from the lock-in amplifier. The time-domain data was directly processed using ASYST.

3.6 Summary and conclusions

We have described the experimental apparatus we constructed to characterize the coherent emission from excitons in GaAs quantum wells. The ultrafast emission is resolved in both the time- and frequency-domain using intensity and interferometric techniques of unprecedented resolution, when compared to traditional experiments on these systems. In the following three chapters we present the first experimental results of transient four- and six-wave mixing measurements investigating the ultrafast dynamic response of both the amplitude and the instantaneous frequency of the emission.

References

[3.1] S. Schmitt-Rink, D.S. Chemla, and D.A.B. Miller: *Linear and nonlinear optical properties of semiconductor quantum wells*, Advances in Physics, Vol.38, No.2, pp.89-188 (1989).

[3.2] J.J. LePore: *An improved technique for selective etching of GaAs and $Ga_{1-x}Al_xAs$*, Journal of Applied Physics, Vol.51, No.12, pp.6441-6442 (1980).

[3.3] P.N. Butcher and D. Cotter: *The Elements of Nonlinear Optics*, Cambridge University Press, pp.212-214 (1990).

[3.4] N. Peyghambarian, S.W. Koch, A. Mysyrowicz: *Introduction to Semiconductor Optics*, Prentice-Hall, Ch.3 (1993).

[3.5] D.A.B. Miller, D.S. Chemla, D.J. Eilenberger, P.W. Smith, A.C. Gossard, W.T. Tsang: *Large room-temperature optical nonlinearity in GaAs/$Ga_{1-x}Al_xAs$ multiple quantum well structures*, Applied Physics Letters, Vol.41, No.8, pp.679-681 (1982).

[3.6] D.E. Spence, P.N. Kean, and W. Sibbett: *60-fs pulse generation from a self-mode-locked Ti:sapphire laser*, Optics Letters, Vol.16, No.1, pp.42-44 (1991).

[3.7] T. Brabec, Ch. Spielmann, P.F. Curley, F. Krausz: *Kerr lens mode locking*, Optics Letters, Vol.17, No.18, pp.1292-1294 (1992).

[3.8] B. Proctor and F. Wise: *Quartz prism sequence for reduction of cubic phase in a mode-locked Ti:Al_2O_3 laser*, Optics Letters, Vol.17, No.18, pp.1295-1297 (1992).

[3.9] J.M. Jacobson, K. Naganuma, H.A. Haus, J.G. Fujimoto, A.G. Jacobson: *Femtosecond pulse generation in a Ti:Al_2O_3 laser by using second- and third-order intracavity dispersion*, Optics Letters, Vol.17, No.22, pp.1608-1610 (1992).

[3.10] C.-P. Huang, M.T. Asaki, S. Backus, M.M. Murnane, H.C. Kapteyn, H. Nathel: *17-fs pulses from a self-mode-locked Ti:sapphire laser*, Optics Letters, Vol.17, No.18, pp.1289-1291 (1992).

[3.11] M.T. Asaki, C.-P. Huang, D. Garvey, J. Zhou, H.C. Kapteyn, M.M. Murnane: *Generation of 11-fs pulses from a self-mode-locked Ti:sapphire laser*, Optics Letters, Vol.18, No.12, pp.977-979 (1993)

[3.12] J. Squier, F. Salin, G. Mourou, D. Harter: *100-fs pulse generation and amplification in Ti:Al_2O_3*, Optics Letters, Vol.16, No.5, pp.324-326 (1991).

[3.13] T.B. Norris: *Femtosecond pulse amplification at 250 kHz with a Ti:sapphire regenerative amplifier and application to continuum generation*, Optics Letters, Vol.17, No.14, pp.1009-1011 (1992).

[3.14] L.R. Brovelli, U. Keller, T.H. Chin: *Design and operation of antiresonant Fabry-Perot saturable semiconductor absorbers for mode-locked solid-state lasers*, Journal of the Optical Society of America B - Optical Physics, Vol.12, No.2, pp.311-322 (1995).

[3.15] R. Szipocs, K. Ferencz, Ch. Spielmann, F. Krausz: *Chirped multilayer coatings for broadband dispersion control in femtosecond lasers*, Optics Letters, Vol.19, No.3, pp.201-203 (1994).

[3.16] A. Stingl, Ch. Spielmann, F. Krausz, R. Szipocs: *Generation of 11-fs pulses from a Ti:sapphire laser without the use of prisms*, Optics Letters, Vol.19, No.3, pp.204-206 (1994).

[3.17] W.H. Knox: *Generation and kilohertz-rate amplification of femtosecond optical pulses around 800nm*, Journal of the Optical Society of America B, Vol.4, No.11, pp.1771-1776 (1987).

[3.18] W.H. Knox: *Femtosecond optical pulse amplification*, IEEE Journal of Quantum Electronics, Vol.24, No.2, pp.388-397 (1988).

[3.19] T. Yajima and Y. Taira: *Spatial optical parametric coupling of picosecond light pulses and transverse relaxation effect in resonant media*, Journal of the Physical Society of Japan, Vol.47, No.5, pp.1620-1626 (1979).

[3.20] A.E. Siegman: *Lasers*, University Science Books, pp.675-679 (1986).

[3.21] J.M. Khosrofian and B.A. Garetz: *Measurement of a Gaussian laser beam diameter through the direct inversion of knife-edge data*, Applied Optics, Vol.22, No.21, pp.3406-3410 (1983).

[3.22] A.E. Siegman: *Lasers*, University Science Books, pp.331-339 (1986).

[3.23] J.-C. Diels: *Femtosecond dye lasers*, in *Dye Laser Principles: With Applications*, Academic Press, pp.103-115 (1990).

[3.24] J.-C. Diels, J.J. Fontaine, I.C. McMichael, F. Simoni: *Control and measurement of ultrashort pulse shapes (in amplitude and phase) with femtosecond accuracy*, Applied Optics, Vol.24, No.9, pp.1270-1282 (1985).

[3.25] N. Peyghambarian, S.W. Koch, A. Mysyrowicz: *Introduction to Semiconductor Optics*, Prentice-Hall, pp.380-383 (1993).

[3.26] Y.R. Shen: *The Principles of Nonlinear Optics*, John Wiley & Sons, Chapters 6 and 7 (1984).

[3.27] J. Paye: *The chronocyclic representation of ultrashort light pulses*, IEEE Journal of Quantum Electronics, Vol.28, No.10, pp.2262-2273 (1992).

[3.28] J.-P. Foing, J.-P. Likforman, M. Joffre, A. Migus: *Femtosecond pulse phase measurement by spectrally resolved up-conversion: application to continuum compression*, IEEE Journal of Quantum Electronics, Vol.28, No.10, pp.2285-2290 (1992).

[3.29] D.J. Kane and R. Trebino: *Single-shot measurement of the intensity and phase of an arbitrary ultrashort pulse by using frequency-resolved optical gating*, Optics Letters, Vol.18, No.10, pp.823-825 (1993).

[3.30] R. Trebino and D.J. Kane: *Using phase retrieval to measure the intensity and phase of ultrashort pulses: frequency-resolved optical gating*, Journal of the Optical Society of America A, Vol.10, No.5, pp.1101-1111 (1993).

[3.31] K.W. DeLong, R. Trebino, D.J. Kane: *Comparison of ultrashort pulse frequency-resolved-optical-gating traces for three common beam geometries*, Journal of the Optical Society of America B, Vol.11, No.9, pp.1595-1608 (1994).

[3.32] K.W. DeLong, R. Trebino, J. Hunter, W.E. White: *Frequency-resolved optical gating with the use of second-harmonic generation*, Journal of the Optical Society of America B, Vol.11, No.11, pp.2206-2215 (1994).

[3.33] J. Paye, M. Ramaswamy, J.G. Fujimoto, E.P. Ippen: *Measurement of the amplitude and phase of ultrashort light pulses from spectrally resolved autocorrelation*, Optics Letters, Vol.18, No.22, pp.1946-1948 (1993).

[3.34] G. Taft, A. Rundquist, M.M. Murnane, H.C. Kapteyn, K.W. DeLong, R. Trebino, I.P. Christov: *Ultrashort optical waveform measurements using frequency-resolved optical gating*, Optics Letters, Vol.20, No.7, pp.743-745 (1995).

[3.35] D.S. Chemla, J.-Y. Bigot, M.-A. Mycek, S. Weiss, W. Schafer: *Ultrafast phase dynamics of coherent emission from excitons in GaAs quantum wells*, Physical Review B, Vol.50, No.12, pp.8439-8453 (1994).

[3.36] J. Shah: *Ultrafast luminescence spectroscopy using sum frequency generation*, IEEE Journal of Quantum Electronics, Vol.24, No.2, pp.276-288 (1988).

[3.37] H. Mahr and M.D. Hirsch: *An optical up-conversion light gate with picosecond resolution*, Optics Communications, Vol.13, No.2, pp.96-99 (1975).

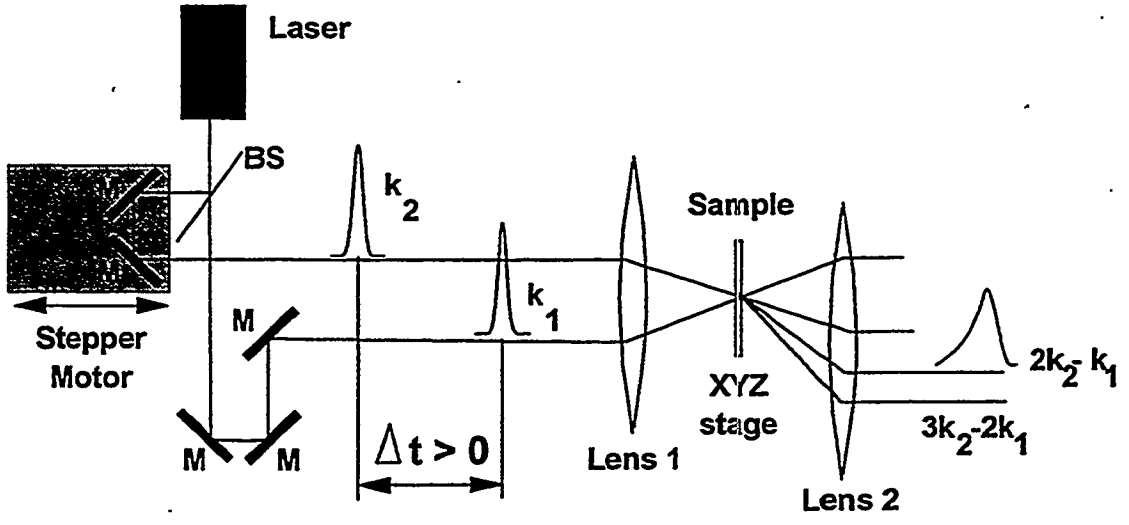

Figure 3.1: Optical set-up for transient multi-wave mixing experiments generating four-wave ($2k_2$-k_1) and six-wave ($3k_2$-$2k_1$) mixing signals in the directions shown. The convention for positive time-delay ($\Delta t > 0$) is also shown. BS = beam splitter. M = mirror.

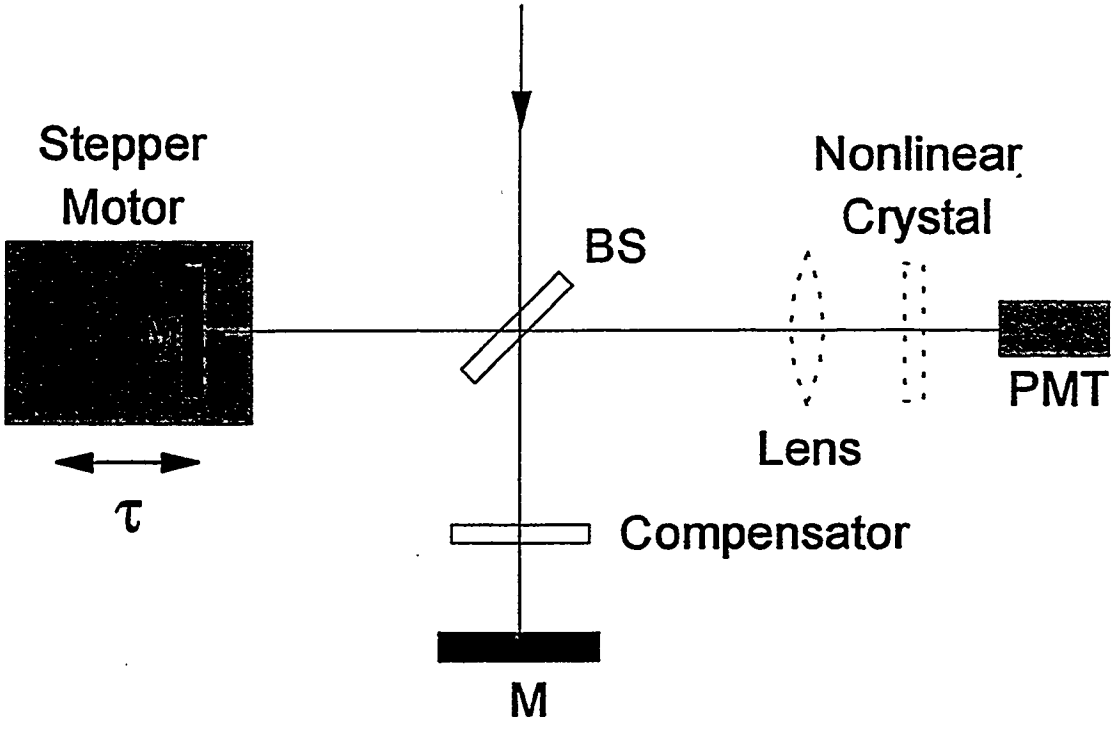

Figure 3.2: Michelson interferometer for interferometric autocorrelations. M = mirror. BS = beam splitter. PMT = photomultiplier tube. The lens and nonlinear crystal (dashed components) are used only for second-order autocorrelations; for first-order autocorrelations they are removed.

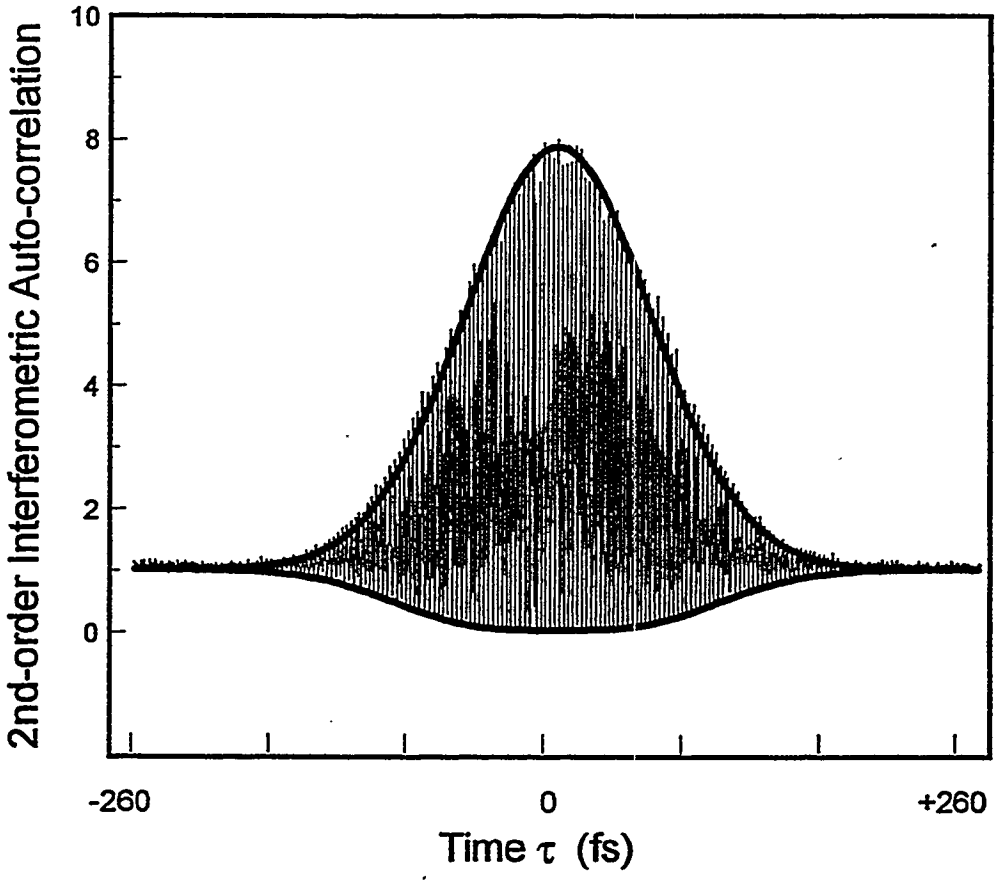

Figure 3.3: Second-order interferometric autocorrelation of a Ti:Sapphire laser pulse with duration approximately 80 fs. The thin line (fringe pattern) is the measured data and the thick line is the envelope of a theoretical prediction for a chirp-free Gaussian pulse.

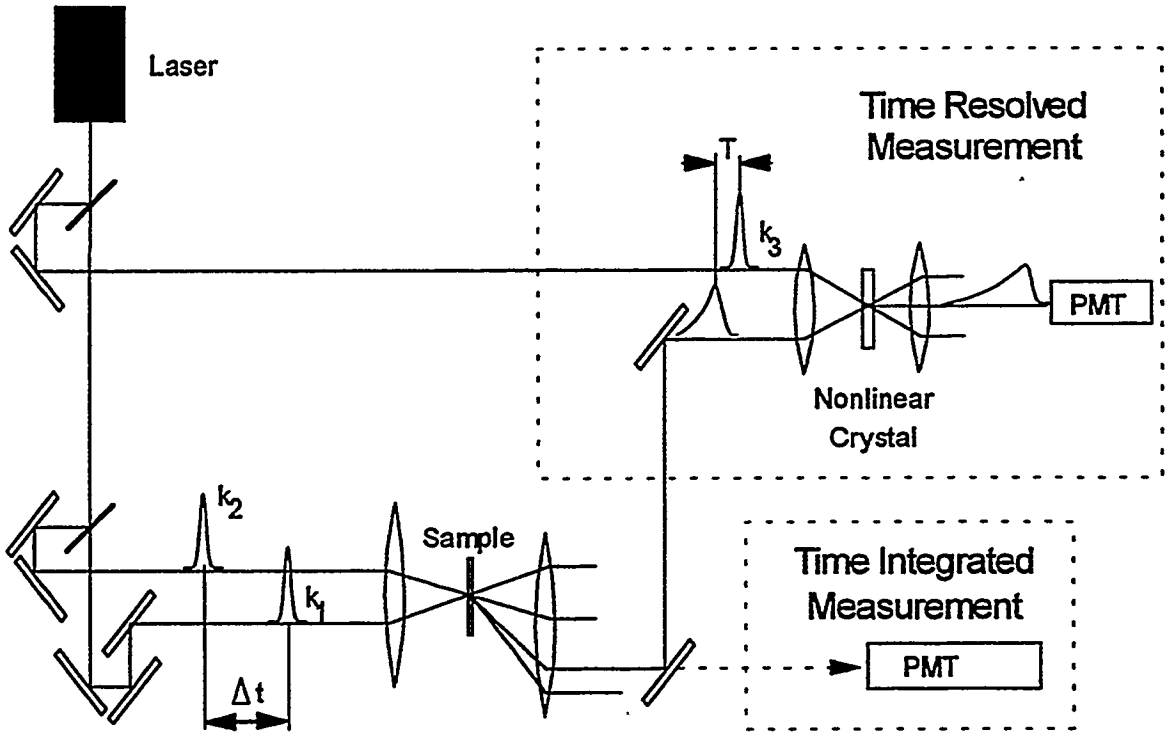

Figure 3.4: Optical set-up for time-integrated (TI) and time-resolved (TR) multi-wave mixing measurements for amplitude characterization of the coherent emission.

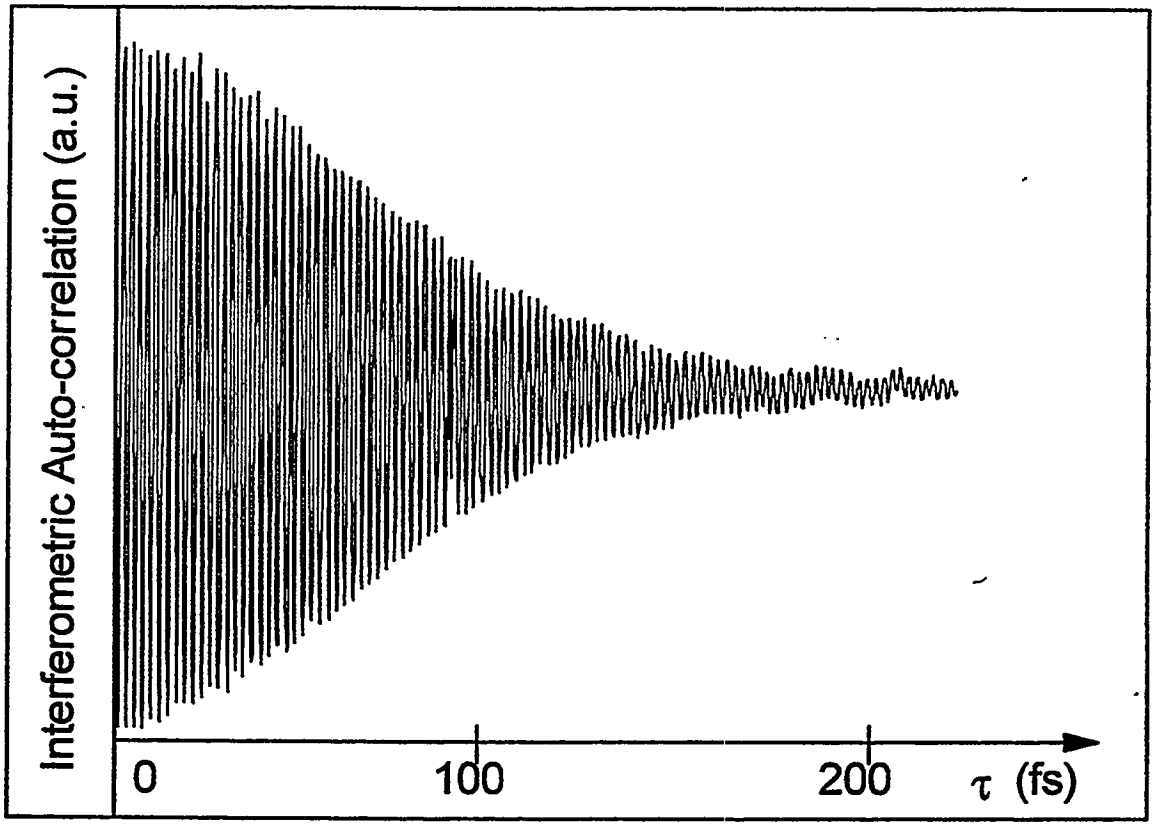

Figure 3.5: Typical first-order interferometric autocorrelation of the ultrashort laser pulse from the Ti:sapphire oscillator. Time delay $\tau = 0$ represents co-incidence of pulses from the two-arms of the Michelson interferometer of Fig.3.2.

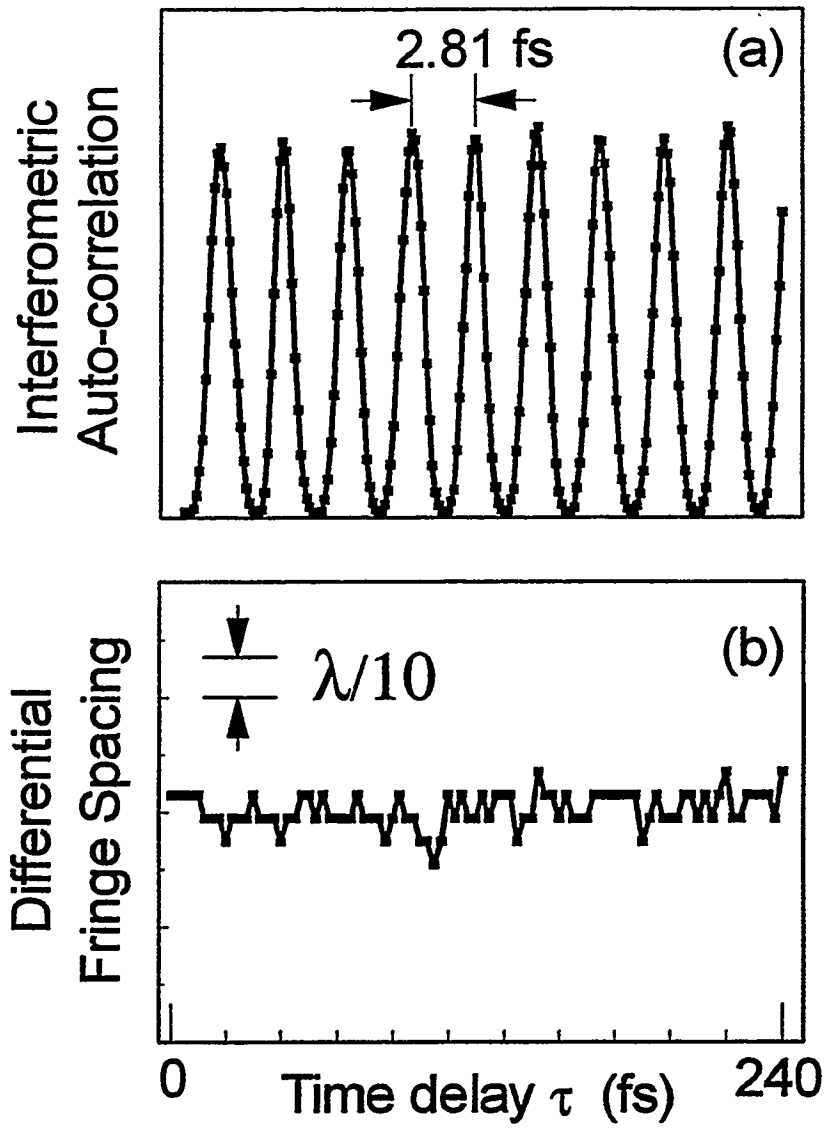

Figure 3.6(a): The resolution of the interferometric measurement is determined by the number of steps per fringe (21) and the duration of the optical cycle (2.81 fs), giving a minimum time-delay smaller than 140 attoseconds.

Figure 3.6(b): The reproducibility of the experiment is measured from the differential fringe spacing of two successive autocorrelation measurements of the laser pulse. The accuracy of the experiment is observed to be approximately $\lambda / 10$.

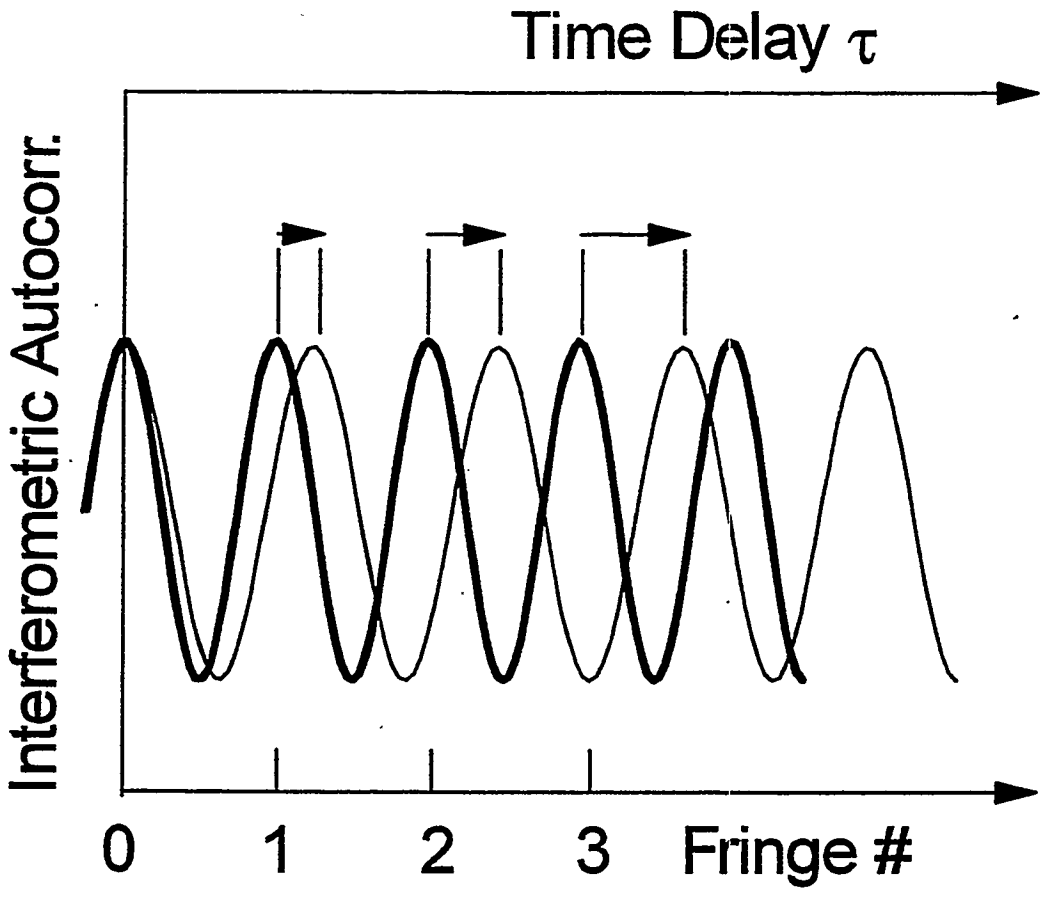

Figure 3.7: The differential fringe spacing DFS(τ) (magnitude shown by arrows) is determined by comparing the position of interferometric autocorrelation fringes of the signal pulse (thin line) with the position of the corresponding fringes of the reference pulse from the laser (thick line). The case of "linear chirp" is sketched here.

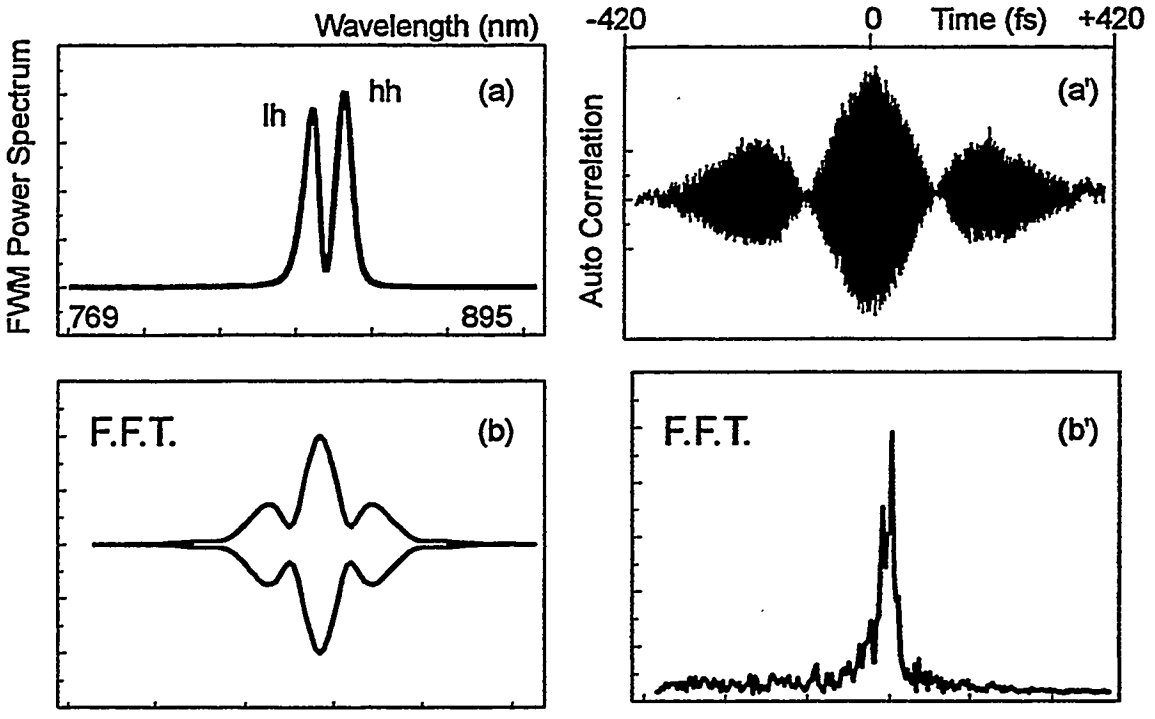

Figure 3.8: Four-wave mixing power spectrum measurement (a) and first-order interferometric autocorrelation (a') taken under identical experimental conditions. For comparison, their fast Fourier transforms are shown in (b) and (b'), respectively.

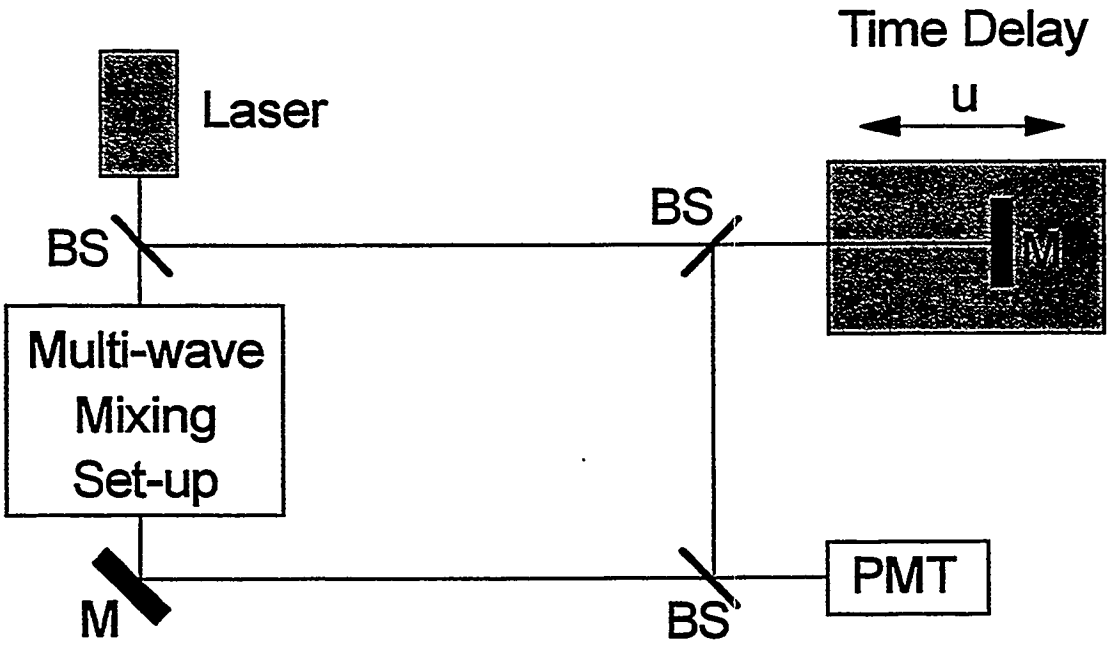

Figure 3.9: Mach-Zender interferometer for first-order interferometric cross-correlations of the multi-wave mixing signal with a reference pulse from the laser. A mirror mounted on a mechanical stepper motor provides time delay u. M = mirror. BS = beam splitter. PMT = photomultiplier tube.

Chapter 4

Four-Wave Mixing: Ultrafast Amplitude Decay

4.1 Introduction

It is known that Coulomb correlation influences both the linear and the nonlinear optical response of excitons in GaAs quantum wells (QWs), as demonstrated, for example, by pump-probe experiments. [4.1] In this chapter, we investigate the effects of Coulomb interaction on time-resolved four-wave mixing (TR FWM) measurements. If Coulomb correlation plays a role, then, in addition to the prompt contribution to the coherent FWM emission due to phase-space filling (PSF), we expect to observe a delayed contribution arising from polarization wave scattering (PWS), as mediated by the Coulomb potential. (See Ch.2.)

Historically, the first transient FWM experiments performed on semiconductors involved time-integrated (TI) measurements. As explained in Chapters 2 and 3, these TI measurements were viewed as being equivalent to time resolving the emission itself, since such is the case for independent two-level systems. [4.2] However, once signatures for Coulomb correlation appeared in TI FWM from semiconductors [4.3] [4.4], there was a clear need for TR FWM, where all the information lost to integration could be recovered

and observed. Time resolution was initially achieved by using streak cameras in experiments on mixed crystals where dephasing times are several hundred picoseconds. [4.5] The first TR FWM measurements on semiconductor QWs by cross-correlation (using upconversion techniques to optically gate the emission, see Ch.3) were made using ps pulses. [4.6] [4.7] Following the development of stable, tunable, fs-pulsed lasers in the near-IR [4.8], more thorough and quantitative studies could be embarked upon, including studies at low temperatures. [4.9]

Here we present results from the first attempt to fully characterize the transient nonlinear optical response of quasi-2D room temperature excitons in GaAs on a femtosecond time scale. [4.10] [4.11] [4.12] [4.13] We begin by measuring the amplitude of the coherent emission from the sample in this and the following chapter and present measurements of the instantaneous frequency in Ch.6.

After a brief description of some experimental details not outlined in previous chapters, the TR FWM data is presented in section 4.2. Upon comparison with the TI FWM lineshapes, it is clear that the simple two-level system description of FWM coherent emission is not valid for this system. This is confirmed in section 4.3 when the TR FWM data is fit to numerical solutions obtained from the nonlinear Schrodinger equation. Proper fits can only be obtained when Coulomb correlation is included. These important and new results are summarized and conclusions are drawn in section 4.4.

4.2 Experimental results

The sample investigated for this study is a multiple quantum well (MQW) structure consisting of 47 periods of 98Å GaAs wells and 96Å $Al_{0.3}Ga_{0.7}As$ barrier layers. It was prepared as described in Ch. 3 and held at room temperature for all experiments. The transmission spectrum of the MQW sample is shown as the solid curve in Fig. 4.1, which also shows a typical power spectrum for the excitation laser pulses (dashed curve) used in these experiments. The Ti:Sapphire laser was tuned to selectively excite the n=1 heavy-hole exciton, as shown in the figure, for all experiments described in this chapter.

Two-pulse time-integrated (TI) and time-resolved (TR) four-wave mixing (FWM) experiments were performed. All measurement techniques and timing conventions for excitation pulses were defined in the previous chapter. For the data presented in this chapter, the temporal overlap of the two excitation pulses k_1 and k_2 (i.e. time delay $\Delta t = 0$) was found by two independent methods. One technique marked $\Delta t = 0$ by using the location of the intersection point of the TI FWM signals measured in directions $2k_2$-k_1 and $2k_1$-k_2, as shown in Fig.4.2. For finite pulses, this procedure is known to give an accurate estimate of zero time delay. [4.14] (Note that all FWM data presented in this dissertation were measured in direction $2k_2$-k_1. The signal in the opposite FWM direction, $2k_1$-k_2, was measured solely for the purpose of establishing zero time delay.) The other technique marked $\Delta t = 0$ by measuring the intensity autocorrelation of the laser pulse at the location of the sample itself. The two methods for establishing $\Delta t = 0$ were found to differ by less than 4 fs, which is well within our experimental error.

4.2.1 Free induction decay

Figure 4.3 shows a series of TR FWM signals measured at excitation density $N_x \approx 3x10^{11}cm^{-2}$ and for time-delays between $\Delta t = -40$ fs and $\Delta t = +140$ fs. Note that on the abscissa the zero of absolute time, $t = 0$, is not marked. Rather, the TR FWM traces are presented relative to one another, with the time calibration noted. As mentioned in Ch.3, it is impossible for us to measure precisely the origin of absolute time ($t = 0$) in the TR measurements. However, as explained in detail in section 4.3, once these TR FWM data are fit to numerical calculations for the coherent emission in direction $2k_2$-k_1, it will be possible to locate $t = 0$. This is an important point, because knowledge of $t = 0$ will greatly contribute to our understanding of the exciton dynamics affecting the coherent emission.

Even without knowledge of $t = 0$, there is much to be learned from these data as they are presented here. First, we note that the temporal lineshapes are smooth and regular, without discontinuities. This point will be important to remember when considering the interpretation of instantaneous frequency measurements in Ch.6. Second, the overall duration of the coherent emission is rather fast, $\approx$ 200 fs, relative to the duration of the $\approx$ 80 fs (FWHM) laser pulses. This indicates that the polarization dephasing time T_2 is fast, which will be verified below. Third, upon closer examination the TR lineshapes are asymmetric, non-exponential, and vary with time-delay. The implications of this will be discussed in detail in following sections of this chapter. Fourth, the timing of the emission clearly varies with time-delay. Recalling the analysis of Yajima

and Taira [4.2] (see Ch.2) for a collection of non-interacting two-level systems under δ-function pulsed excitation, we expect the timing of the FWM emission to depend upon time-delay in a specific way. In fact, the exact dependence is determined by the degree of inhomogeneous broadening in the system. Thus, one important result of the TR FWM data presented here is that by carefully measuring the timing of the emission one can determine whether or not the system is homogeneously broadened.

We demonstrate this fact immediately by plotting the relative positions of the maxima of the TR FWM signals from Fig.4.3 vs. the time-delay Δt, as shown by the filled circles in Fig. 4.4. Also marked on the figure are the evolutions with time-delay expected for free induction decay signals (hollow circles) and for photon echoes (triangles). Recall that in the analysis of Yajima and Taira, for $\Delta t > 0$ a homogeneously broadened system emits a FID signal in direction $2k_2$-k_1 immediately following the arrival of pulse k_2, or, at time $t = \Delta t$. On the other hand, a strongly inhomogeneously broadened system emits a photon echo only once time Δt has elapsed after pulse k_2 is incident, or, at time $t = 2\Delta t$. As plotted in the figure, for $\Delta t > 0$ this corresponds to a line of slope equal to 1 for FID (hollow circles) and 1/2 for photon echo (triangles). From the figure it is clear that our data reflect a free induction decay (FID) process [4.15], not a photon echo, and arise from a homogeneously broadened collection of quasi-2D excitons. Additional TR FWM data taken at higher excitation density $N_x \approx 10^{12}cm^{-2}$ are shown in Figures 4.5 and 4.6 and confirm this result. (We note that for $\Delta t < 0$ the analysis of Yajima and Taira predicts no FWM emission. Experimentally, however, we do measure a signal for $\Delta t < 0$ due to the

overlap of the finite excitation pulses for small Δt.) In this way, TR FWM provides a means of determining unambiguously whether or not the system being studied is homogeneously broadened. Importantly, there is no way of determining this property of the system from the conventional TI FWM measurement alone.

The FID we observe is understood when one considers that the experiments are performed at room temperature, where collisional broadening with the large population of thermal phonons homogenizes the exciton line. At low temperatures, a homogeneously broadened exciton line would normally require heterostructures made from very high quality materials, since fluctuations in layer thickness are a source of inhomogeneous broadening. (Indeed, the photon echo behavior expected from the inhomogeneously broadened system of a QW at low temperature has been verified experimentally by others. [4.7]) For the purpose of purely studying the ultrafast dynamics of excitons, we prefer a homogeneously broadened system, where each exciton "sees" the same environment and which responds with a free induction decay. For this reason the experiments were performed at room temperature, the only disadvantage being a relatively fast polarization dephasing time T_2. This leads to the overall short duration of the coherent emission, as we saw in the TR FWM signals above. In the following sections we will measure T_2 directly from the FWM data using the conventional method of TI FWM and contrast this result with the analysis of the TR FWM lineshape.

4.2.2 Time-resolved vs. time-integrated data

Having demonstrated that the system is homogeneously broadened from the TR FWM results, we turn to the TI FWM data both to check the internal consistency of our results and to extract an estimate for the polarization dephasing time T_2. We begin by examining the TI FWM signal shown as the solid line in Fig.4.7, taken under the same excitation conditions as the TR FWM data of Fig.4.3, and noting a few qualitative features. The profile of the TI signal is only slightly asymmetric, indicating a polarization dephasing time T_2 which is fast relative to the excitation laser pulse duration. This is consistent with the observations from the TR FWM measurement and is not surprising in light of the fact that we are working both at room temperature and at the exciton saturation density $N_{sat} \approx 3x10^{11}cm^{-2}$, where we expect collisions with phonons and other excitons to increase the dephasing rate of the coherent polarization established in the sample. Notice also that the TI FWM curve peaks around $\Delta t \approx +50$ fs and not at $\Delta t = 0$. This effect is well understood from modeling done for two-level systems under resonant excitation by finite pulses [4.16] and it results from a combination of finite pulse effects and finite, non-zero polarization dephasing time T_2. In fact, this result tends to support our measurement of $\Delta t = 0$.

Importantly, we can verify the internal consistency of our TR and TI FWM results by numerically integrating the TR FWM data in Fig.4.3 for each time-delay and comparing the result to the TI FWM signal measured directly with the GaAs slow detector. Fig.4.7 shows the results of the numerical integration (crosses) and the measurement of the peak amplitude (hollow circles) normalized and superimposed upon the direct TI FWM measurement (solid line). The data, whether integrated numerically or by the detector, are

clearly in good agreement and give us confidence in the internal consistency of the TR and TI measurements.

Using the fact that the system under study is homogeneously broadened, we can now examine the TI FWM lineshape in greater detail by recalling the analysis presented in Ch.2. [4.2] For noninteracting two-level systems resonantly excited by δ-function pulses, the TI FWM signal decays exponentially as $\exp(-2\Delta t/T_2)$ for FID from homogeneously broadened systems. Let us apply this analysis to the TI FWM measurement taken at lower excitation density $N_x \approx 10^{11}cm^{-2}$, shown as curve (b) in Fig.4.8, and we extract a dephasing time T_2 of $\approx 135 \pm 5$ fs. This simple analysis represents the conventional approach taken in FWM experiments: the TI FWM signal is measured and dephasing time T_2 deduced from it. Importantly, it is worth emphasizing that for *non-interacting* two-level systems this approach is valid. From this perspective, in fact, there is not much to be gained from going to the trouble of measuring the TR FWM signal: both TI and TR FWM lineshapes decay exponentially and reflect the polarization dephasing time T_2 in the sample. Indeed, as we saw above, by numerically integrating the TR signal one reproduces the TI lineshape! (Even the issue of homogeneous broadening, which is settled by TR measurements, may also be determined more easily, perhaps, by TI three-pulse FWM experiments. [4.17]) The critical assumption made when applying this analysis to semiconductors is that the collection of resonantly excited quasi-2D excitons, in this case, responds as a collection of independent and non-interacting two-level systems would respond. In fact, as we show immediately, this is not correct and the conventional analysis presented above for deducing T_2 is wrong.

The error becomes obvious when we compare the lineshape of the TI FWM signal to that of the TR FWM signal. From the analysis presented in Ch.2 for independent two-level systems [4.2], *both* TI and TR FWM lineshapes are expected to decay exponentially, with the same time dependence. This is understood as being a reflection of the exponential decay of the coherent polarization in the medium, metered by the dephasing time T_2. Fig.4.8 compares the TI FWM signal analysed above (curve (b)) with the TR FWM signal (curve (a)) taken at $\Delta t = 0$ and under identical excitation conditions. The curves have been normalized and the unrelated time axes have been shifted to bring the maxima into coincidence for comparison. Clearly there is an enormous difference between the two curves. The TR FWM lineshape does not decay exponentially, and is, in fact, much broader than the TI FWM trace. (One might expect the TR FWM trace to be slightly broader, since the upconversion is realised not with δ-function pulses, but with finite pulses. However, this is a small effect and certainly cannot explain the nonexponential decay we observe.) Furthermore, the degree of discrepancy between the TR and TI curves strongly depends upon the excitation density, as demonstrated by the data presented in Fig.4.9, which are taken at higher excitation density $N_x \approx 4x10^{11}cm^{-2}$. At higher density we still observe a distinct difference between TR and TI FWM, but the non-exponential decay of the TR trace is clearly more pronounced at lower density. These observations are all consistent with effects due to Coulomb correlation, as described in Ch.2, where there is a delayed polarization wave scattering (PWS) contribution to the emission arising from interactions among excitons, thus leading to a non-exponential profile for the TR FWM signal. This effect will be demonstrated explicitly in the next

section. We note that after the above experiments were performed, another group obtained numerical solutions to the semiconductor Bloch equations (SBE) for excitation conditions matching our experiment. [4.18] They compared TR FWM traces for several Δt and the lineshapes of TI vs. TR FWM signals and found excellent agreement with our measurements. They, also, attributed their findings to Coulomb interaction.

We understand the density dependence of our results by noting that at higher excitation densities there are more free electron hole pairs present due to exciton ionization and these free carriers act to screen the Coulomb correlation. It is for this reason, less screening at lower densities, that the non-exponential decay of the TR signal is more pronounced in Fig.4.8 than in Fig.4.9. This description will be discussed in greater detail in the next section. For now, a final point to emphasize is that by its very nature, the TI measurement loses information (during integration) that can only be found from measuring the TR FWM lineshape directly. Assuming that the TR and TI measurements provide equivalent information is incorrect for FWM experiments in semiconductors.

4.3 Numerical analysis

We may quantify the qualitative description given above by fitting the TR FWM data to the lineshape predicted by the nonlinear Schrodinger equation for the exciton transition amplitude. [4.19] [4.20] This description was introduced in the Appendix and shown to be equivalent to the formalism presented in detail in Ch.2. For convenience, we rewrite Eqn.8 of the Appendix, separating terms for clarity

$$\frac{\partial\psi(t)}{\partial t}=-i(\Omega-\frac{i}{T_2})\psi(t)+i\mu E(t)-i\mu E(t)\frac{|\psi(t)|^2}{|\psi_{sat}|^2}-iV|\psi'(t)|^2\psi(t) \qquad \text{Eqn.4-1}$$

where the notation for the renormalized transition frequency has been changed from ω to Ω. As described in Ch.2, the first two terms on the right hand side describe the linear response, while the last two describe the nonlinear response. Recall that the first nonlinear term originates from the Pauli exclusion principle and accounts for the effect of phase space filling (PSF) in the semiconductor. It is analogous to a saturation term and for high fields it acts to reduce the dipole coupling of the exciton to the applied field. The second nonlinear term describes the effect of Coulomb correlation as excitons at one site ψ' interact with excitons at another site ψ via the potential V. This term accounts for polarization wave scattering (PWS), which produces a contribution to the coherent FWM emission which is *delayed* with respect to the prompt PSF contribution.

Using the perturbation expansion described in Ch.2, we solve Eqn.4-1 numerically, in the mean-field approximation, to third order in the field for the coherent emission in direction $2k_2$-k_1. We further include the effect of upconversion of the emitted signal (see Ch.3) to completely reproduce the TR FWM result for our experimental conditions. The adjustable parameters are: pulse duration, dephasing time T_2, and the ratio of nonlinearities (Coulomb correlation to saturation density) $V|\psi_{sat}|^2$. The excitation laser pulses are known to be Gaussian in shape and their duration is deduced from the measured non-collinear intensity autocorrelation assuming transform limited pulses. The dephasing

time is first estimated from TI FWM results and then adjusted, along with the ratio of nonlinearities, to best fit the data.

Figure 4.10 shows fits of the numerical analysis to series of TR FWM data taken at excitation density $N_x \approx 10^{11}cm^{-2}$. In the figure, the dash-dotted lines give the PSF contribution from Pauli exclusion, while the dashed lines give the PWS contribution from Coulomb correlation. The thin solid line represents the sum of these two contributions and is seen to match the data very well. Importantly, we find that it is impossible to fit these TR FWM data without including the effect of Coulomb correlation. From the figures it is easy to obtain an intuitive understanding of this. The PSF contribution is nearly instantaneous, beginning immediately after the arrival of the second pulse (and limited only by the fact that we have finite pulses). The PWS contribution, on the other hand, is delayed with respect to the PSF contribution. This occurs because PWS requires *coherent* polarization to be present in the sample. Naturally, the time before which the polarization loses its coherence is $\approx T_2$, so the PWS via Coulomb interaction is delayed by this amount of time, as we will show below. This combination of a prompt plus a delayed contribution is the signature for Coulomb correlation in TR FWM and leads to an overall decay which is non-exponential. Such a decay is impossible to reproduce from PSF alone.

It is important to note that the *entire TR FWM series* vs. Δt is fit for a single origin of absolute time ($t = 0$), for a fixed relative magnitude, and, naturally, for a single excitation pulse: i.e. these are parameters which are *not* adjusted to make these fits. We note that this procedure gives us the best estimate we can possibly have for the true zero of absolute time t. Thus, the only parameters adjusted for the fits are T_2 and $V|\psi_{sat}|^2$,

which are summarized in Table 4.1(a). From the table it is clear that for a *fixed* excitation density, T_2 and $V|\psi_{sat}|^2$ vary with time delay Δt. Although at first this fact was surprising to us, upon reflection it makes sense when one recalls that the two excitation pulses k_1 and k_2 are *not* identical. In fact, the intensity of k_2 is twice that of k_1. Therefore, the effective excitation density in the sample will vary depending upon the timing of the excitation pulses, Δt. As explained before, at higher excitation densities, the dephasing time T_2 decreases and the Coulomb correlation V is screened. For this reason, T_2 is smaller for $\Delta t < 0$, when the more intense pulse k_2 is incident on the sample first. This effect, specifically that T_2 varies with Δt, is now known as excitation induced dephasing (EID) [4.21] and was confirmed by fits to TR FWM data taken at higher excitation density. Also listed in the table is the percentage of the TR FWM signal arising from the PWS contribution. As expected, the highest percentage $\approx 75\%$ occurs for $\Delta t < 0$, when the FWM emission is dominated by the effects of Coulomb correlation. As the time-delay increases for $\Delta t > 0$, the percentage decreases since the induced polarization has more time to dephase, thus reducing the relative contribution of PWS.

We should note that the T_2 used to fit all the TR data in this section are consistent with the dephasing times we will present in the next chapter from six-wave mixing (SWM) experiments under similar excitation conditions. Furthermore, the T_2 deduced from the TI FWM measurements are clearly seen to be unreliable and inconsistent with those deduced from TR FWM and SWM. The reasons are now obvious: the conventional analysis of TI FWM data neglects effects due to EID and due to the contribution from Coulomb correlation. An example is the value for T_2 extracted from the TI FWM measurement at

low excitation density $N_x \approx 10^{11}cm^{-2}$ in Fig.4.8: $T_2 \approx 135 \pm 5$ fs is inconsistent with SWM data. On the contrary, the value obtained from analysis of the corresponding TR FWM trace at $\Delta t = 0$ gives a value much larger: $T_2 \approx 190 \pm 5$ fs. It is worth emphasizing that in the TR FWM experiment, Δt remains fixed, so excitation of the sample is constant. This is not true for TI FWM, which measures variations as a function of Δt and therefore contains in its lineshape a superposition of excitation conditions.

The real strength of the TR FWM numerical analysis appears when we compare the fits for several excitation densities. Because of effects due to EID, we only compare TR FWM lineshapes for coincident pulses ($\Delta t = 0$), as shown in Fig.4.11 and summarized in Table 4.1(b). At the highest density, the TR FWM signal is entirely due to PSF and the dephasing time is extremely short. At these densities, band gap renormalization effects become important: the semiconductor continuum states shift below the excitation frequency, excitons dissociate and create free electron-hole pairs, which shorten the relaxation time and screen the Coulomb interaction. [4.1] As the density is lowered, the polarization dephasing time T_2 increases and the PWS contribution to the emission therefore increases, until it dominates the emission at the lowest densities we were able to measure. Interestingly, the saturation density for GaAs QWs is $N_{sat} \approx 3x10^{11}cm^{-2}$ and from these data the Coulomb correlation appears to rapidly "turn on" below this density. Table 4.1(b) shows this explicitly as the percentage of the TR FWM signal due to PWS jumps from $\approx 14\%$ when $N_x > N_{sat}$, to $\approx 60\%$ when N_x falls below N_{sat}. This is consistent with our qualitative descriptions of screening and dephasing in the sample. At the lower densities, the coherent polarization, and hence PWS, has sufficient time to build up before

dephasing processes destroy it. We may directly observe this growth by noting how the timing of the peak of the TR FWM signal varies with excitation density. As indicated before, these fits to the TR data represent the only way of determining accurately the location of t = 0. Now we see the importance of that information: as the density is lowered, the polarization maintains its coherence for a longer time and the contribution to the emission arising from Coulomb correlation is therefore emitted at a later time ($\approx T_2$). This effect is clearly demonstrated in these data where the position of the peak of the TR FWM signal varies from $\approx$ 15 fs at the highest density to $\approx$ 160 fs at the lowest density.

4.4 Conclusions

We have shown that there is much to be gained by directly measuring the amplitude of the coherent emission from semiconductors. TR FWM measurements have not only confirmed that the room temperature excitons in the quantum well sample are homogeneously broadened, they have demonstrated that effects due to Coulomb correlation in such systems can *dominate* the emission at low excitation densities. In performing the analyses which lead to these results we also discovered, for the first time, that the dephasing time T_2 can vary as a function of the time-delay between pulses: an effect later dubbed "excitation induced dephasing" [4.21] in the literature. Importantly, it is clear from these results that conventional TI FWM measurements alone are not sufficient for a thorough understanding of the exciton dynamics. In fact, we have shown

that TI measurements can hide information which is found by analysis of the measured TR lineshape.

The data presented here represent the first quantitative measurements and analyses of the effects of Coulomb correlation on the TR FWM emission from room temperature excitons in GaAs QWs. We can further test the ideas which led us to these results by measuring the next higher order of wave-mixing signal under similar excitation conditions. Although higher order effects on FWM have previously been considered in relation to Coulomb correlation [4.4] [4.22], until now the *direct* effects of Coulomb interactions on the six-wave mixing (SWM) signal itself have not been investigated. The TI and TR lineshapes of SWM measurements are presented in the following chapter.

References

[4.1] S. Schmitt-Rink, D.S. Chemla, D.A.B. Miller: *Linear and nonlinear optical properties of semiconductor quantum wells*, Advances in Physics, Vol.38, No.2, pp.89-188 (1989).

[4.2] T. Yajima and Y. Taira: *Spatial optical parametric coupling of picosecond light pulses and transverse relaxation effect in resonant media,* Journal of the Physical Society of Japan, Vol.47, No.5, pp.1620-1626 (1979).

[4.3] K. Leo, M. Wegener, J. Shah, D.S. Chemla, E.O. Gobel, T.C. Damen, S. Schmitt-Rink, W. Schafer: *Effects of coherent polarization interactions on time-resolved*

degenerate four-wave mixing, Physical Review Letters, Vol.65, No.11, pp.1340-1343 (1990).

[4.4] M. Wegener, D.S. Chemla, S. Schmitt-Rink, W. Schafer: *Line shape of time-resolved four-wave mixing*, Physical Review A, Vol.42, No.9, pp.5675-5683 (1990).

[4.5] G. Noll, U. Siegner, S.G. Shevel, E.O. Gobel: *Picosecond stimulated photon echo due to intrinsic excitations in semiconductor mixed crystals*, Physical Review Letters, Vol.64, No.7, pp.792-795 (1990).

[4.6] L. Schultheis, M.D. Sturge, J. Hegarty: *Photon echoes from two-dimensional excitons in GaAs-AlGaAs quantum wells*, Applied Physics Letters, Vol.47, No.9, pp.995-997 (1985).

[4.7] M.D. Webb, S.T. Cundiff, D.G. Steel: *Observation of time-resolved picosecond stimulated photon echoes and free polarization decay in GaAs/AlGaAs multiple quantum wells*, Physical Review Letters, Vol.66, No.7, pp.934-937 (1991).

[4.8] D.E. Spence, P.N. Kean, W. Sibbett: *60-fs pulse generation from a self-mode-locked Ti:sapphire laser*, Optics Letters, Vol.16, No.1, pp.42-44 (1991).

[4.9] D.S. Kim, J. Shah, T.C. Damen, W. Schafer, F. Jahnke, S. Schmitt-Rink, K. Kohler: *Unusually slow temporal evolution of femtosecond four-wave-mixing signals in intrinsic GaAs quantum wells: direct evidence for the dominance of interaction effects*, Physical Review Letters, Vol.69, No.18, pp.2725-2728 (1992).

[4.10] M.-A. Mycek, S. Weiss, J.-Y. Bigot, S. Schmitt-Rink, D.S. Chemla, W. Schaefer: *Femtosecond time-resolved free-induction decay of room-temperature excitons in GaAs quantum wells*, Applied Physics Letters, Vol.60, No.21, pp.2666-2668 (1992).

[4.11] S. Weiss, M.-A. Mycek, J.-Y. Bigot, S. Schmitt-Rink, D.S. Chemla: *Collective effects in excitonic free induction decay: do semiconductors and atoms emit coherent light in different ways?*, Physical Review Letters, Vol.69, No.18, pp.2685-2688 (1992).

[4.12] S. Weiss, M.-A. Mycek, J.-Y. Bigot, S. Schmitt-Rink, D.S. Chemla: *Observation of many body effects in the femtosecond temporal profile of quasi-2D exciton free induction decay,* in Ultrafast Phenomena VIII, (J.-L. Martin et al., Eds.), Springer Verlag, p.466 (1993).

[4.13] J.-Y. Bigot, M.-A. Mycek, S. Weiss, R.G. Ulbrich, D.S. Chemla: *Amplitude decay and instantaneous frequency dynamics of excitonic polarization in semiconductor quantum wells,* in Coherent Optical Interactions in Semiconductors, (R.T. Phillips, Ed.), Plenum Press, New York, pp.245-260 (1994).

[4.14] J.G. Fujimoto and E.P. Ippen: *Transient four-wave mixing and optical pulse compression in the femtosecond regime,* Optics Letters, Vol.8, No.8, pp.446-448.

[4.15] see, for example, L. Allen and J.H. Eberly: *Optical resonance and two-level atoms,* Dover Publications (1987).

[4.16] A.M. Weiner: *Femtosecond optical pulse generation and dephasing measurements in condensed matter,* Ph.D. dissertation, MIT, pp.102-108 (1984).

[4.17] A.M. Weiner, S. De Silvestri, E.P. Ippen: *Three-pulse scattering for femtosecond dephasing studies: theory and experiment,* Journal of the Optical Society of America B, Vol.2, No.4, pp.654-661 (1985).

[4.18] W. Schafer: *Manybody-effects in nonlinear optics of semiconductor structures*, in *Optics of Semiconductor Nanostructures*, F. Henneberger, S. Schmitt-Rink, E.O. Gobel, eds., Academie Verlag, pp. 34-37 (1993).

[4.19] S. Schmitt-Rink, S. Mukamel, K. Leo, J. Shah, D.S. Chemla: *Stochastic theory of time-resolved four-wave mixing in interacting media*, Physical Review A, Vol.44, No.3, pp.2124-2129 (1991).

[4.20] S. Schmitt-Rink, D.S. Chemla, H. Haug: *Nonequilibrium theory of the optical Stark effect and spectral hole burning in semiconductors*, Physical Review B, Vol.37, No.2, pp.941-955 (1988).

[4.21] H. Wang, K. Ferrio, D.G. Steel, Y.Z. Hu, R. Binder, and S.W. Koch: *Transient nonlinear optical response from excitation induced dephasing in GaAs*, Physical Review Letters, Vol.71, No.8, pp.1261-1264 (1993).

[4.22] S. Wu, X.-C. Zhang, R.L. Fork: *Direct experimental observation of interactive third and fifth order nonlinearities in a time- and space-resolved four-wave mixing experiment,* Applied Physics Letters, Vol.61, No.8, pp.919-921 (1992).

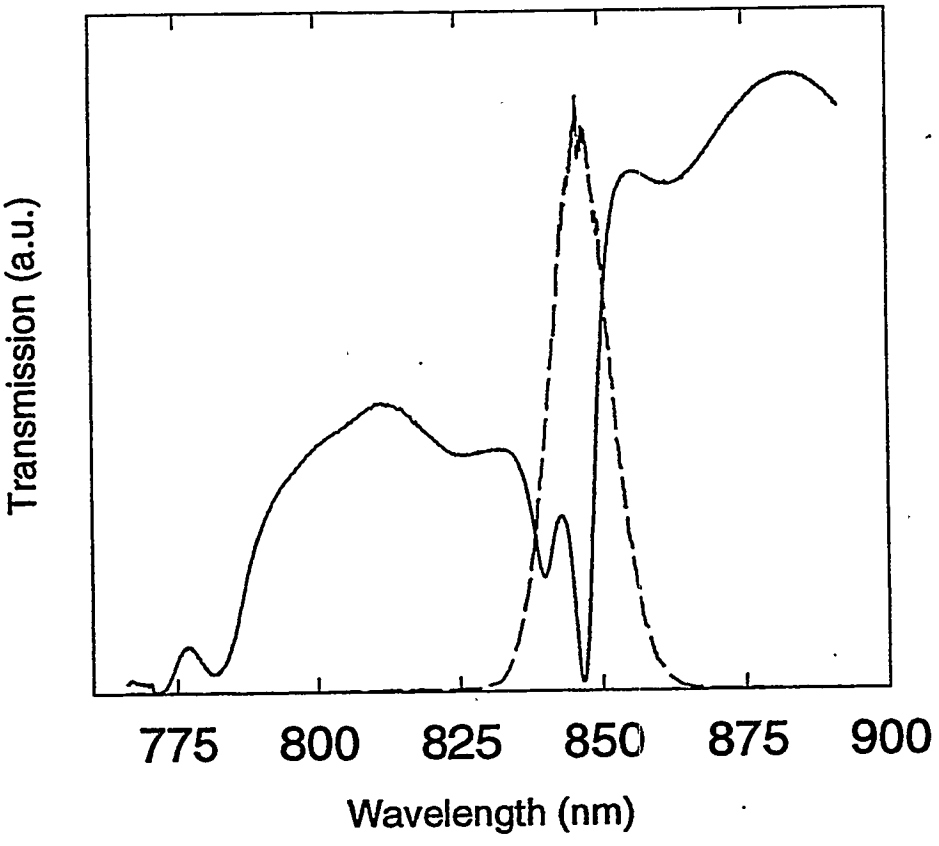

Figure 4.1: Transmission spectrum of the multiple quantum well sample at room temperature (solid line) and the power spectrum of the excitation laser pulse (dashed line). The pronounced dips in the transmission at approximately 840nm and 846nm are the n=1 light-hole and heavy-hole excitons, respectively.

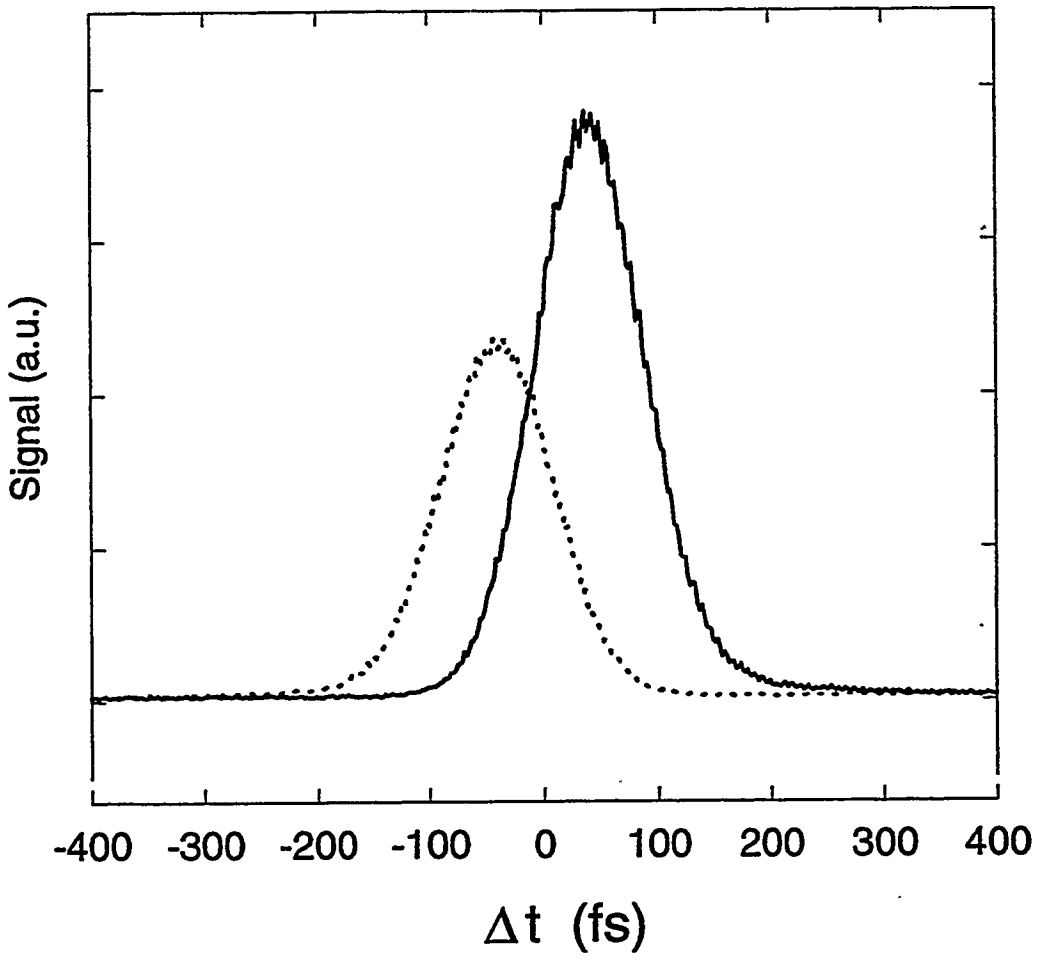

Figure 4.2: Finding time delay $\Delta t = 0$ using the intersection of TI FWM signals from directions $2k_1$-k_2 (dotted line) and $2k_2$-k_1 (solid line), for typical experimental conditions: excitation density $N_x \approx 3x10^{11}cm^{-2}$ and laser pulse duration (78 ± 3) fs.

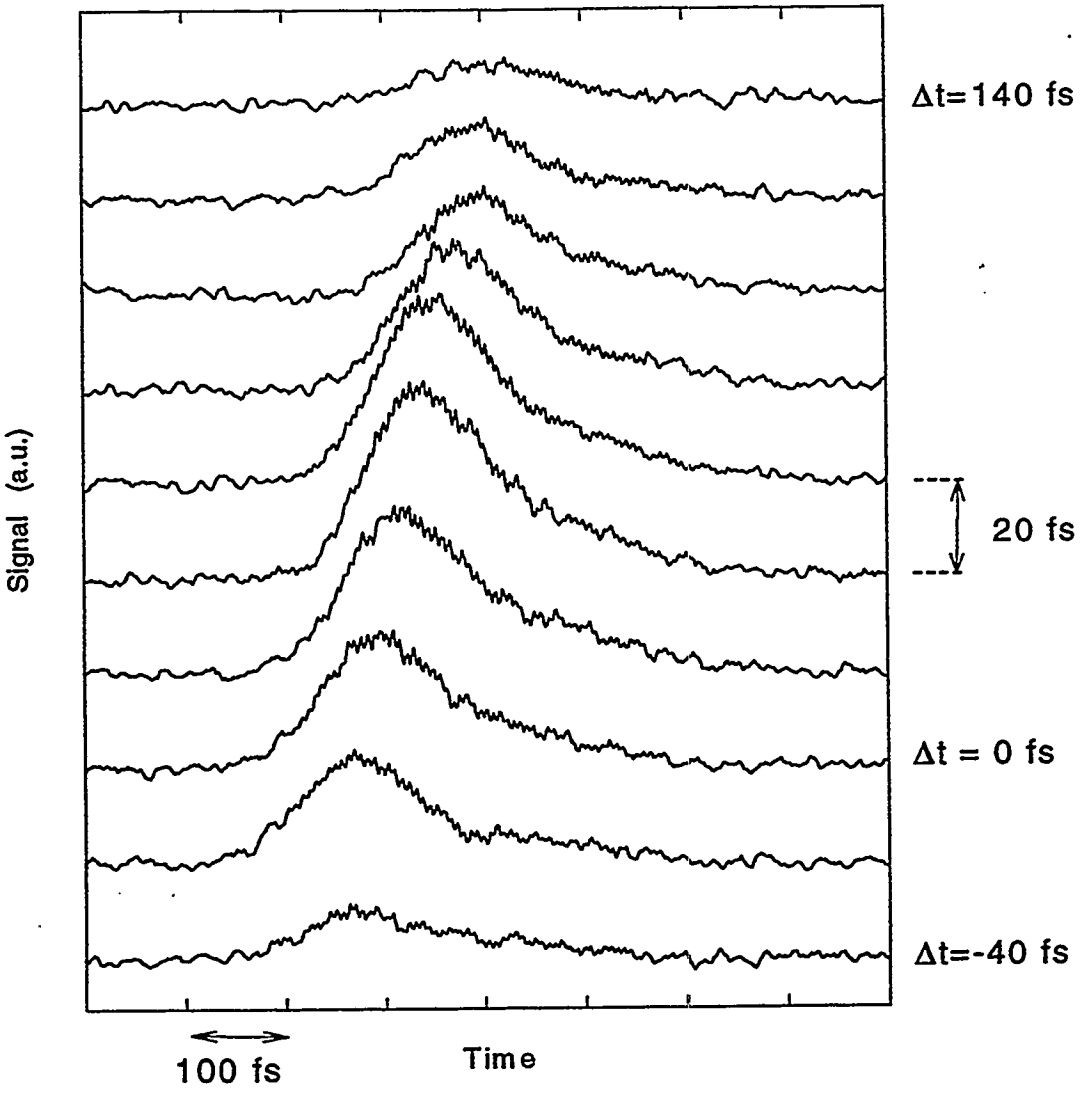

Figure 4.3: TR FWM signals, offset for clarity, for a range of time delays Δt between -40fs and +140fs. The data were taken for an excitation density $N_x \approx 3x10^{11}cm^{-2}$ and for an excitation laser pulse duration of (78 ± 3)fs.

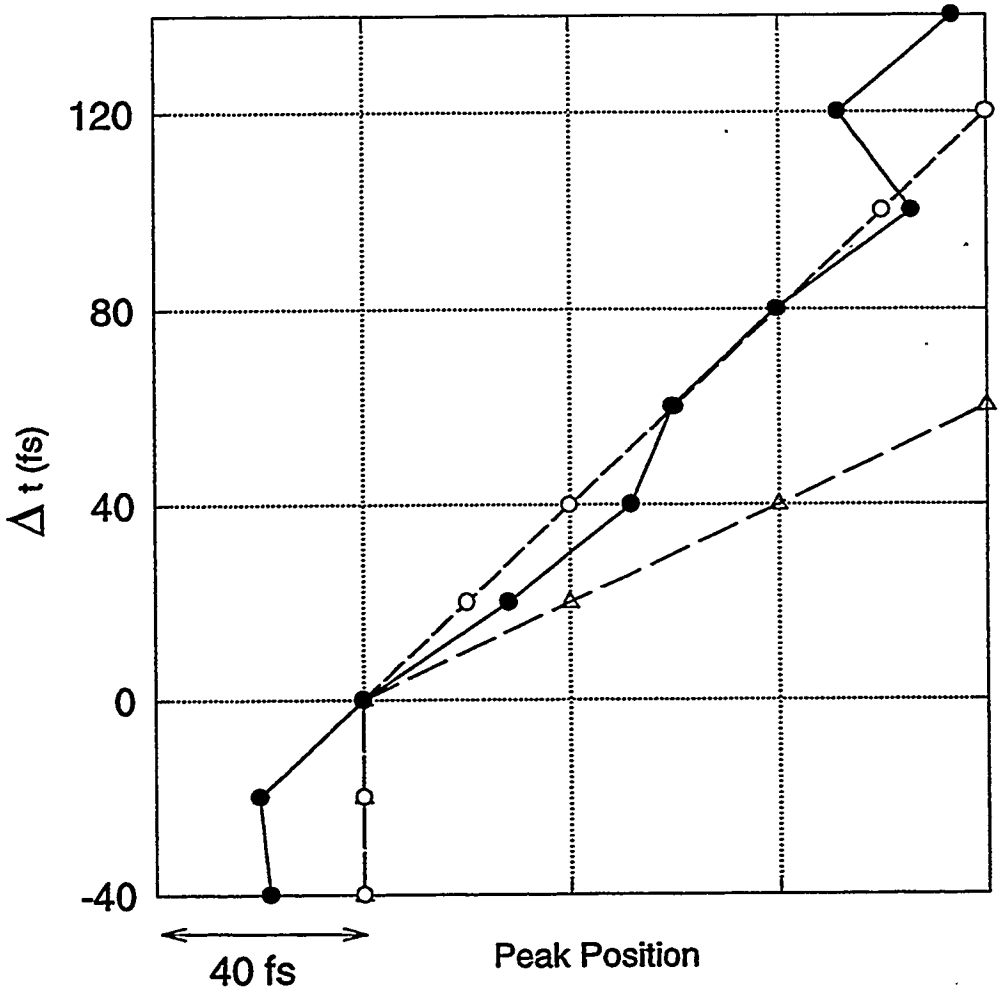

Figure 4.4: Relative positions of the maxima of the TR FWM signals shown in Fig.4.3 vs. time delay Δt (filled circles). Evolution expected for free induction decay signals (hollow circles) and for photon echoes (triangles).

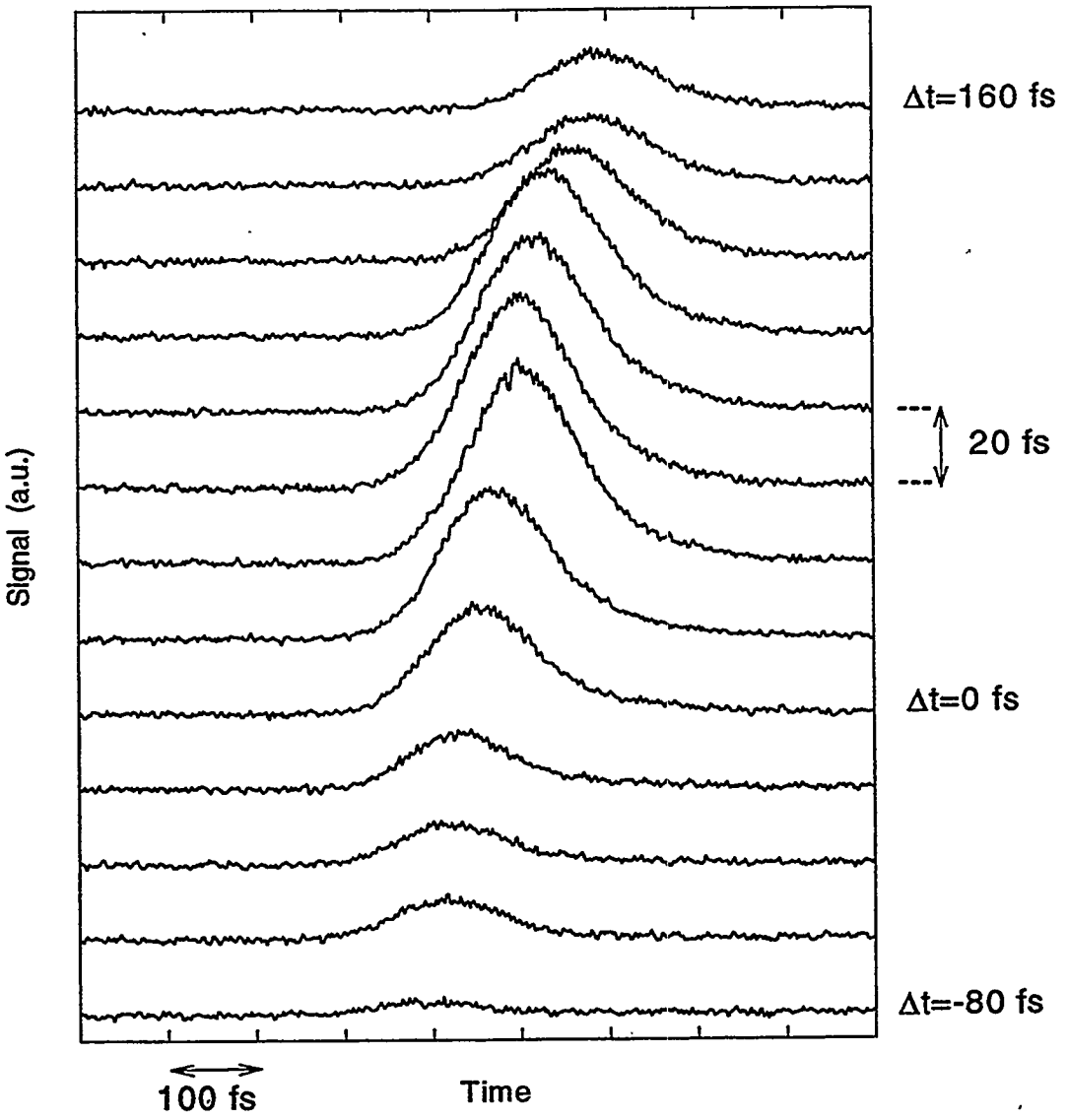

Figure 4.5: TR FWM signals, offset for clarity, for a range of time delays Δt between -80fs and +160fs. The data were taken for an excitation density $N_x \approx 10^{12}cm^{-2}$ and for an excitation laser pulse duration of (78 ± 3)fs.

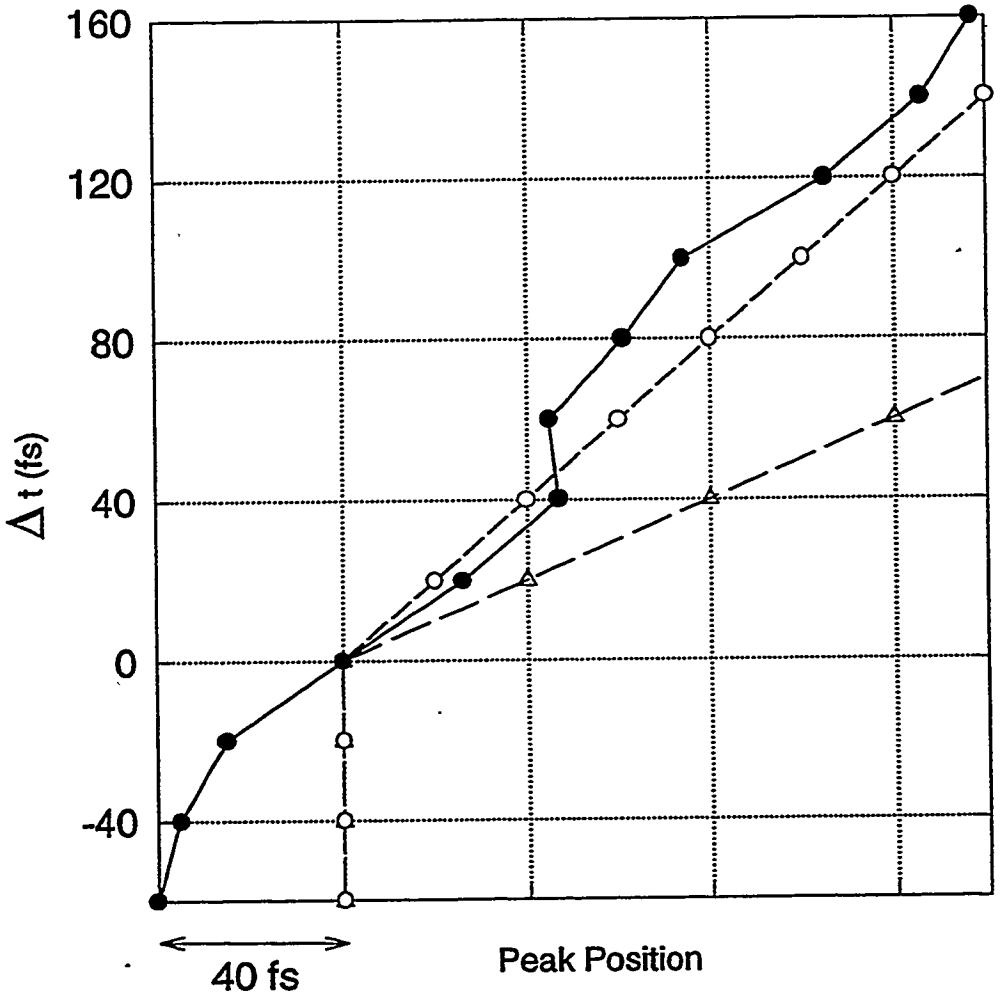

Figure 4.6: Relative positions of the maxima of the TR FWM signals shown in Fig.4.5 vs. time delay Δt (filled circles). Evolution expected for free induction decay signals (hollow circles) and for photon echoes (triangles).

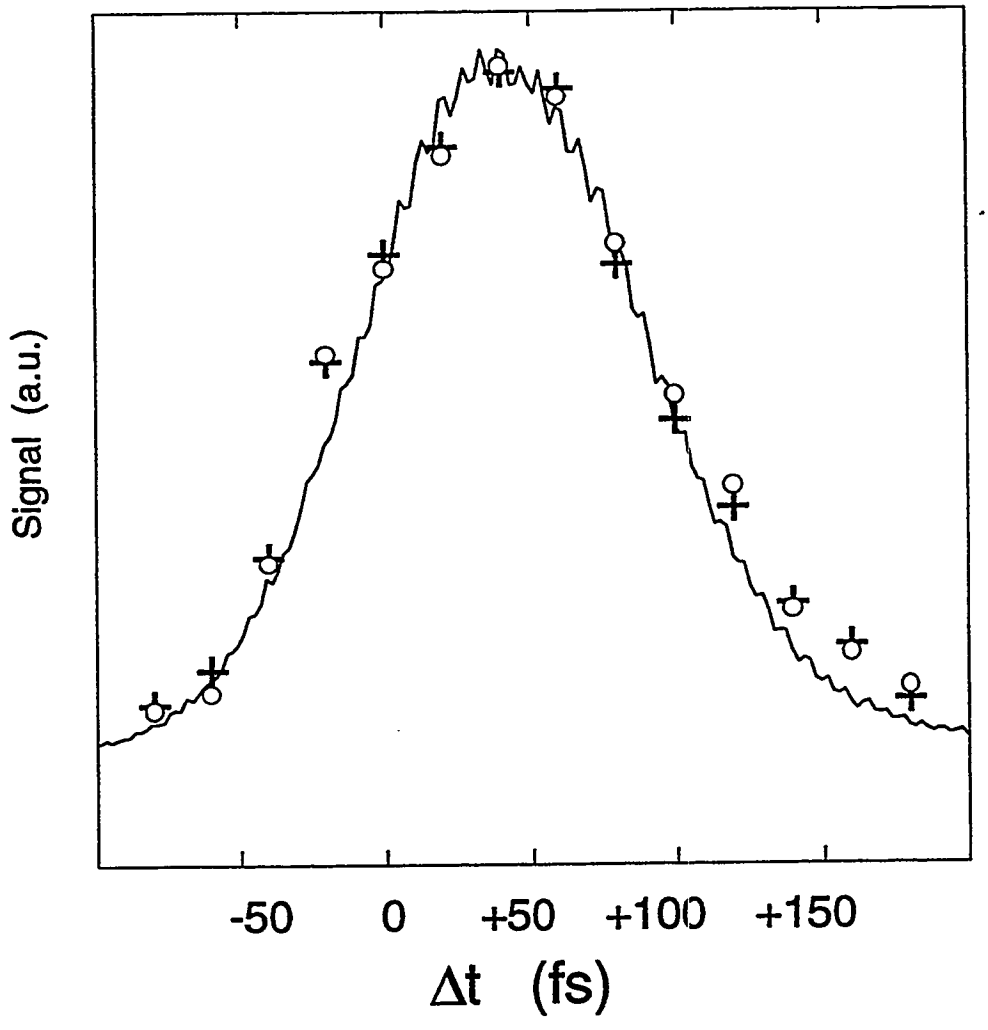

Figure 4.7: TI FWM signal measured directly with the GaAs slow detector (solid line). Numerical integration (crosses) and maximum amplitude (hollow circles) of the TR FWM data shown in Fig.4.3. All data points are normalized to the peak of the TI FWM signal and all data are taken at excitation density $N_x \approx 3x10^{11}cm^{-2}$ and with an excitation laser pulse duration of (78 ± 3)fs.

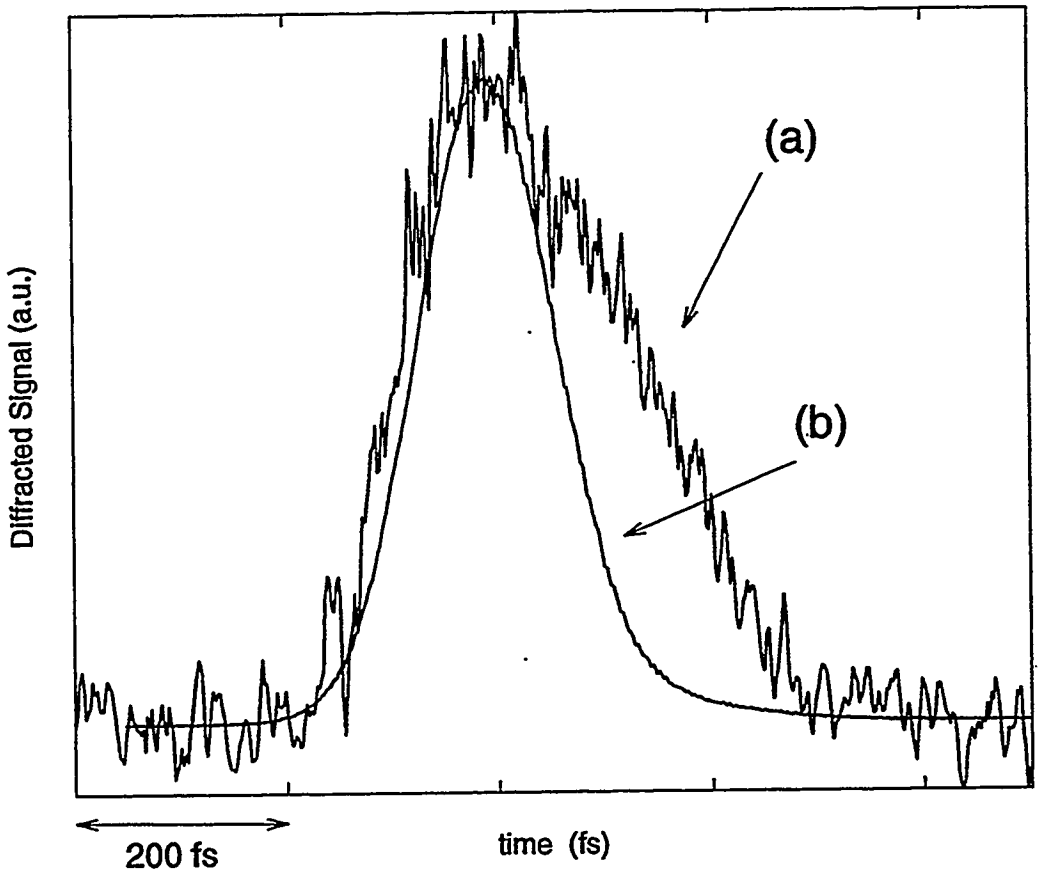

Figure 4.8: (a) TR FWM signal recorded for $\Delta t = 0$ and (b) the corresponding TI FWM signal. All data are taken for excitation density $N_x \approx 10^{11}cm^{-2}$ and with an excitation laser pulse duration of (96 ± 2)fs.

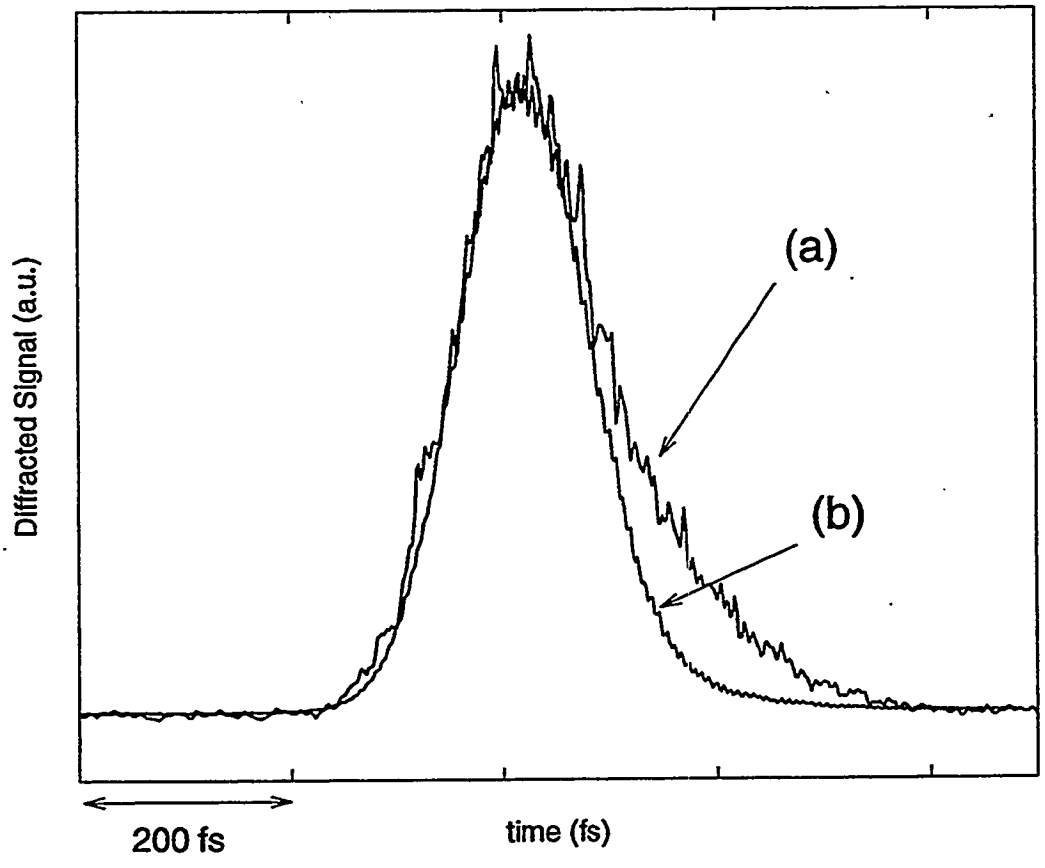

Figure 4.9: (a) TR FWM signal recorded for $\Delta t = 0$ and (b) the corresponding TI FWM signal. All data are taken for excitation density $N_x \approx 4x10^{11}cm^{-2}$ and with an excitation laser pulse duration of (98 ± 2)fs.

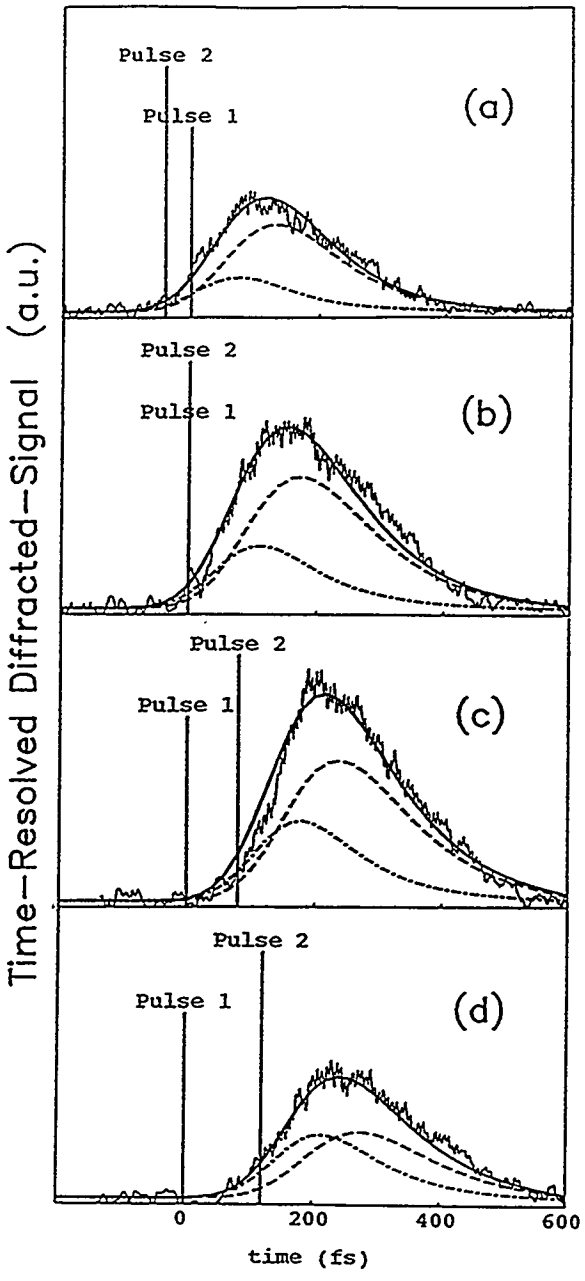

Figure 4.10: Numerical fits to TR FWM data taken at excitation density $N_x \approx 10^{11}cm^{-2}$ and with an excitation laser pulse duration of (98 ± 2) fs for time-delays Δt = (a)-40 fs, (b)0 fs, (c)+80 fs, (d)+120 fs. The dash-dotted lines give the phase-space filling contribution, the dashed lines give the Coulomb contribution, and the solid lines give their sum.

Δt (fs)	T_2 (fs)	$V\|\psi_{sat}\|^2$	%
-40	160 ± 5	.009	75.0
0	190 ± 5	.009	71.6
+80	190 ± 5	.011	67.4
+120	190 ± 5	.009	54.8

Table 4.1(a): Parameters from fits to TR FWM data in Fig.4.10, $N_x \approx 10^{11} cm^{-2}$, and the percentage of the TR FWM signal arising from the Coulomb (PWS) contribution to the signal.

N_x (cm^{-2})	T_2 (fs)	$V\|\psi_{sat}\|^2$	%
$1x10^{13}$	10 ± 5	0	0
$1x10^{12}$	70 ± 5	.002	1.8
$4x10^{11}$	130 ± 5	.0033	14.1
$2x10^{11}$	190 ± 5	.007	60.4
$1x10^{11}$	190 ± 5	.009	71.6

Table 4.1(b): Parameters from fits to TR FWM data in Fig.4.11, $\Delta t = 0$, and the percentage of the TR FWM signal arising from the Coulomb (PWS) contribution to the signal.

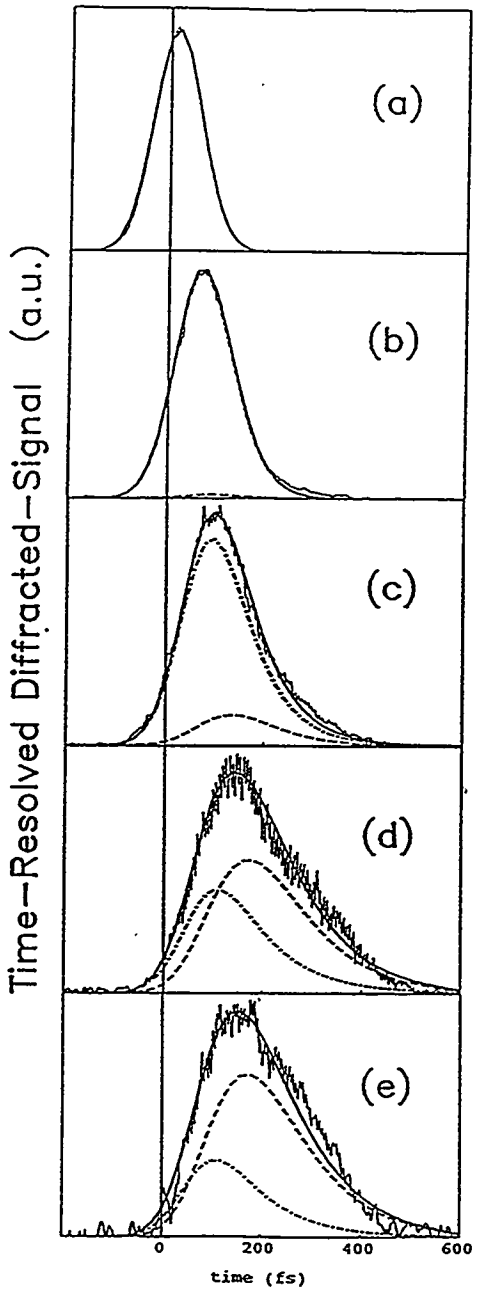

Figure 4.11: Numerical fits to the TR FWM data taken at $\Delta t = 0$ and for a series of excitation densities $N_x \approx$ (a)10^{13}, (b)10^{12}, (c)$4x10^{11}$, (d)$2x10^{11}$, and (e)10^{11} cm^{-2}. The dash-dotted lines give the phase-space filling contribution, the dashed lines give the Coulomb contribution, and the solid lines give their sum.

Chapter 5

Six-Wave Mixing: Time-Integrated and Time-Resolved Measurements

5.1 Introduction

Coherent transient wave-mixing experiments with ultrashort laser pulses can reveal important dynamics in the many-body interactions between excitons in quantum wells. As we saw in the previous chapter, the presence of Coulomb correlation significantly modifies the temporal lineshape of four-wave mixing (FWM) signals measured at low excitation densities. In order to quantify and compare the relative contributions of the various nonlinearities involved (phase space filling and Coulomb correlation), however, numerical fits to the time-resolved (TR) FWM data were necessary. In the present chapter, we demonstrate for the first time that the lineshape of time-integrated (TI) six-wave mixing (SWM) reflects the presence of Coulomb correlation in a *simple, direct, and unambiguous* manner.

It is commonly assumed that TI measurements of higher order coherent wave-mixing signals (i.e. orders higher than FWM) will not reveal any information about the dephasing processes of the system being studied. [5.1] This assumption, coupled with the experimental difficulties associated with measuring the small signals arising from fifth-

order processes, explains why wave-mixing experiments usually do not measure diffracted signals beyond the first-order, FWM, signal. In fact, we derived this result explicitly in Ch.2 for SWM emission from a collection of independent two-level systems under resonant excitation by δ-function excitation pulses [5.2], where the analysis further showed that all information related to the dephasing of the polarization is contained in the TR SWM measurement. However, these assumptions were shown to be *incorrect* when effects arising from Coulomb interaction were included in the model, as is necessary for the case of coherent emission from semiconductors. Here, we verify these theoretical predictions experimentally by measuring the TI and TR SWM emission from GaAs quantum wells at several excitation densities.

In section 5.2 we begin our presentation of the experimental results by showing that at high excitation densities, when Coulomb interactions are screened, it is possible to extract reliable dephasing information *only* from the TR SWM measurement. We then lower the excitation density and directly measure signatures of Coulomb correlation in the TI SWM lineshape. In section 5.3 we summarize our results and conclude our analysis of the ultrafast amplitude decay of coherent wave mixing emission from semiconductors.

5.2 Experimental results

The sample we investigated in the SWM experiments was the optically thin GaAs multiple quantum well structure described in Ch.4. The transmission spectrum of the sample and the power spectrum of the excitation laser pulse used in the experiments are shown in

Fig.4.1. All measurements were performed at room temperature using transform-limited, ≈ 100 fs laser pulses from a Ti:sapphire laser tuned to selectively excite the n=1 heavy-hole exciton. As we demonstrated in Ch.4, under these experimental conditions the exciton in our system was homogeneously broadened through collisions with thermal phonons. Thus, our wave-mixing signals corresponded to a free-induction decay process with density dependent dephasing times less than one picosecond. The SWM emission in direction $3k_2$-$2k_1$ was measured via both TI and TR experiments. All measurement techniques and timing conventions for excitation pulses were defined in Ch.3. The temporal overlap of excitation pulses in directions k_1 and k_2 (i.e. $\Delta t = 0$) was found by measuring the noncolinear intensity autocorrelation of the excitation laser pulse at the location of the sample.

5.2.1 SWM measurements at high excitation densities

At excitation densities greater than the saturation density for the sample $N_{sat} \approx 3x10^{11}cm^{-2}$, excitons quickly ionize from collisions with other excitons and with phonons. Thus, under these conditions, the Coulomb interaction between excitons is screened due to the presence of a relatively large number of free carriers. [5.3] In this case, the strength of the Coulomb term (which is parametrized by 'V' in the equations in Ch.2) is approximately zero and the excitons are non-interacting. As we saw in Ch.4, the system of excitons then behaves like a collection of independent two-level systems. Recall that in the absence of interactions, SWM emission is present only when the two excitation pulses are incident on the sample at the same time, i.e. when time-delay $\Delta t = 0$. (See Eqn.2-

12(b).) In this case, the TI SWM signal derived for δ-function excitation pulses is given only by a coherent spike at $\Delta t = 0$. (This result is true for all successive wave-mixing orders (m) where $m \geq 2$.) For finite pulse widths, therefore, we would expect the TI SWM signal to follow the laser pulse and to be *symmetric* around $\Delta t = 0$.

This theoretical prediction has been verified experimentally and is shown in Fig.5.1. The solid line in the figure is the TI SWM signal taken at high excitation density $N_x \approx 10^{13}cm^{-2}$. We see that it is symmetric with respect to $\Delta t = 0$ with no obvious decay. For comparison, we overlay with the intensity autocorrelation of the excitation laser pulse used in the experiment raised to the 5/2 power (dotted curve). Clearly, over several orders of magnitude the two signals have the same temporal dependence, with no asymmetry in the TI signal. In this sense, at high excitation densities the TI SWM measurement is given by a coherent spike determined by the temporal overlap of the excitation pulses and provides no information on the polarization dephasing time T_2.

Under these conditions, then, we expect that all of the dephasing information is contained in the TR SWM lineshape, which is predicted to decay exponentially with time constant $T_2/2$. (See Eqn.2-12(a).) In this way, an estimate of T_2 can be extracted directly from the TR SWM measurement. In Fig.5.2 we compare the TI and TR SWM traces taken at high excitation density $N_x \approx 10^{13}cm^{-2}$. Indeed, the TR lineshape has a slightly asymmetric exponential decay for positive times, which is not present in the TI lineshape. To demonstrate that this asymmetry is a reflection of the polarization dephasing time T_2, we measured the TR SWM signal for decreasing excitation density. Recall that because the collision rate decreases at lower excitation densities, we expect T_2 to increase, as has

been demonstrated many times via FWM experiments. (See, for example Ch.4., [5.3], [5.4].) Fig.5.3 shows TR SWM lineshapes taken at $\Delta t = 0$ for three excitation densities. We should point out that because SWM is a fifth-order process, the smallest signal that we could upconvert for time-resolution was produced at an excitation density $N_x \approx 10^{12}cm^{-2}$. This is above the saturation density for the sample $N_{sat} \approx 3x10^{11}cm^{-2}$ and therefore high enough to effectively screen the Coulomb interaction. For this reason, in this experiment, we could lower the density of excitons by as much as an order of magnitude and still be in the regime of non-interacting excitons. Fig.5.3(a) shows that at the highest density, $N_x \approx 10^{13}cm^{-2}$, the dephasing is so fast that we are nearly limited in resolution by the duration of the laser pulses. Nonetheless, we estimate from the measurement a polarization dephasing time $T_2 \approx 54$ fs. As we lower the density to $N_x \approx 4x10^{12}cm^{-2}$ (Fig.5.3(b)), the TR lineshape develops a clear exponential decay from which we estimate a dephasing time $T_2 \approx 84$ fs. Finally, Fig.5.3(c) shows that at the lowest density we could measure, $N_x \approx 2x10^{12}cm^{-2}$, the dephasing time has increased to approximately 132 fs. Clearly, as the density is lowered the polarization established in the sample maintains its coherence for longer times, and therefore we observe a slower exponential decay to the TR SWM trace.

These TI and TR SWM observations are consistent with the theoretical predictions for independent two-level systems. It is also important to note that these estimates of T_2 are in good agreement with values obtained from FWM under identical experimental conditions. This is plotted in Fig.5.4, which compares values for the dephasing time T_2 extracted from SWM (circles) and FWM (squares) measurements for several excitation

densities. The agreement gives us confidence in both the internal consistency of our results and in the interpretation of the data.

5.2.2 SWM measurements at low excitation densities

If the model we are using to interpret the data is correct, we should also be able to measure another important theoretical prediction: that there is in SWM an unambiguous signature for Coulomb correlation which is easily observed from a qualitative analysis of the TI signal. Recall from the discussion surrounding Eqn.2-12(b) that if one includes in the model effects arising from Coulomb interactions, then there is SWM emission at time delays other than $\Delta t = 0$ and the presence of interactions produces an *asymmetry* in the TI signal. This effect arises because the polarization remaining in the system after the pulsed-excitation field is no longer present continues to interact with the population grating via the Coulomb potential, thus producing a diffracted signal. This process was called polarization wave scattering (PWS) in Ch.2. The dynamics of the interaction of the polarization with the grating are such that the usual (in the absence of interactions) time development of the coherent emission is significantly changed. It is this asymmetry which is the signature of Coulomb correlation in TI SWM. As we demonstrate below and contrary to the complicated analyses used to interpret FWM data, this signature is observed quickly and easily from the TI SWM data.

As we demonstrated by the FWM results presented in Ch.4, by lowering the exciton density to a point below the saturation density for GaAs, $N_{sat} \approx 3x10^{11}cm^{-2}$, the Coulomb interaction between excitons is no longer efficiently screened by free carriers.

The dynamics of these interactions then significantly affect the wave-mixing emission and cannot be ignored. Because SWM is a fifth-order process, the emission at such low densities was very small and it was not possible to detect the upconverted TR SWM signal. However, it was possible to perform the TI SWM experiment and data from such a measurement is shown in Fig.5.5. The exciton density in this experiment was $N_x \approx 2.7 \times 10^{11} cm^{-2}$ and at this density an asymmetry in the TI measurement was clearly visible in a simple logarithmic plot of the data. This is an entirely different response from the TI SWM data taken at higher excitation density (Figs.5.1 and 5.2) where, in the absence of interactions, we observed the TI SWM measurement to be a symmetric coherent spike around $\Delta t = 0$.

Clearly, at low densities the presence of Coulomb interactions allows for the scattering of the induced polarization off the grating, which occurs even when the two excitation laser pulses are not in the sample at the same time. Thus, the interactions arising from PWS produce an emitted SWM signal for $\Delta t \neq 0$. In fact, our observations are consistent with the slower decay of the emission expected for positive time delays. (See Eqn.2-12(b)). Thus, we interpret the pronounced asymmetry in the TI signal measured here as the signature of exciton-exciton interactions via Coulomb correlation in SWM.

5.3 Summary and conclusions

We have presented experimental evidence for many-body interactions via Coulomb correlation, as observed for the first time from SWM measurements at low excitation densities. By changing the excitation density we observe clear variations in both the polarization dephasing time T_2 and the effective strength of the Coulomb interaction. These results are entirely consistent with the theoretical model presented in Ch.2. and with the FWM data from Ch.4. Importantly, an unambiguous signature of these collective exciton dynamics was observed from only a simple qualitative analysis of the TI SWM measurement.

We have shown in Chs. 4 and 5 that TI and TR *amplitude* measurements of the coherent emission from semiconductor quantum wells at room temperature can reveal signatures attributed to Coulomb correlation, as predicted by the theoretical models of Ch.2. Another important, yet heretofore ignored, prediction of these models is that Coulomb correlation affects both the *amplitude* and the *phase* of the coherent emission. In the next chapter we conclude our treatment of the full characterization of the coherent wave mixing emission from semiconductors, by presenting measurements of the ultrafast instantaneous frequency dynamics.

References

[5.1] A.M. Weiner: *Femtosecond optical pulse generation and dephasing measurements in condensed matter*, Ph.D. dissertation, MIT, pp.150-153 (1984).

[5.2] S. Wu, X.-C. Zhang, R.L. Fork: *Direct experimental observation of interactive third and fifth order nonlinearities in a time- and space-resolved four-wave mixing experiment,* Applied Physics Letters, Vol.61, No.8, pp.919-921 (1992).

[5.3] L. Schultheis, J. Kuhl, A. Honold, C.W. Tu: *Ultrafast phase relaxation of excitons via exciton-exciton and exciton-electron collisions,* Physical Review Letters, Vol.57, No.13, pp.1635-1638 (1986).

[5.4] J.-Y. Bigot, M.T. Portella, R.W. Schoenlein, J.E. Cunningham, C.V. Shank: *Two-dimensional carrier-carrier screening in a quantum well,* Physical Review Letters, Vol.67, No.5, pp.636-639 (1991).

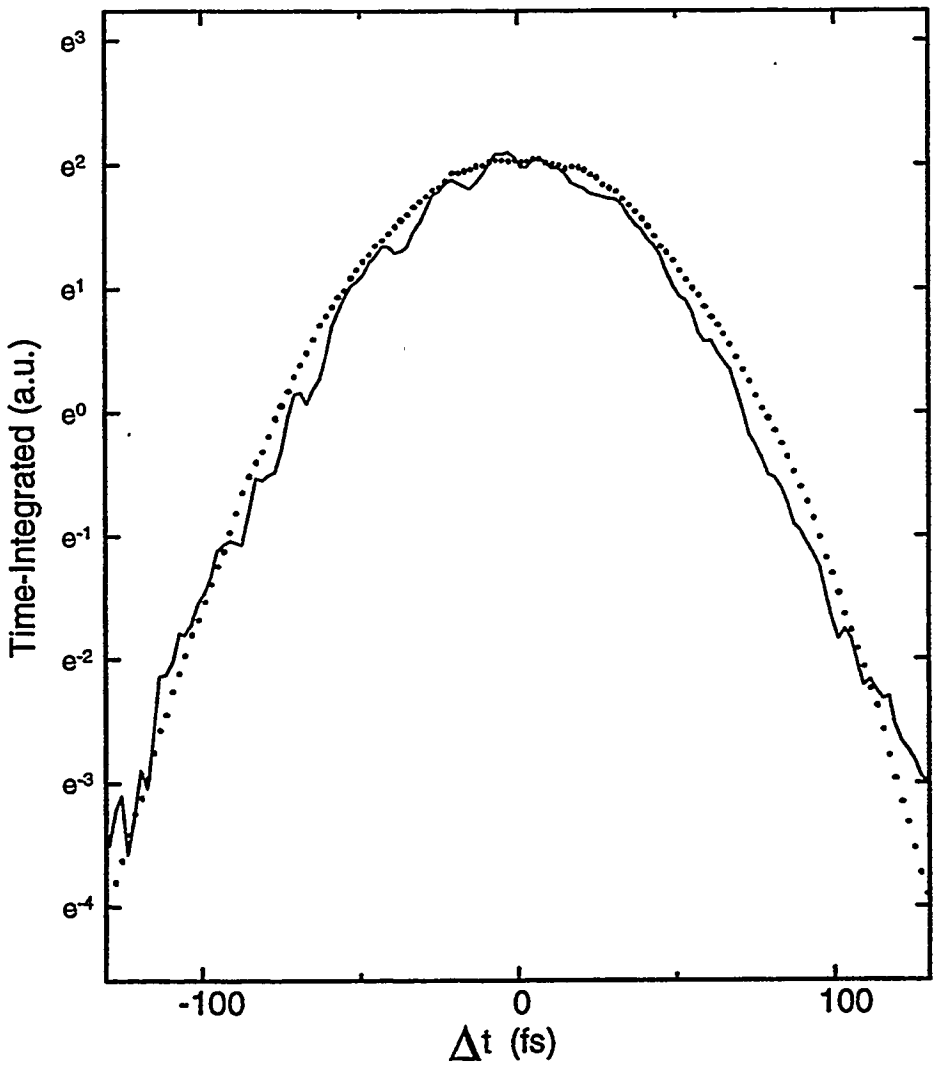

Figure 5.1: TI SWM lineshape measured at high excitation density $N_x \approx 10^{13}cm^{-2}$ (solid curve) compared with the noncolinear autocorrelation trace of the excitation laser pulse raised to the power 5/2 (dotted curve).

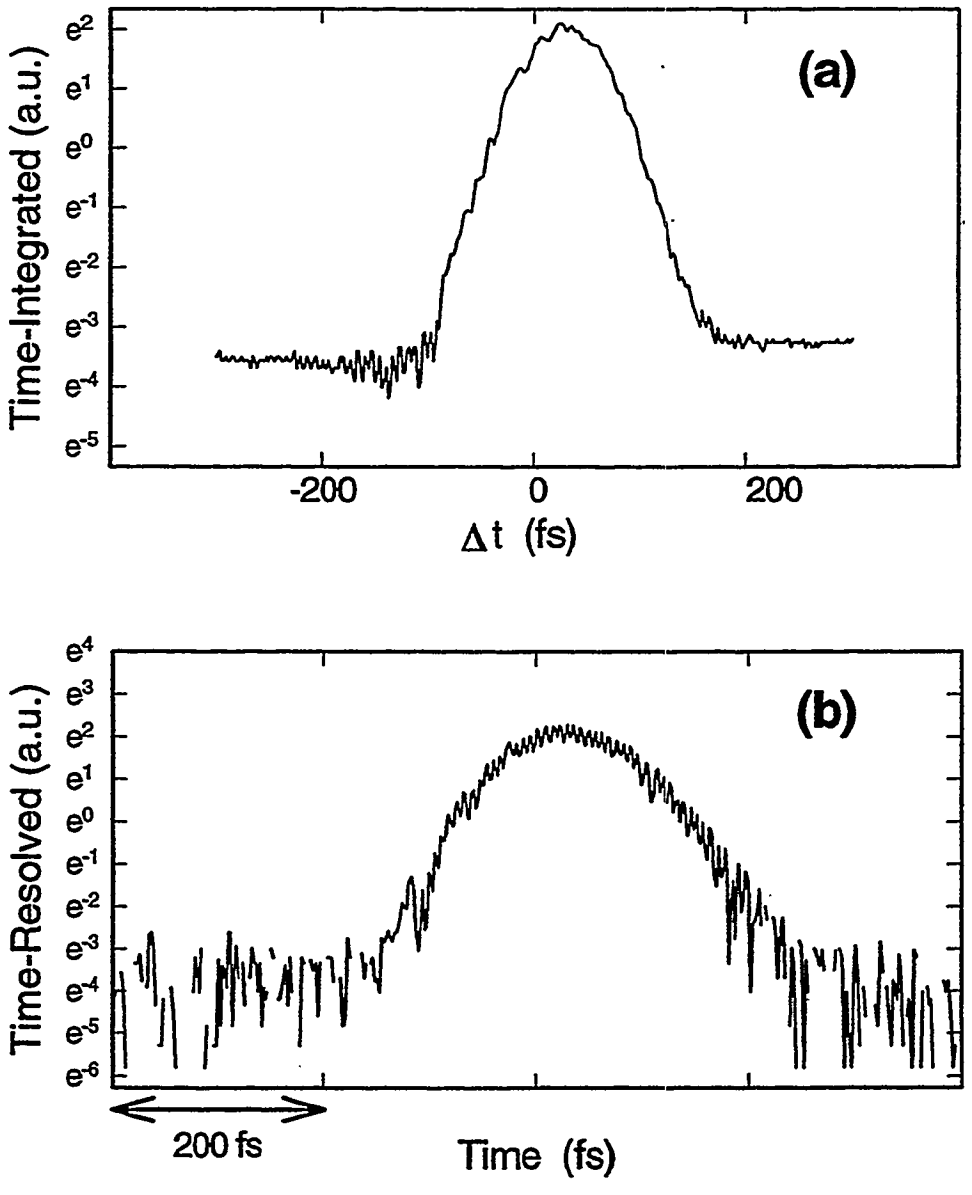

Figure 5.2: Symmetric TI SWM lineshape (a) vs. asymmetric TR SWM lineshape at Δt = +80fs (b). All data were taken at high excitation density $N_x \approx 10^{13} cm^{-2}$.

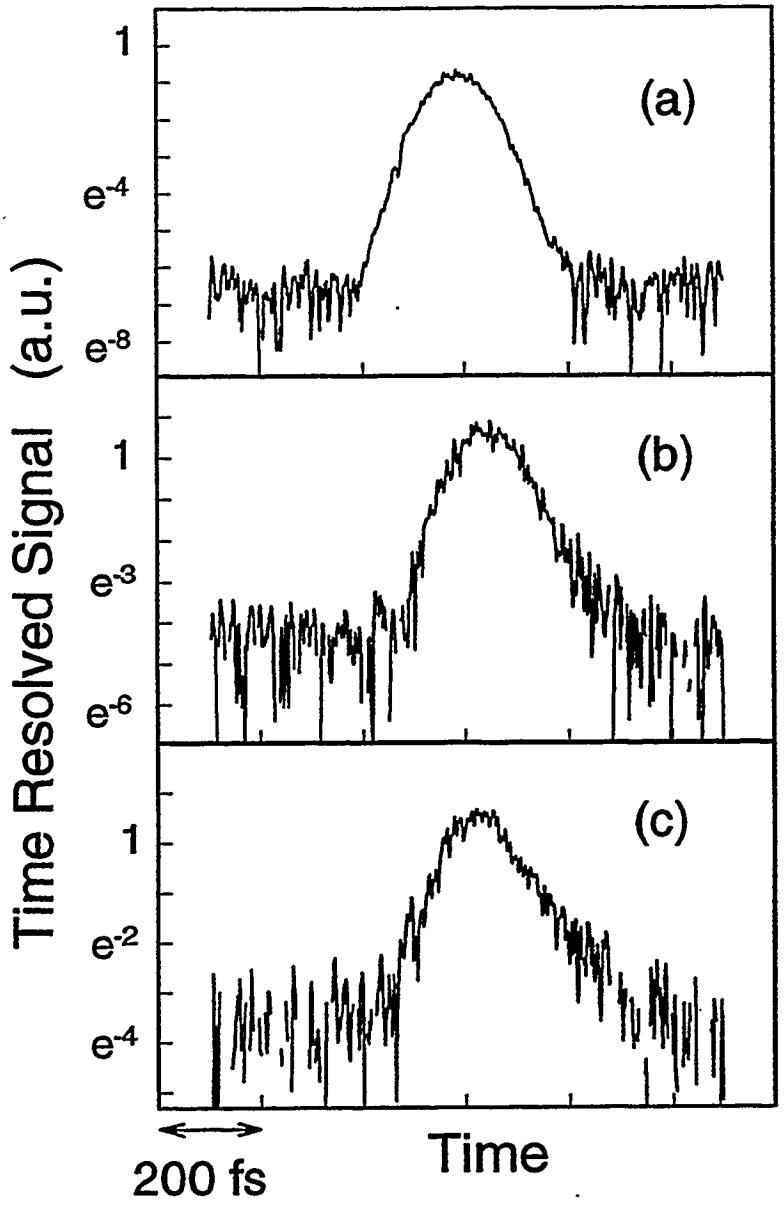

Figure 5.3: TR SWM lineshapes measured at $\Delta t = 0$ for excitation densities (a) $N_x \approx 10^{13}cm^{-2}$, (b) $N_x \approx 4x10^{12}cm^{-2}$, and (c) $N_x \approx 2x10^{12}cm^{-2}$. The dephasing times extracted from the TR decays are: (a) $T_2 \approx 54fs$; (b) $T_2 \approx 84fs$; (c) $T_2 \approx 132fs$.

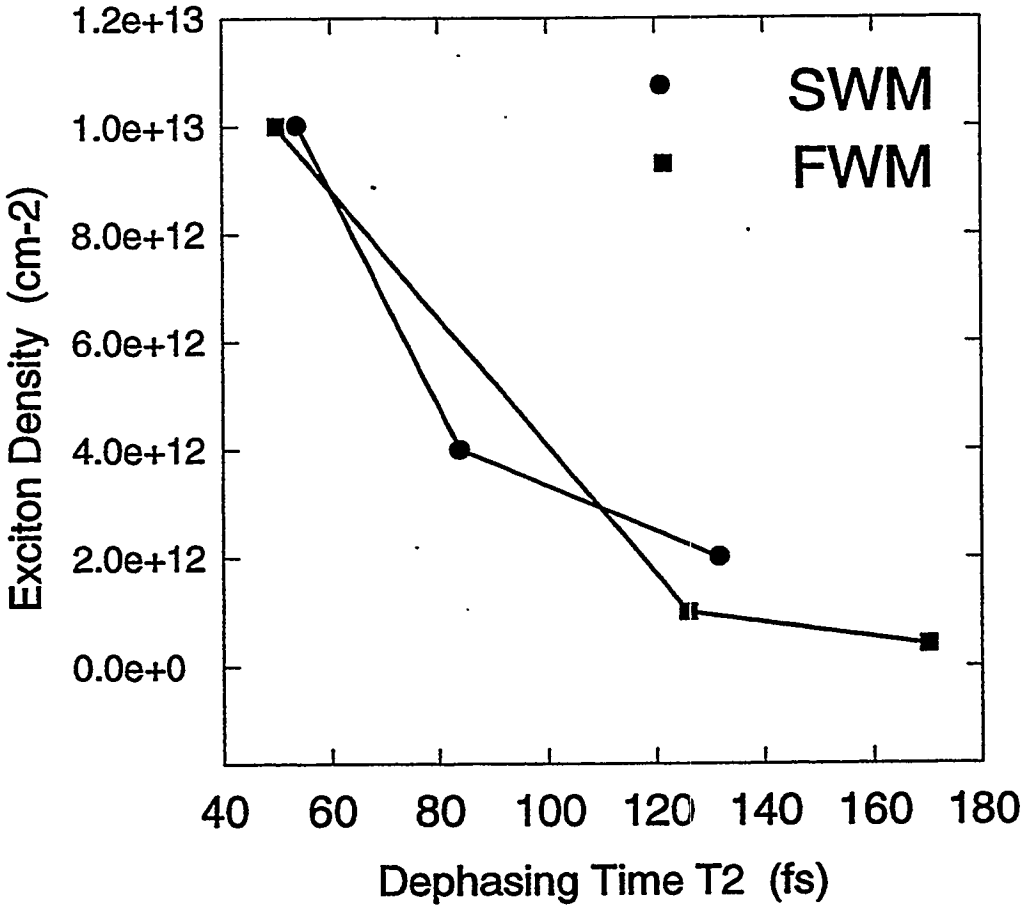

Figure 5.4: Comparison of dephasing times T_2 extracted from SWM (circles) and FWM (squares) measurements for several excitation densities.

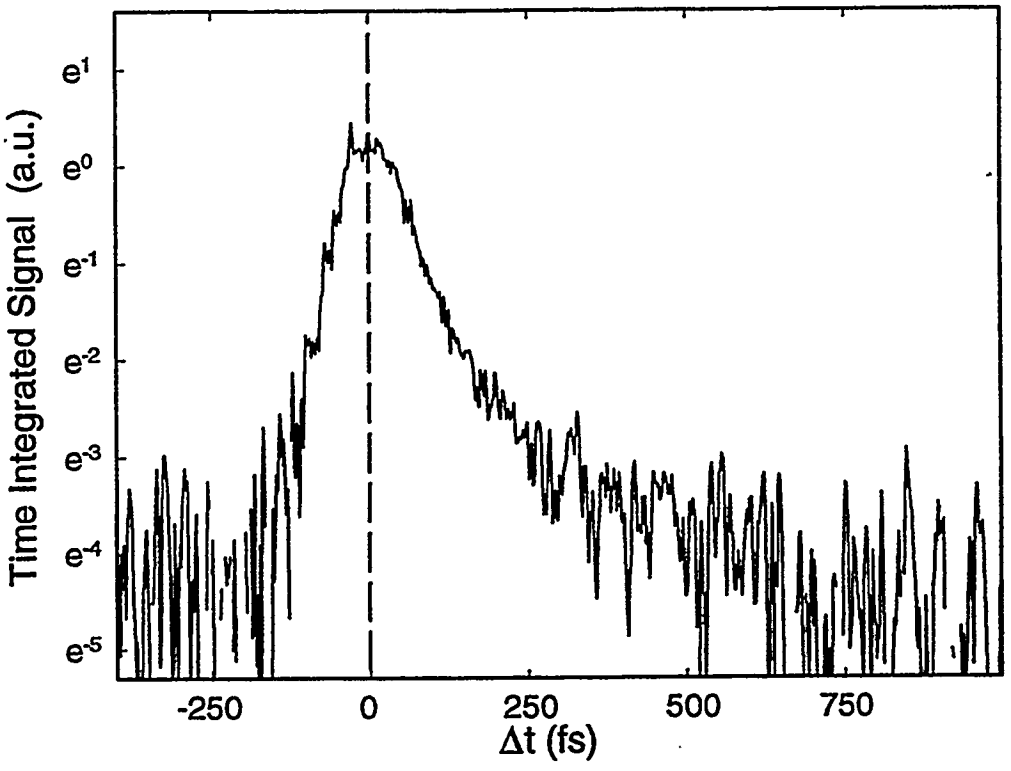

Figure 5.5: TI SWM trace at low excitation density $N_x \approx 2.7 \times 10^{11} cm^{-2}$. The dashed line is a visual aid to demonstrate the asymmetry of the curve.

Chapter 6

Ultrafast Response via Four-Wave Mixing: Phase Measurements

6.1 Introduction

We have shown that time-integrated (TI) and time-resolved (TR) multi-wave mixing measurements are both important techniques for detecting signatures of Coulomb correlation in the ultrafast coherent emission from semiconductors. Both four- and six-wave mixing (FWM, SWM) signals detected in TI and TR experiments fit very well into the theoretical predictions for the *amplitude* of the multi-wave mixing emission presented in Ch.2. For example, as demonstrated in Ch.4, at the lowest excitation densities the TR FWM profile displayed both prompt and delayed contributions to the emission. This allowed us to directly resolve the instantaneous nonlinear polarization response due to phase-space filling (PSF) and the time-delayed polarization-wave scattering (PWS) response due to Coulomb correlation. Importantly, the theoretical models in Ch.2 also indicate that the PSF and PWS contributions to the coherent emission are "out of phase," thus predicting a dynamic instantaneous frequency evolution throughout the duration of the emitted pulse, resulting from Coulomb correlation. In the absence of Coulomb correlation, there is no such change of phase, i.e. the emitted pulse is chirp-free.

Using the interferometric techniques described in Ch.3., we set out to fully characterize the FWM signal from 2-D excitons in GaAs quantum wells. This requires resolving not only the amplitude of the ultrashort emitted pulse, but also the *phase*. We find that by combining frequency domain power spectrum measurements with interferometric time domain measurements, coupled with our knowledge of the amplitude decay from Ch.4, we obtain information on the instantaneous frequency dynamics of the coherent emission. Our results demonstrate for the first time that Coulomb correlation does, in fact, affect both the amplitude and the phase of multi-wave mixing signals from semiconductors. [6.1] [6.2] [6.3]

The chapter is organized as follows. After discussing the experimental method in section 6.2, we present the results of our time- and frequency-domain characterization. We begin, in section 6.3, with a demonstration of the techniques used in this chapter by directly measuring a quantum beat in the FWM emission from a "three-level" system created by simultaneous excitation of the heavy-hole (hh) and light-hole (lh) excitons in the quantum well. We then present measurements of the coherent emission from selectively excited hh-excitons and study the effect of Coulomb correlation on the instantaneous frequency dynamics in section 6.4. As in Chs.4 and 5, our observations are in good agreement with the predictions of the theoretical models presented in Ch.2. Finally, we summarize our results and conclude the discussion in section 6.5.

6.2 Experiment

We performed transient, two-pulse FWM experiments on a multiple quantum well (MQW) structure consisting of 50 periods of 95 Å wide GaAs wells with 45 Å wide $Al_{0.3}Ga_{0.7}As$ barrier layers. The sample was prepared as described in Ch.3 and held at room temperature for all experiments. The absorption spectrum of the sample is presented in Fig.6.1, which clearly shows the n = 1 hh-exciton at energy 1.467 eV and the n = 1 lh-exciton at energy 1.482 eV. A typical power spectrum of the 80-100 fs long pulses from the Ti:sapphire oscillator is illustrated by the shaded region in the figure. The laser is specified completely in Ch.3 The FWHM (full width at half-maximum) of the laser pulse power spectrum was typically around 30 meV. Thus, it was large enough to easily cover both the hh- and lh-exciton resonances, which are separated by 15 meV. The laser pulse was tuned around the n = 1 excitons, as explained below, to allow for simultaneous excitation of both the hh- and lh-excitons or selective excitation of the hh-exciton only.

We measure the FWM emission in direction $2k_2$-k_1, as explained in Chs. 2 and 3. To characterize the instantaneous frequency dynamics, we measure three quantities described in detail in Ch.3:

1.) The FWM power spectrum, $S_{PS}(\omega, \Delta t)$ (Eqn.3-5).

2.) The first-order interferometric auto-correlation measurement of the FWM emission, $S_{1\text{-}IAC}(\tau,\Delta t)$ (Eqn.3-6), referred to hereafter as the IAC measurement.

3.) The first-order interferometric cross-correlation measurement of the FWM emission, $S_{1\text{-}ICC}(u,\Delta t)$ (Eqn.3-7), referred to hereafter as the ICC measurement.

These measurements provide us with a *simultaneous* time-frequency description of the FWM signal, which we interpret in light of the amplitude characterization discussed in Ch.4.

It is important to recall that the instantaneous frequency dynamics itself is determined from a *differential* measurement: the differential fringe spacing (DFS(τ)), explained in detail in Ch.3. The DFS(τ) is obtained by first measuring the IAC of the signal we are interested in characterizing and then measuring the shift of those IAC fringes relative to a reference. The ideal "ruler" we use as a reference is the IAC fringe pattern of the transform-limited laser pulse traveling through the same optical elements as the signal. In this way the differential measurement corrects for all sources of dispersion in the optical set-up, which add chirp to both the signal and the reference pulse. Recall that the DFS(τ) reproduces the temporal evolution of the phase, as illustrated for the case of "linear" chirp (a simple frequency shift) in Fig.3.7. For this simplified case it is easy to see that if the signal and the reference are at the same frequency, the DFS(τ) measurement will be a straight line of zero slope. On the other hand, if the signal and the reference are at different frequencies (as in Fig.3.7), then the DFS(τ) measurement will be a straight line of non-zero slope. Naturally, by measuring the slope of the DFS(τ) measurement one can determine the actual instantaneous frequency of the signal, since one knows the reference frequency from power spectrum measurements of the laser pulse. Furthermore, a *nonlinear* DFS(τ) evolution thus indicates higher-order, nonlinear phase changes during the temporal evolution of the signal, i.e. the presence of chirp on the signal pulse itself. Thus, we interpret any instantaneous frequency changes observed on the DFS(τ)

measurement of the FWM signal as an effect due solely to the intrinsic dynamics of Coulomb correlated excitons in the MQW sample. We begin our investigation of the instantaneous frequency dynamics of the coherent FWM emission by simultaneously exciting both hh- and lh-excitons in the next section. Then, in section 6.4, we examine the dynamic nonlinear optical response exhibited by hh-excitons when they alone are selectively excited.

6.3 Quantum beats

It is instructive to examine the simultaneous excitation of hh- and lh-excitons for several reasons. First, the IAC measurement provides a beautiful visual demonstration of the phenomenon of quantum beats in the coherent emission from semiconductor heterostructures. Second, it reveals the instantaneous frequency dynamics behind the beating process, which has never been measured experimentally for such systems. Third, it clearly illustrates the precision of the interferometric measurements we will use to study the effects of Coulomb correlation on the phase of the coherent FWM emission, in section 6.4.

In order to simultaneously excite both the hh- and lh-exciton resonances, the excitation laser is tuned so that the central wavelength of the pulse is at approximately 1.482 eV, the energy of the lh-exciton. Because of the spectral bandwidth of the ultrashort pulse, the hh-exciton resonance is also excited. In this case, we expect the coherent FWM emission to contain contributions from both excited resonances. This is

indeed the case, as illustrated in Fig.6.2, which shows the power spectrum of the FWM emission (thick curve) for time-delay $\Delta t = 0$ and excitation density $N_x \approx 3x10^9$ cm^{-2}. As expected, we see two large peaks in the FWM power spectrum at the energies of the hh- and lh-exciton. The excitation laser pulse (thin curve) is shown for comparison. It is important to note that two pieces of information are missing from the power spectrum measurement. First, it is not clear whether the FWM emission comes from two distinct and independent two-level systems, the hh-exciton and the lh-exciton, or from a single "three-level" system consisting of the hh- and lh-excitons quantum mechanically coupled to a common ground state. Second, the power spectrum measurement indicates that radiation is emitted at both the hh- and lh-exciton energies, but it does not reveal the dynamics of the instantaneous frequency during the course of the emission.

We can address both these points by examining the response in the time-domain. The distinction between the transient response from two independent two-level systems and from a single three-level system has been investigated experimentally for a variety of systems including dilute atomic vapors [6.4] and semiconductor heterostructures [6.5] [6.6] [6.7]. When two closely spaced resonances are excited simultaneously, we expect to observe a beating modulation in the time-domain, which was observed by these experiments. Recently, an experimental method using TR FWM was developed to distinguish between quantum beats from a three-level system and polarization interference from two independent two-level systems. [6.8] The method was demonstrated for specially designed GaAs MQW structures, but the basic idea is simple. If the excitation laser pulse creates a collection of identical three-level systems, then the entire system is

homogeneously broadened and therefore the coherent emission is a free-induction decay (FID) process. On the other hand, if the excitation pulse creates two distinct collections of independent two-level systems, then the entire system is inhomogeneously broadened and therefore the coherent emission is a photon echo.

We have already demonstrated in Ch.4. that by time-resolving the FWM emission via intensity cross-correlation and plotting the relative positions of the maxima of the TR FWM signals vs. Δt, we could distinguish between FID and photon echo processes. (See Figs.4.4 and 4.6.) Here we use the same principle with the first-order *interferometric* cross-correlation (ICC) measurement described above. Fig.6.3 shows a typical ICC trace of the FWM emission for simultaneous excitation of the hh- and lh-exciton resonances. The data are taken at low excitation density $N_x \approx 3x10^{10}$ cm^{-2} and for $\Delta t = 0$. The beating pattern expected in the time-domain is clearly visible in the figure. The beating modulation on the ICC envelope has a measured period, T, of approximately 280 fs. This corresponds well to the energy separation, ΔE, between the hh- and lh-excitons: $\Delta E = 15$ meV $= (h\,\Delta\nu) = (h / T)$ gives T = 275 fs. We use the amplitude information afforded by the ICC envelope to determine whether the beat we observe is a quantum beat or the result of polarization interference. As explained above, we vary the time-delay Δt and measure the relative position of the first peak of the ICC envelope. Results of the measurements for two excitation densities are shown as the filled circles in Fig.6.4. Also plotted in the figure are the evolutions expected for FID signals (hollow circles) and for photon echoes (triangles), following the analysis of Yajima and Taira for non-interacting systems under δ-function pulsed excitation. (See Ch.2 and reference [6.9].) At both low

excitation density (a) $N_x \approx 3x10^{10}$ cm^{-2} and high excitation density (b) $N_x \approx 3x10^{11}$ cm^{-2} the data clearly follow the evolution of a FID decay signal from a homogeneously broadened system. (We note that for $\Delta t < 0$ the analysis of Yajima and Taira predicts no FWM emission. Experimentally the signals measured for $\Delta t < 0$ are due to the finite duration of the 100 fs excitation pulses plus contributions from PWS via Coulomb correlation. In any case, the signals at $\Delta t < 0$ do not affect the results stated here.) Thus, these ICC measurements indicate that the coherent FWM emission is a FID signal from a homogeneously broadened system. This is consistent with the room temperature measurements on a similar quantum well sample presented in Ch.4. Thus, under simultaneous excitation of the hh- and lh-exciton resonances, the modulation in the ICC envelope of the FWM signal is the result of a quantum beat from a collection of three-level systems.

We now determine the instantaneous frequency dynamics missing from the FWM power spectrum shown in Fig.6.2, by measuring the first-order interferometric auto-correlation (IAC) of the FWM emission taken under identical experimental conditions. The result is shown in Fig.6.5(a). As with the ICC, we observe a pronounced beating modulation in the envelope of the fringes. The beat period measured from this data is approximately 275 fs, which is in excellent agreement with the separation in energy between hh- and lh-excitons, as described above. We determine the instantaneous frequency dynamics of this FWM emission by measuring the DFS(τ) (Fig.6.5(b)), as described above. (The reference used for DFS(τ) is the IAC of the laser pulse whose power spectrum is also shown in Fig.6.2.) Simultaneously comparing the FWM power

spectrum (Fig.6.2), the IAC of Fig.6.5(a), and the DFS(τ) of Fig.6.5(b), we can see the evolution of the instantaneous frequency of the emitted FWM pulse. Between $\tau = 0$ and $\tau \approx 60$ fs the slope of DFS(τ) is zero, which means that the FWM emission is at the frequency of the laser, which is the frequency of the lh-exciton resonance. Thus, initially the FWM emission is dominated by the contribution from the lh-exciton. Gradually, though, the frequency of the emission begins to shift and between $\tau \approx 80$ - 120 fs there is an abrupt phase shift of π as the emission goes through the first beat node in Fig.6.5(a). Finally, after about 120 fs, DFS(τ) is again nearly linear with a non-zero slope. The measured value of the slope indicates that after approximately 120 fs the FWM emission is dominated by the contribution from the hh-exciton. Because of the fundamental quantum limit imposed by the uncertainty principle, the change of frequency during the beating process is not instantaneous. In fact, the change of phase takes ≈ 60 fs to complete, which places the measured duration of the quantum beat only about 40% above the quantum limit.

To demonstrate the simplicity behind this type of interferometric analysis, we show as the thick curve in Fig.6.6 a close-up of the fringes around the first beat node ($\tau \approx 100$ fs) presented in the IAC of Fig.6.5(a). Note that the amplitude of the curve first decreases and then increases as the fringes pass through the beat node itself. For comparison and as a reference we have superimposed fringes (thin curve) taken from around $\tau \approx 0$ in the IAC of Fig.6.5(a). On the left side of the figure we have aligned the two curves so that they are in phase. It is clear that the beat node fringes step out of phase with the "reference"

curve after only about 12 optical cycles. Thus the IAC and corresponding DFS(τ) clearly indicate the instantaneous frequency dynamics of the coherent emission missing from the FWM power spectrum measurement of Fig.6.2 alone. In this way, using the three techniques simultaneously, we obtain information on the dynamics of the phase evolution of the ultrafast coherent emission from the sample.

6.4 Instantaneous frequency dynamics

To measure the effects of Coulomb correlation on the instantaneous frequency dynamics it is best to remove the complications added by the quantum beating from simultaneously excited resonances. For this reason, we tune the excitation laser pulse to a position slightly below the hh-exciton resonance. In this way we selectively excite a collection of hh-excitons only. We use the same techniques of FWM power spectrum, IAC, and DFS(τ) shown for the case of quantum beats above to obtain simultaneous time and frequency measurements of the nonlinear optical response. We extract the phase information from the DFS(τ) and observe effects which we attribute to Coulomb correlation.

At low excitation density $N_x \approx 3x10^9$ cm^{-2} and for time-delay $\Delta t = 0$, Fig.6.7 shows the results of these three measurements for the FWM emission induced under the excitation conditions described above. The power spectrum is shown as the thick curve in Fig.6.7(a), which also shows the power spectrum of the detuned excitation laser pulse

(thin curve) for comparison. Clearly the FWM power spectrum is highly asymmetric, indicating the presence of chirp on the emitted FWM pulse. The power spectrum measurement shows a pronounced contribution to the FWM emission from the hh-exciton with some FWM frequency components at the central frequency of the laser. We verify the presence of chirp directly by measuring the IAC and the corresponding DFS(τ) under identical excitation conditions, Fig.6.7(b) and (c). The IAC measurement shows a very long decay, extending out to over 400 fs, at this low density due to the slow polarization dephasing time (T_2), as was illustrated via TR FWM measurements in Ch.4 and TR SWM measurements in Ch.5. The corresponding DFS(τ) shows the nonlinear phase dynamics (chirp) expected from the power spectrum measurements and also gives the temporal evolution of the instantaneous frequency. From the DFS(τ) we see that the FWM emission actually starts out with the dominant contribution from the hh-exciton (the non-zero slope of the DFS(τ) corresponds to the de-tuning of the reference laser pulse relative to the hh-exciton) and after approximately 250 fs the FWM emission drifts to the frequency of the laser (zero slope portion of the DFS(τ)). Again, by simultaneously measuring the time and frequency domain response we obtain information not revealed by power spectrum measurements alone. As explained in Ch.2, this dynamic frequency change is caused by the combination of the instantaneous contribution to the FWM emission, due to phase space filling (PSF), and the delayed contribution to the FWM emission, from polarization wave scattering (PWS) via Coulomb correlation. Thus the presence of Coulomb correlation at this low excitation density *does* effect the instantaneous frequency dynamics of the FWM emission. This is consistent with the

models presented in Ch.2 and with the results of FWM and SWM amplitude measurements presented in Chs.4 and 5. In this sense, the nonlinear phase dynamics is a "signature" for Coulomb correlation.

To verify that these effects are the result of Coulomb correlation we varied the excitation density and performed these same measurements. From the discussions of Chs.4 and 5 we demonstrated that at high excitation densities effects due to Coulomb correlation disappear. This occurs because at high excitation densities there are more free electron-hole pairs present, due to exciton ionization via collisions, which act to screen the Coulomb correlation. Thus at high excitation density the system of excitons is reduced to a collection of independent two-level systems. In Fig.6.8 we present FWM power spectrum data taken at $\Delta t = 0$ over a wide range of excitation densities: (a) $N_x \approx 3x10^9$ cm^{-2}; (b) $N_x \approx 1.2x10^{10}$ cm^{-2}; (c) $N_x \approx 6x10^{10}$ cm^{-2}; (d) $N_x \approx 3x10^{11}$ cm^{-2}. At the lowest density we have the data presented in Fig.6.7(a). As the excitation density is raised the FWM power spectrum becomes more symmetric and eventually approaches the lineshape of the laser. We interpret the increasing symmetry as a reflection of the reduced Coulomb correlation resulting from increased screening at high excitation densities. These results are qualitatively equivalent to the trends observed in the TR FWM traces we fit numerically in Ch.4. As the excitation density is raised, the polarization dephasing time T_2 decreases, thus diminishing the delayed PWS contribution to the emission. This leaves only the instantaneous PSF contribution and so, at high excitation densities, the FWM emission becomes chirp-free.

We further confirm this interpretation by directly measuring the FWM instantaneous frequency dynamics via the IAC and corresponding DFS(τ), as shown in Fig.6.9 for low and high excitation densities:(b) $N_x \approx 3x10^9$ cm^{-2} and (c) $N_x \approx 3x10^{11}$ cm^{-2}. For comparison, the IAC and corresponding DFS(τ) for the excitation laser pulse are shown in Fig.6.9(a). The low excitation density FWM data shows the long decay coupled with the nonlinear phase dynamics discussed above. The high excitation density FWM data is completely different from the low density result. First, the decay of the high density IAC is very fast, almost as fast as the 100 fs laser pulse itself. This is due to the fast polarization dephasing time T_2 at high excitation density, as shown with the amplitude TR FWM data in Ch.4. Second, the corresponding DFS(τ) is a straight line, indicating a constant phase throughout the emitted FWM pulse. This absence of nonlinear phase dynamics is attributed to the screening of the Coulomb correlation at high excitation densities. Thus, these direct time-domain measurements are consistent with both the interpretation of the power spectra measurements described above and with the results obtained via amplitude FWM measurements in Ch.4.

6.5 Summary and conclusions

We have measured the ultrafast FWM emission from 2-D excitons in GaAs MQWs in both the time and frequency domains via power spectrum and interferometric correlation experiments. By comparing the simultaneous measurements, we observed quantum beats

in the nonlinear optical response from multiply excited resonances. The accuracy of these interferometric measurements is sufficient to determine that the duration of the beat is only about 40% above the fundamental quantum limit.

Furthermore, we have demonstrated for the first time that the instantaneous frequency dynamics of the FWM emission from semiconductors is strongly influenced by the presence of Coulomb correlation. The signature for Coulomb correlation detected here is qualitatively consistent with the theoretical model for dense media presented in Ch.2 and with the experimental results obtained in amplitude measurements of the FWM signal presented in Ch.4. Our results are also consistent, qualitatively, with numerical solutions to the semiconductor Bloch equations (SBE). [6.3] Importantly, our measurements have also highlighted *limitations* to the SBE, which currently provide the most complete description of semiconductor nonlinear optical response. In the next chapter we discuss how these limitations indicate new directions for future research.

References

[6.1] J.-Y. Bigot, M.-A. Mycek, S. Weiss, R.G. Ulbrich, D.S. Chemla: *Instantaneous frequency dynamics of coherent wave mixing in semiconductor quantum wells*, Physical Review Letters, Vol.70, No.21, pp.3307-3310 (1993).

[6.2] J.-Y. Bigot, M.-A. Mycek, S. Weiss, R.G. Ulbrich, and D.S. Chemla: *Amplitude decay and instantaneous frequency dynamics of excitonic polarization in*

semiconductor quantum wells, in *Coherent Optical Interactions in Semiconductors*, (R.T. Phillips, Ed.), Plenum Press, New York, pp.245-260 (1994).

[6.3] D.S. Chemla, J.-Y. Bigot, M.-A. Mycek, S. Weiss, W. Schafer: *Ultrafast phase dynamics of coherent emission from excitons in GaAs quantum wells*, Physical Review B, Vol.50, No.12, pp.8439-8453 (1994).

[6.4] J.E. Rothenberg and D. Grischkowsky: *Observation of a 1.9 ps polarization beat*, Optics Letters, Vol.10, No.1, pp.22-24 (1985).

[6.5] E.O. Gobel, K. Leo, T.C. Damen, J. Shah, S. Schmitt-Rink, W. Schafer, J.F. Muller, K. Kohler: *Quantum beats of excitons in quantum wells*, Physical Review Letters, Vol.64, No.15, pp.1801-1804 (1990).

[6.6] K. Leo, E.O. Gobel, T.C. Damen, J. Shah, S. Schmitt-Rink, W. Schafer, J.F. Muller, K. Kohler, P. Ganser: *Subpicosecond four-wave mixing in $GaAs/Al_xGa_{1-x}As$ quantum wells*, Physical Review A, Vol.44, No.11, pp.5726-5737 (1991).

[6.7] K. Leo, J. Shah, E.O. Gobel, T.C. Damen, S. Schmitt-Rink, W. Schafer, J.F. Muller, K. Kohler: *Quantum beats of excitons in quantum wells*, Modern Physics Letters B, Vol.5, No.2, pp.87-93 (1991).

[6.8] M. Koch, J. Feldman, G. von Plessen, E.O. Gobel, P. Thomas, K. Kohler: *Quantum beats versus polarization interference: An experimental distinction*, Physical Review Letters, Vol.69, No.25, pp.3631-3634 (1992).

[6.9] T. Yajima and Y. Taira: *Spatial optical parametric coupling of picosecond light pulses and transverse relaxation effect in resonant media*, Journal of the Physical Society of Japan, Vol.47, No.5, pp.1620-1626 (1979).

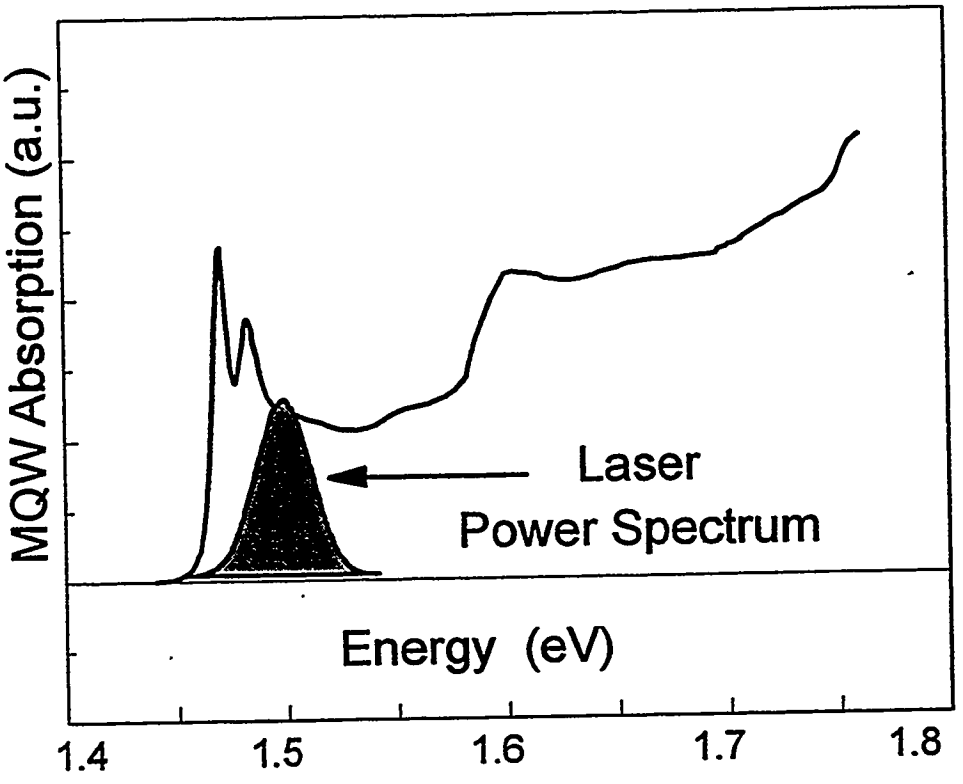

Figure 6.1: Absorption spectrum of the multiple quantum well sample at room temperature (solid line) showing the n=1 heavy- and light-hole excitons at 1.467 eV and 1.482 eV, respectively. The power spectrum of a typical excitation laser pulse (shaded region) is also shown. In these experiments, the laser was tuned above and below the heavy-hole resonance.

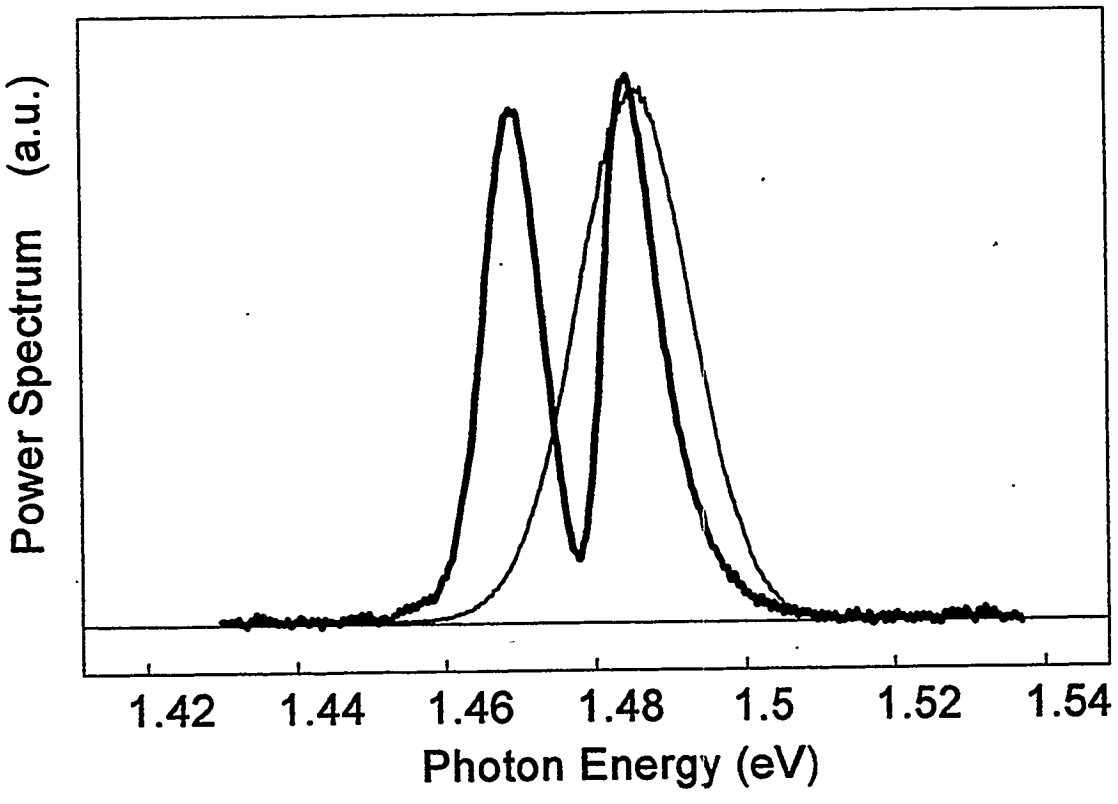

Figure 6.2: Four-wave mixing emission power spectrum (thick line) showing contributions from both the heavy- and light-hole excitons. The data is taken for excitation resonant with the light-hole exciton at excitation density $N_x \approx 3x10^9$ cm^{-2} and for time-delay $\Delta t = 0$. The excitation laser pulse (thin line) is shown for comparison.

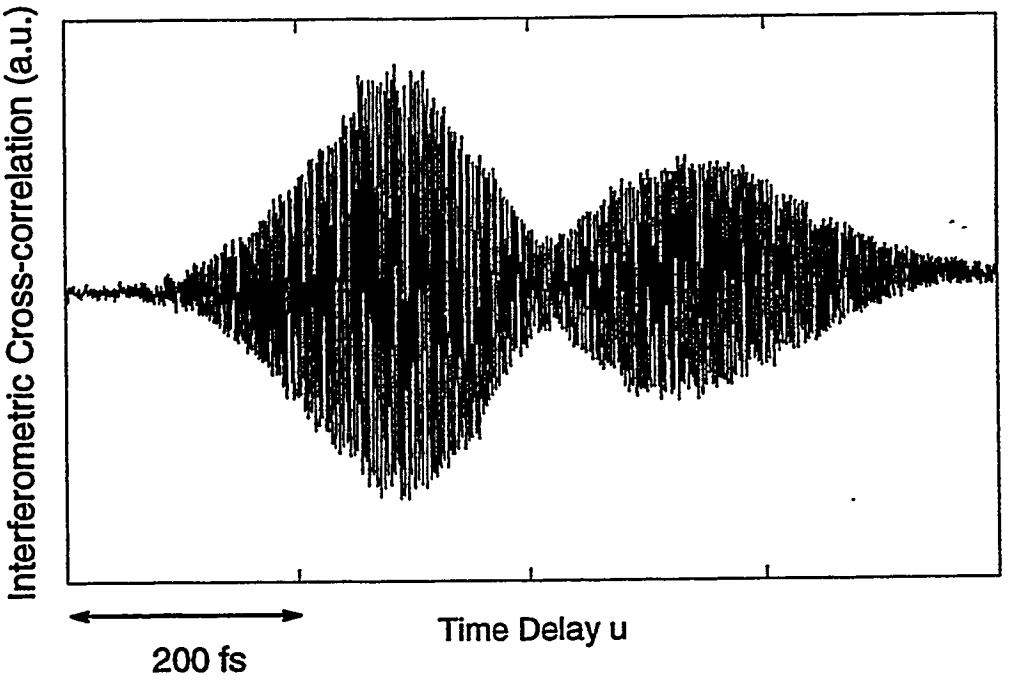

Figure 6.3: First-order interferometric cross-correlation of the FWM signal emitted for simultaneous excitation of the heavy- and light-hole excitons. The beating modulation of the envelope is obvious. The data are taken at low excitation density $N_x \approx 3x10^{10}$ cm^{-2} and time-delay $\Delta t = 0$.

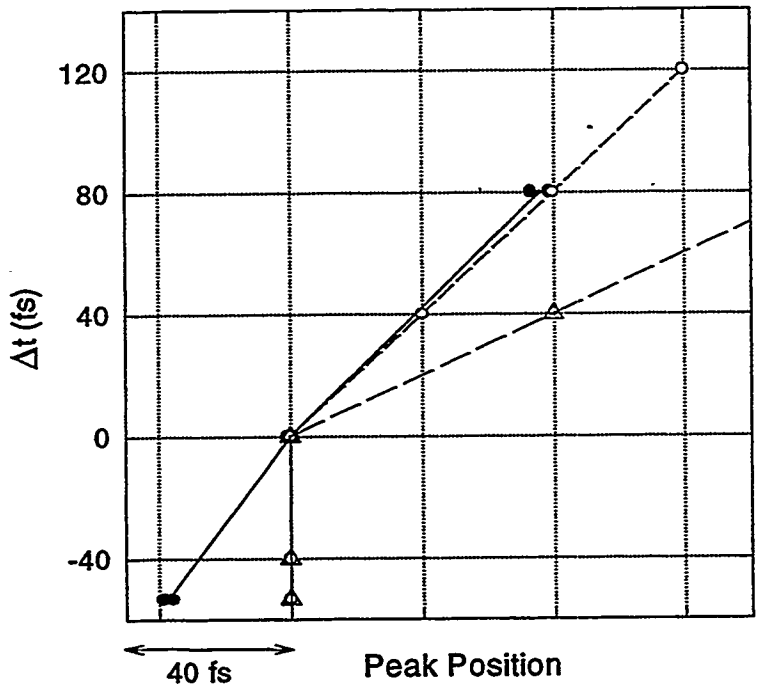

(a)

Figure 6.4(a): Relative positions of the maxima of the interferometric cross-correlation signals vs. time-delay Δt (filled circles). Evolutions expected for free induction decay signals (hollow circles) and for photon echoes (triangles) are also plotted. Data are taken for excitation density $N_x \approx 3x10^{10}$ cm^{-2}, as in Fig.6.3.

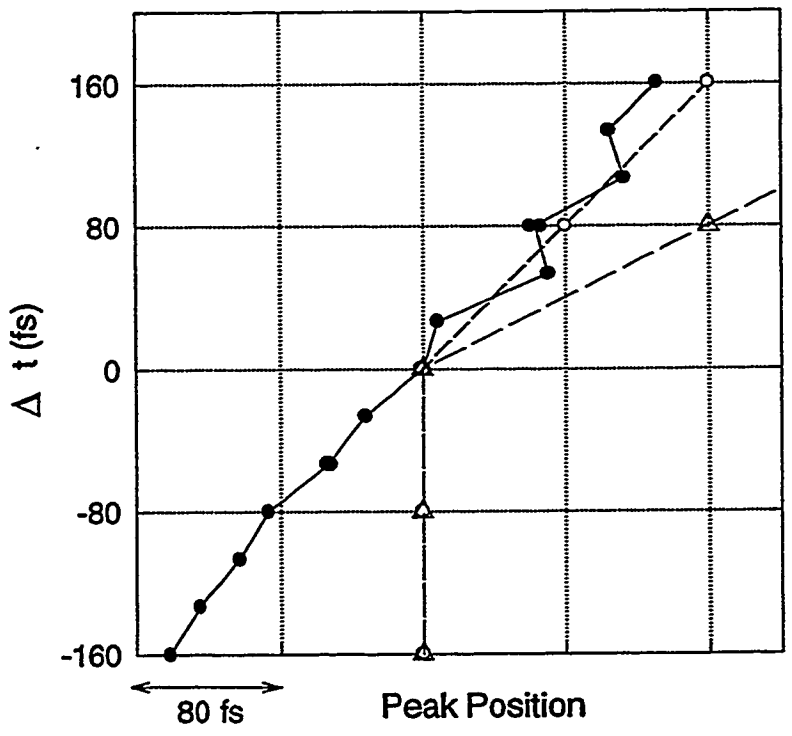

Figure 6.4(b): Relative positions of the maxima of the interferometric cross-correlation signals vs. time-delay Δt (filled circles). Evolutions expected for free induction decay signals (hollow circles) and for photon echoes (triangles) are also plotted. Data are taken for excitation density $N_x \approx 3 \times 10^{11}$ cm^{-2}.

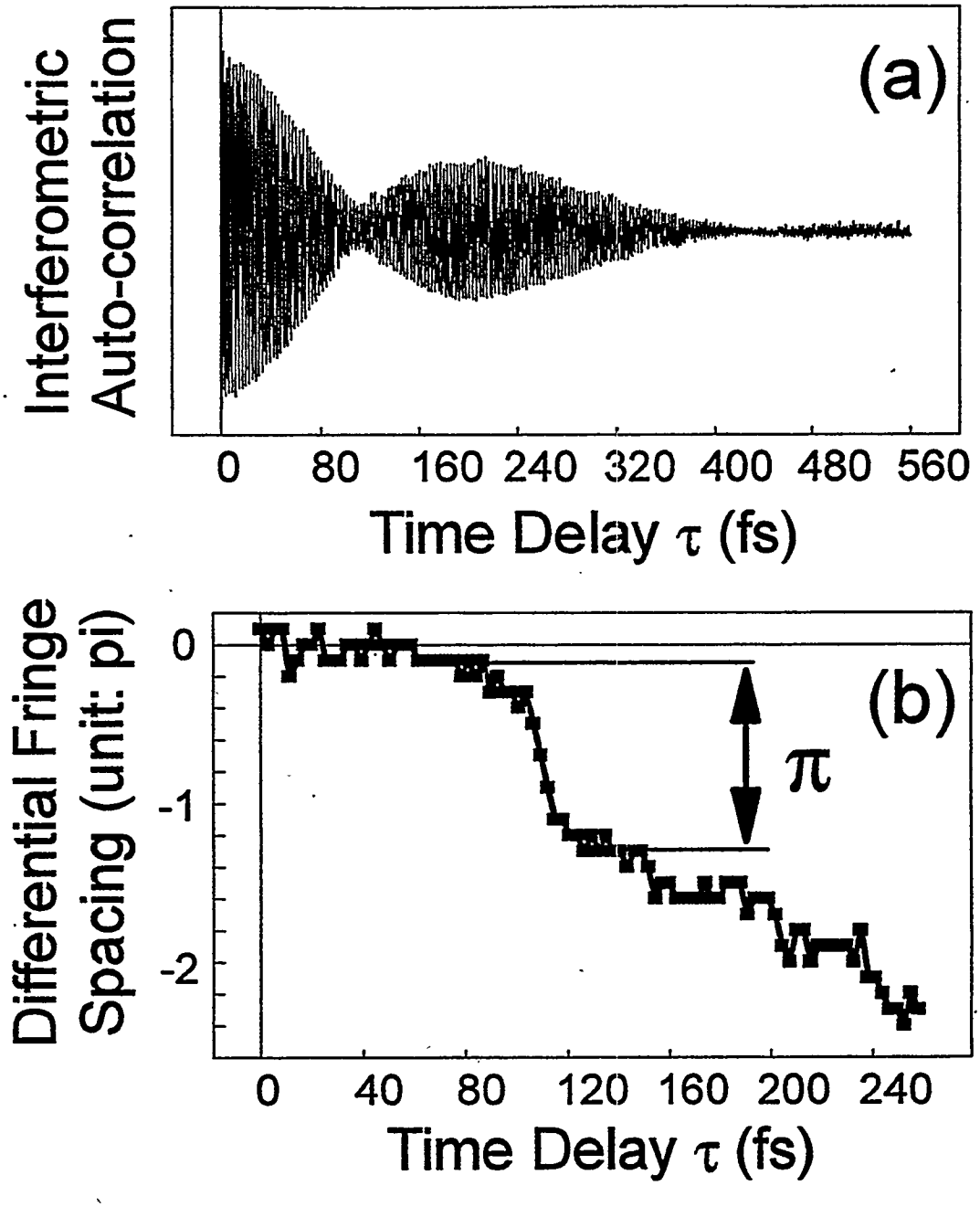

Figure 6.5: (a) First-order interferometric autocorrelation of the FWM signal, whose power spectrum is presented in Fig.6.2. (b) The corresponding DFS(τ) clearly showing the change of phase around the first beat node at approximately $\tau = 100$ fs.

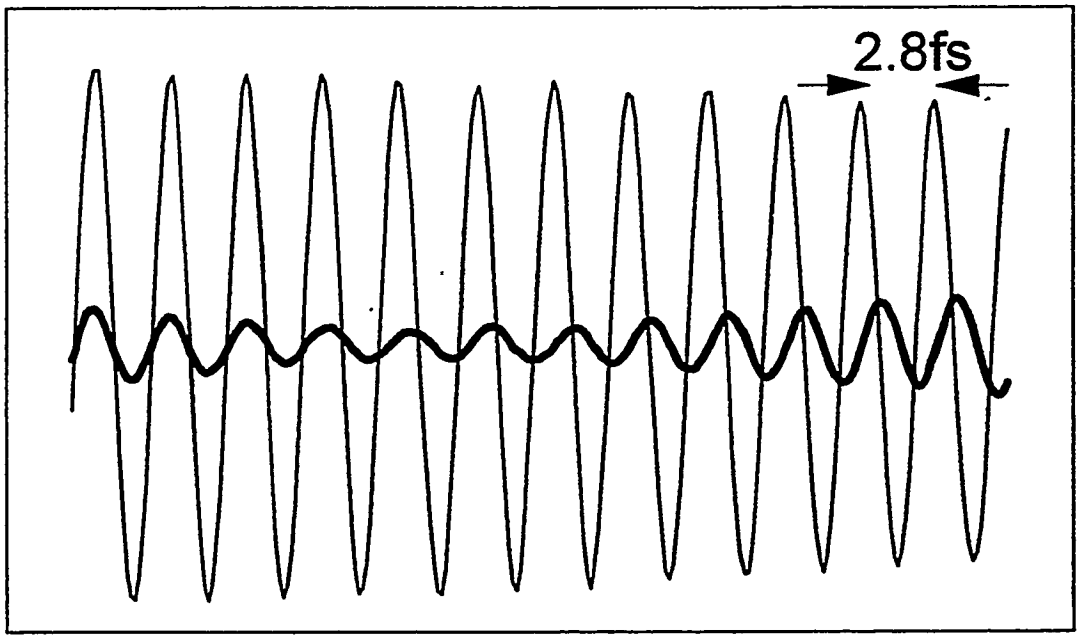

Figure 6.6: Close-up view of fringes from the experimentally measured interferometric autocorrelation of Fig.6.5. For comparison, the thin curve is taken from $\tau = 0$ fs and the thick curve is taken from around the beat node at approximately $\tau = 100$ fs. It is clear after only 12 fringes (33 fs) that the two curves are stepping out of phase with one another.

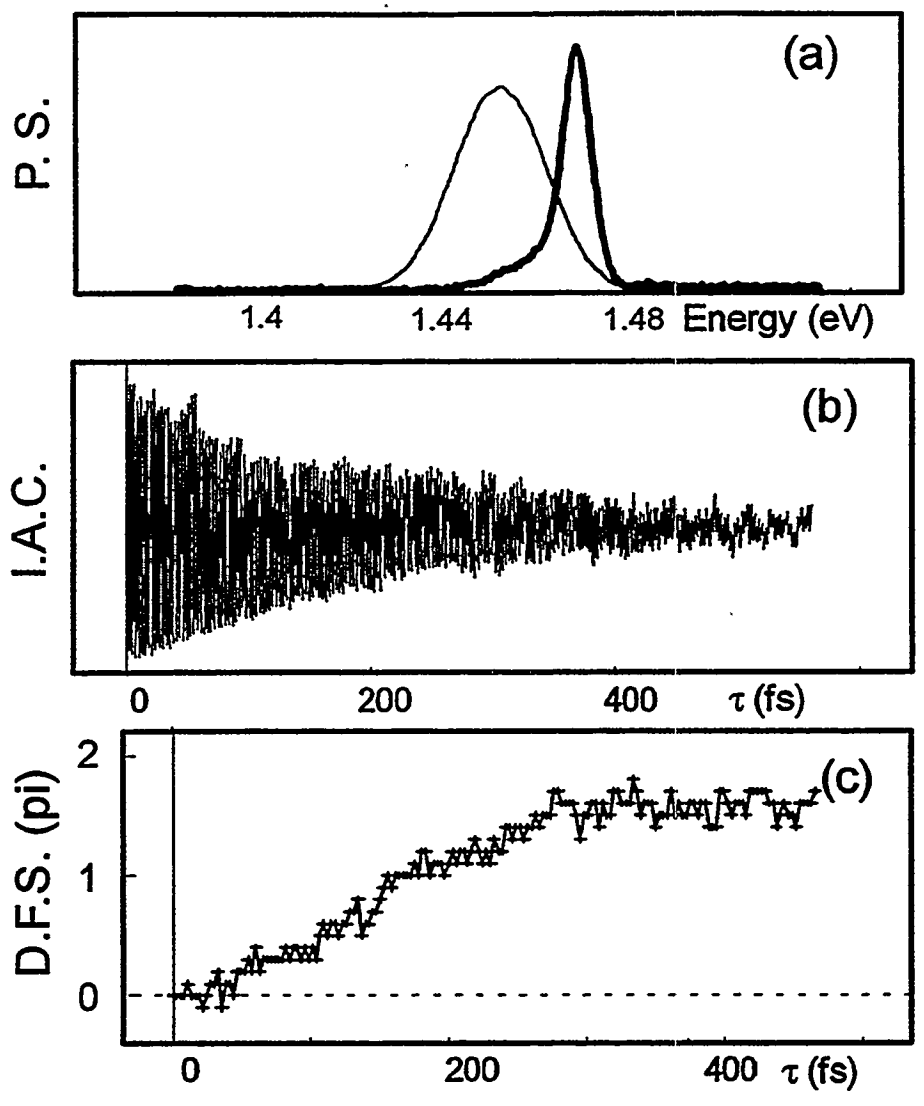

Figure 6.7: FWM data taken for selective excitation of the heavy-hole exciton at time-delay $\Delta t = 0$ and low excitation density $N_x \approx 3x10^9$ cm^{-2}. The FWM power spectrum (a) (thick line) is asymmetric compared to the laser pulse (thin line). The interferometric autocorrelation (b) of the FWM emission, taken under identical excitation conditions, is shown together with the corresponding differential fringe spacing (c).

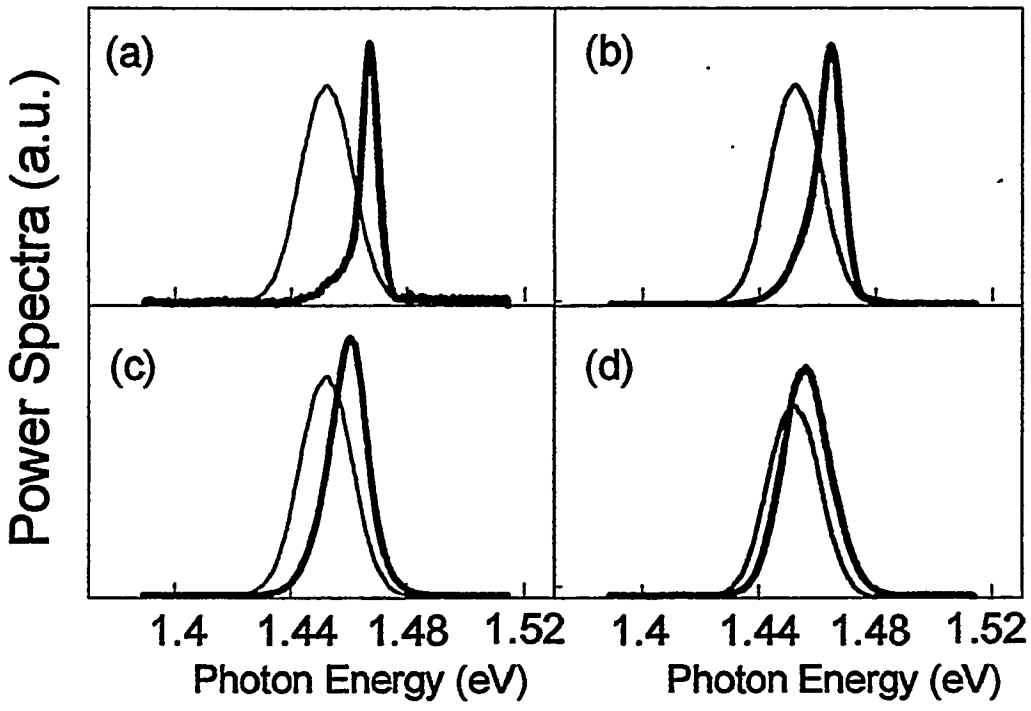

Figure 6.8: Power spectra of the FWM emission (thick curves) for time-delay $\Delta t = 0$ and excitation densities: (a) $N_x \approx 3x10^9 cm^{-2}$; (b) $N_x \approx 1.2x10^{10} cm^{-2}$;(c) $N_x \approx 6x10^{10} cm^{-2}$; (d) $N_x \approx 3x10^{11} cm^{-2}$. The power spectra of the excitation laser pulse (thin curves) is shown for comparison. For this experiment, the laser is tuned slightly below the heavy-hole exciton resonance.

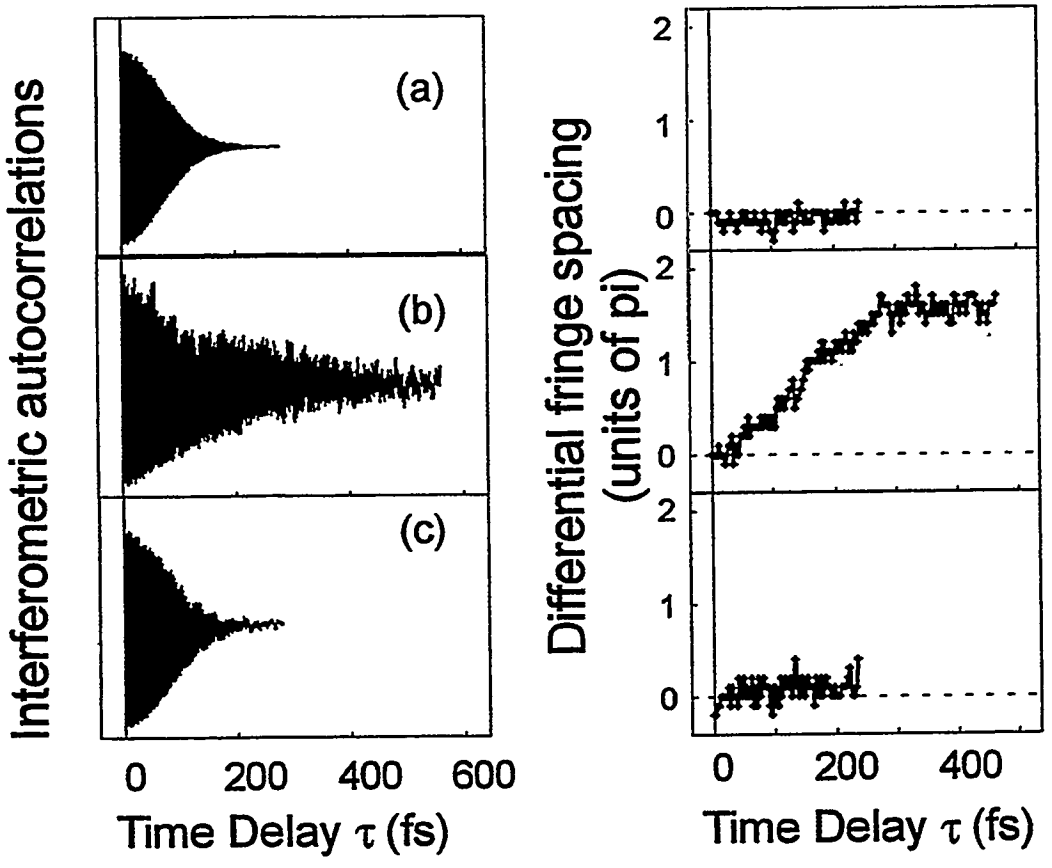

Figure 6.9: Interferometric autocorrelation traces and the corresponding differential fringe spacing DFS(τ) for the FWM signals whose power spectra are presented in Fig.6.8. FWM data is shown for the lowest and highest excitation densities recorded: (b) $3x10^{9}cm^{-2}$, (c) $3x10^{11}cm^{-2}$. The excitation laser pulse, tuned for selective excitation below the heavy-hole exciton, is shown in (a) for comparison.

Chapter 7

Conclusions

7.1 Principal results

We have measured the transient nonlinear optical response of GaAs multiple quantum well structures at room temperature via multi-wave mixing experiments in order to study the effects of Coulomb correlation on the ultrafast dynamics of quasi-2D excitons. To interpret our results, we have modeled the semiconductor as a homogeneously broadened ensemble of *interacting* two-level systems. Upon solving the equation of motion for the density matrix, we obtained analytical forms for the nonlinear polarization induced in the material under impulsive excitation. This led to a series of "signatures" for Coulomb correlation in both the amplitude and phase of four- and six-wave mixing (FWM, SWM) signals. For example, when Coulomb correlation is included in the model:

1.) the time-resolved (TR) FWM signal has a *delayed* contribution to the emission, arising from polarization wave scattering (PWS), in addition to the usual prompt response from field scattering.

2.) the time-integrated (TI) FWM measurement has a signal, also arising from the scattering of polarization waves, which appears at *negative* time-delays.

3.) the TI SWM lineshape is *asymmetric*, instead of resembling a coherent spike, with a slower decay for positive time-delays, again from PWS.

4.) the FWM emission exhibits a *nonlinear phase* evolution, because the prompt and delayed contributions to the nonlinear signal are out of phase.

Naturally, these signatures were unknown for dilute media, where interactions are neglected and the TI FWM measurement alone is therefore sufficient to extract information on the polarization dephasing rate. In fact, the signature for Coulomb correlation in TI FWM (see 2.), above) was the first one recorded for experiments in semiconductor heterostructures. [7.1] In this dissertation, we have presented evidence for the other three.

To realize these measurements, we constructed an apparatus for transient, multi-wave mixing experiments consisting of a modelocked Ti:sapphire oscillator delivering transform limited pulses of duration ≈100 fs, an optical set-up in the two-beam geometry for generating the FWM and SWM signals, and an electronic lock-in detection scheme interfaced to a personal computer. Our samples were optically thin, ≈100 Å GaAs multiple quantum well structures held at room temperature. We measured both the TI and TR multi-wave mixing signal, the power spectrum of the coherent emission, and the instantaneous frequency of the signal. The phase measurements were achieved via interferometric correlations, which had a temporal resolution of better than 140 attoseconds.

The TR FWM measurements provided much information on the dynamics of the quasi-2D excitons in our system. After verifying the internal consistency of the TR FWM measurements with the TI result, we studied the behavior of the TR FWM signal vs. the time-delay between excitation pulses and determined that the ensemble of excitons in our

sample was homogeneously broadened. The coherent emission from the sample thus corresponded to a free induction decay process, which is consistent with the theoretical analysis above. Using this result, we were able to fit the TR FWM traces taken for a series of excitation densities and time-delays to numerical solutions of the theoretical model, based on realistic excitation conditions. From the fits, we learned that the TI measurement hides information that can be extracted from an analysis of the TR signal. For instance, the temporally delayed PWS arising from Coulomb correlation (see 1.), above) can *dominate* the coherent emission at low excitation densities, where the potential remains unscreened. This leads to a non-exponential decay of the TR FWM lineshape, which is easily distinguished from the TI response. From the fits, we also determined that the polarization dephasing time T_2 depends upon both the excitation density, as expected, and, surprisingly, the *timing* of the excitation pulses. We will say more about this unexpected result in the following section. For the first time, a numerical analysis of the *TR* FWM lineshape provided quantitative information regarding the effects of Coulomb correlation on the nonlinear polarization induced in GaAs quantum wells. [7.2]

In addition to the amplitude FWM measurements, we also examined the higher order nonlinear response of our samples via TI and TR SWM experiments. TR SWM measurements verified that the dependence of the polarization dephasing time T_2 on the excitation density was consistent with the results found independently through the TR FWM measurements described above. TI SWM measurements at high excitation densities reproduced the symmetric, coherent spike expected for independent two-level systems, while TI measurements at low densities had an *asymmetric* lineshape. This asymmetry

indicated that there was a PWS contribution to the induced nonlinear polarization in addition to the contribution from field scattering. Thus, by measuring the fifth-order nonlinear optical response of room temperature excitons in GaAs quantum wells, we presented for the first time experimental evidence supporting the signature of Coulomb correlation (see 3.), above) in TI SWM. [7.3]

Beyond the traditional amplitude measurements of FWM and SWM, we also presented the first measurements of the *phase* of the ultrafast coherent emission from GaAs quantum wells. Using a differential technique to analyse interferometric correlation data, we compared the time domain response of the FWM emission to frequency domain power spectra measurements. We observed quantum beats in the emission of simultaneously excited heavy-hole (hh) and light-hole excitons, which is consistent with the interpretation of a homogeneously broadened system found from TR FWM measurements. When the hh-exciton alone was selectively excited, we measured both the power spectrum and the instantaneous frequency dynamics of the coherent FWM emission and found that they depended upon excitation density. In particular, at the lowest densities, there was a pronounced nonlinear variation to the phase of the FWM signal, which disappeared with increased excitation density. This observation was found to be consistent with the interpretation of a time-delayed, and out-of-phase, PWS contribution to the FWM emission (see 4.), above). Thus, for the first time, the nonlinear phase dynamics of Coulomb correlated excitons in GaAs quantum wells was verified experimentally. These results were qualitatively consistent with predictions from both the simplified model for dense media, described above, and the full numerical solution to the

semiconductor Bloch equations (SBE). [7.4] Importantly, as we explain below, our results also pointed out limitations to the validity of the SBE.

7.2 Future research directions

The results summarized above offer experimental confirmation of signatures of Coulomb correlation appearing in multi-wave mixing experiments on semiconductors at low excitation densities. These signatures were predicted from a theoretical model for dense media based upon interacting two-level systems and are consistent with numerical solutions to the SBE. [7.5] In addition to obtaining qualitative agreement with theory, we also detected surprising and important limitations to the currently available theoretical models. [7.4] In this section we discuss new directions for future experimental and theoretical research toward a more complete description of the nonlinear optical response of excitons in quantum wells.

An important issue raised by our results was found in the TR FWM measurements, where to obtain numerical fits to the data it was necessary to vary the polarization dephasing time T_2 as the time delay between excitation pulses Δt was changed. This indicates that *during the course of a TI measurement, T_2 is not constant.* This is a very surprising result, when one considers that TI measurements were traditionally performed for the very purpose of determining "the" polarization dephasing time for the system. This effect is understood intuitively in terms of an increased dephasing rate as the exciton density increases during the course of excitation. We expect the effect to be most

important when the polarization dephasing time is not much longer than the duration of the excitation pulses themselves, as is the case for our room temperature experiments. This effect was subsequently and independently confirmed by other groups via FWM measurements on GaAs [7.6] and named "excitation induced dephasing" (EID). Clearly, for a complete description of the semiconductor, theoretical models must be expanded to include dephasing processes resulting from EID.

Another important question to be answered by future research is brought to light by the measurements of the instantaneous frequency dynamics of the FWM signal. Historically the information contained in the phase of the ultrafast coherent emission was ignored and only the amplitude response was studied. This was true because of the experimental difficulties associated with measuring phase for very small, very fast signals and because the amplitude response was well described by numerical solutions to the SBE, which currently provides the most complete description of the nonlinear optical response of semiconductors. We have found that although the response vs. excitation density is in qualitative agreement with theoretical predictions, *some of the approximations used for numerical solutions of the SBE prevent quantitative agreement with both the phase dynamics and the response vs. time-delay between excitation pulses.* These surprising results and the corresponding calculations are well described by reference [7.4]. This discovery, which was only detected via measurements of the instantaneous frequency of the FWM emission, reveals an important limitation of the existing theoretical model. Although much research remains to be done on this subject, the results of reference [7.4] indicate that non-Markovian effects should be included in a complete theoretical

description. This new model must go beyond both the static treatment of screening and the frequency independent description of dephasing.

Finally, on an experimental note, studies of the transient nonlinear optical response of semiconductors have much to gain from steady advances in the fields of ultrashort laser pulse generation and characterization. As solid-state fs-oscillators evolve toward shorter (≈10 fs) pulses, temporal resolution much better than the results presented here becomes available. [7.7] Furthermore, these spectrally broad lasers make possible experiments involving the simultaneous excitation of bound and continuum semiconductor states. Additionally, the development of phase detection schemes applicable not only to high intensity ultrashort laser pulses, but also to low intensity spectroscopic signals, such as those characterized in this dissertation, would be of great benefit. Clearly, there is much to be learned from characterizing the ultrafast coherent emission from semiconductors in both amplitude and phase.

7.3 Concluding remarks

Investigating the transient nonlinear optical response of semiconductors is a rich and interesting field of research for many reasons. It encompasses the diverse sciences (and arts) of ultrafast laser techniques, semiconductor heterostructure growth, nonlinear optical phenomena, and many-body physics. We have presented in this dissertation only a tiny fraction of the current research being performed everyday as this complex field develops.

We hope that the physical insight gained from the discussion here inspires new experiments, improved theoretical models, and a wealth of unanticipated discoveries.

References

[7.1] M. Wegener, D.S. Chemla, S. Schmitt-Rink, and W. Schafer: *Line shape of time-resolved four-wave mixing*, Physical Review A, Vol.42, No.9, pp.5675-5683 (1990).

[7.2] S. Weiss, M.-A. Mycek, J.-Y. Bigot, S. Schmitt-Rink, and D.S. Chemla: *Collective effects in excitonic free induction decay: do semiconductors and atoms emit coherent light in different ways?*, Physical Review Letters, Vol.69, No.18, pp.2685-2688 (1992).

[7.3] M.-A. Mycek, J.-Y. Bigot, D.S. Chemla: *Time-resolved and time-integrated six-wave mixing in GaAs quantum wells: effects due to exciton-exciton interactions*, in Quantum Electronics and Laser Science Conference, OSA Technical Digest Series Vol.3 (Optical Society of America, Washington, DC), pp.9-10 (1993).

[7.4] D.S. Chemla, J.-Y. Bigot, M.-A. Mycek, S. Weiss, W. Schafer: *Ultrafast phase dynamics of coherent emission from excitons in GaAs quantum wells*, Physical Review B, Vol.50, No.12, pp.8439-8453 (1994).

[7.5] W. Schafer: *Manybody-effects in nonlinear optics of semiconductor structures*, in *Optics of Semiconductor Nanostructures*, F. Henneberger, S. Schmitt-Rink, E.O. Gobel, eds., Academie Verlag, pp. 21-50 (1993).

[7.6] H. Wang, K. Ferrio, D.G. Steel, Y.Z. Hu, R. Binder, S.W. Koch: *Transient nonlinear optical response from excitation induced dephasing in GaAs*, Physical Review Letters, Vol.71, No.8, pp.1261-1264 (1993).

[7.7] M.T. Asaki, C.-P. Huang, D. Garvey, J. Zhou, H.C. Kapteyn, M.M. Murnane: *Generation of 11-fs pulses from a self-mode-locked Ti:sapphire laser*, Optics Letters, Vol.18, No.12, pp.977-979 (1993).

Appendix

Optical Response of Interacting Two-level Systems

Beginning with Eqns.11(a), (b) from reference [1], we obtain the Eqns.2-1, 2-2 used in the phenomenological model of Ch.2. We then discuss the equivalent formalism of reference [2] used to numerically fit the time-resolved four-wave mixing data in Ch.4.

We use the notations of reference [1]. Under optical excitation with externally applied field E(t), a collection of N interacting two-level systems satisfies the optical Bloch equations

$$\left[\frac{\partial}{\partial t}+\gamma_2+i(\varepsilon_1-\varepsilon_2)\right]P(t)=i[N-2\nu(t)]|\mu|^2 E_{loc}(t) \qquad \text{Eqn.1}$$

$$\left[\frac{\partial}{\partial t}+\gamma_1\right]\nu(t)=-i\left[P(t)E^*_{loc}(t)-P^*(t)E_{loc}(t)\right] \qquad \text{Eqn.2}$$

where the transition amplitude ψ and population n are given by the polarization $P = N\mu^*\psi$ and the excited state density $\nu = Nn$. Here, the driving field is the Lorentz local field $E_{loc} = E + LP$, as determined by the Lorentz local field factor L, and the transverse and longitudinal relaxation rates are denoted $\gamma_2 = (T_2)^{-1}$ and $\gamma_1 = (T_1)^{-1}$, respectively.

Substituting $E_{loc} = E + LP$, we find that the transition energy is renormalized to $\Omega = \varepsilon_1 - \varepsilon_2 - V$, where $V = N|\mu|^2 L$. Thus, Eqn.1 becomes

$$\left[\frac{\partial}{\partial t}+\gamma_2+i\Omega\right]P(t)=i[1-2n(t)]N|\mu|^2 E(t)-2iVn(t)P(t) \qquad \text{Eqn.3}$$

and, assuming L (and hence V) is real, Eqn.2 becomes

$$\left[\frac{\partial}{\partial t}+\gamma_1\right]v(t)=-i\left[P(t)E^*(t)-P^*(t)E(t)\right] \qquad \text{Eqn.4}$$

To find the behavior of the transition amplitude ψ and population n, we substitute $P = N\mu^*\psi$, $v = Nn$ and cancel the common factor ($N\mu^*$). We also re-label the transverse (γ_2) and longitudinal (γ_1) relaxation rates as $\Gamma = (T_2)^{-1}$ and $\gamma = (T_1)^{-1}$, respectively. Thus, Eqns.3 and 4 become

$$\left[\frac{\partial}{\partial t}+\Gamma+i\Omega\right]\psi(t)=i[1-2n(t)]\mu E(t)-2iVn(t)\psi(t) \qquad \text{Eqn.5}$$

$$\left[\frac{\partial}{\partial t}+\gamma\right]n(t)=-2\mathrm{Im}\left[\mu E(t)\psi^*(t)\right] \qquad \text{Eqn.6}$$

which are identical to the Eqns.2-1, 2-2 used in Ch.2 to derive time-dependence of the first-, third-, and fifth-order polarizations and hence the transient multi-wave mixing response.

It is important to note that the Eqn.1 above is also equivalent to equation (2) of reference [2], which we used for the numerical analysis of Ch.4. We demonstrate this by beginning with Eqn.1 above and substituting $E_{loc} = E + \mathbb{L}P$, finding that the renormalized transition frequency is given by $\omega = (\varepsilon_1 - \varepsilon_2 - NL|\mu|^2)$. Letting $V = 2NL|\mu|^2$ and substituting $P = N\mu^*\psi$, $\nu = Nn$, Eqn.1 becomes

$$\left[\frac{\partial}{\partial t}+\gamma_2+i\omega\right]\psi(t)=i[1-2n(t)]\mu E(t)-iVn(t)\psi(t) \qquad \text{Eqn.7}$$

Making the approximation $n\equiv|\psi|^2$, valid for low excitation densities [3], and changing the notation for the transverse (γ_2) relaxation rate to $\Gamma = (T_2)^{-1}$, Eqn.7 becomes

$$\left[\frac{\partial}{\partial t}+\Gamma+i\omega\right]\psi(t)=i\left[1-\frac{|\psi(t)|^2}{|\psi_{sat}|^2}\right]\mu E(t)-iV|\psi'(t)|^2\psi(t) \qquad \text{Eqn.8}$$

where the saturation density is given by $|\psi_{sat}|^2=1/2$ for two-level systems. As explained in greater detail in Ch.4, the terms on the right side of the equation clearly show the two sources of nonlinearity in the problem. Firstly, phase-space filling due to Pauli exclusion

enters via the saturation term. Secondly, Coulomb correlation enters as excitons at one site ψ' interact with excitons at another site ψ via the potential V.

Equation 8 above is identical to the nonlinear Schrodinger equation (equation (2)) of reference [2] and is employed for the numerical fits to the time-resolved four-wave mixing data presented in Ch.4. The results for the time-dependent first- and third-order polarizations derived from Eqn.8 are equivalent to the formalism presented in detail in Ch.2, using Eqns.5, 6 above.

References

[1] M. Wegener, D.S. Chemla, S. Schmitt-Rink, and W. Schafer: *Line shape of time-resolved four-wave mixing*, Physical Review A, Vol.42, No.9, pp.5675-5683 (1990).

[2] S. Schmitt-Rink, S. Mukamel, K. Leo, J. Shah, D.S. Chemla: *Stochastic theory of time-resolved four-wave mixing in interacting media*, Physical Review A, Vol.44, No.3, pp.2124-2129 (1991).

[3] S. Schmitt-Rink, D.S. Chemla, H. Haug: *Nonequilibrium theory of the optical Stark effect and spectral hole burning in semiconductors*, Physical Review B, Vol.37, No.2, pp.941-955 (1988).

LAWRENCE BERKELEY LABORATORY
UNIVERSITY OF CALIFORNIA
TECHNICAL INFORMATION DEPARTMENT
BERKELEY, CALIFORNIA 94720